DEFECT ENGINEERING OF METAL OXIDE SEMICONDUCTORS

BY

KYONG WOOK NOH

THESIS

Submitted in partial fulfillment of the requirements
for the degree of Master of Science in Chemical Engineering
in the Graduate College of the
University of Illinois at Urbana-Champaign, 2010

Urbana, Illinois

Advisor:

Professor Edmund Seebauer

ABSTRACT

Defects in semiconductors have been studied for many years, with a view toward controlling their behavior through various forms of defect engineering. In the Si-based microelectronics industry, numerous methods to characterize and control the behavior of defects have been developed, including novel techniques such as co-implantation, millisecond annealing, photostimulation and surface engineering. Closely related, yet unique defect engineering efforts have also been made for non-Si based microelectronic applications as well. The accumulated knowledge stemmed from microelectronics should also be able to be extended to metal oxide semiconductors, where promising applications (*e.g.*, gas sensors and photocatalysts) are gaining increased interest. In particular, the use of surface engineering has been extended to titanium dioxide, opening up new possibilities of defect control. For further investigation of these effects, sulfur has been chosen as a surface controlling adsorbate, which can be used to manipulate the surface states. The successful deposition of the element through electrochemical means has been demonstrated on silicon and titanium dioxide substrates. In addition, experimental and computational studies on the behavior of the cation species in titanium dioxide using isotopic tracers have also been carried out, with an emphasis on the effect of surface states. It follows that the surface state can indeed influence the cation defect behaviors in a significant manner, which in turn affects the self-diffusion profiles.

ACKNOWLEDGMENTS

All X-ray photoelectron spectroscopy analysis in this work was carried out in the Frederick Seitz Materials Research Laboratory Central Facilities, University of Illinois, which are partially supported by the U.S. Department of Energy under grants DE-FG02-07ER46453 and DE-FG02-07ER46471. The staff of the SCS machine shop, electronic shop and glass shop is gratefully acknowledged for their assistance in building and maintaining some of the necessary components and equipments that have been used for this work.

I would very much like to thank my advisor, Dr. Edmund Seebauer, for guiding and assisting me through the hardships of research and life. I would also like to thank my colleague, Alice Hollister, for all the useful discussions and help on various subjects. My thanks are also extended to my former and current lab mates who helped make research an enjoyable experience. Lastly, many thanks go to my family and friends for their continuous support and love. Without them, I would not be where I am now.

TABLE OF CONTENTS

LIST OF FIGURES

LIST OF TABLES

1. INTRODUCTION

1.1. Defects in Semiconductors

The technologically useful properties of a semiconductor often depend upon the types and concentrations of the defects it contains. For example, defects mediate dopant diffusion in semiconductors used for microelectronic devices [1-5] in ways that are vital for device fabrication. Defects also affect the performance of semiconductor-based sensors [6], catalysts [7,8], photo-active devices [9-11], and photovoltaic (PV) cells [12]. Defect formation affects semiconductor properties in a variety of ways. Point defects typically affect electronic properties such as carrier type, concentration or mobility [13,14]. Extended defects also affect physical properties, such as strength or toughness [15]. At elevated temperatures, extended defects frequently serve as sources or sinks of point defects. Surfaces do the same, interacting through both bond-exchange [16,17] and electrostatic [16] mechanisms. Most defects can act as sites where electrons and holes recombine with special efficiency [18-20], typically degrading the performance of the host material in applications ranging from optoelectronics to photocatalysis. In order to control the behavior of these defects and maximize the performance of the applications, various means of defect engineering have been developed and implemented.

1.2. Recent Trends in Defect Engineering

Most of the defect engineering originates from the Si-based microelectronics industry, where precisely controlling the electronic properties of Si was vital in the advancement of the technology. Methods such as ion implantation , rapid thermal processing and solid state epitaxial regrowth are examples of techniques developed for the purpose of defect manipulation in Si

microelectronics [21-24]. With the increasing demand to form ultra shallow junctions with feature sizes of tens of nanometers, novel methods have also arose and show promise. These include plasma doping, vacancy engineering, surface manipulation, and photostimulation effects [17,25-29]. In non-Si applications, on the other hand, defect engineering has been relatively less active and was focused more on other aspects. In compound semiconductors for example, much interest was on the role of extended defects like threading dislocations, which is thought to be the main cause of reduction in efficiency and lifetime in optoelectronic applications and photovoltaic cells. Hence, defect engineering in this area was mainly focused on reducing these dislocations by means such as step growth or epitaxial lateral overgrowth [30,31]. The recent extension of microelectronics to non-Si semiconductors, however, opens the possibility of defect engineering that closely resembles that of Si-based microelectronics to be utilized as well.

Metal oxide semiconductors are another set of materials that show unique characteristics. These materials have found use in many useful applications such as gas sensors and photocatalysts [32-35]. While the defect structure and chemistry has been characterized in depth for some oxides, active means of manipulating defects has only been the subject of research recently. Since many of the related applications require the small scale geometries of nanoparticles (*e.g.*, nanowires) rather than large singe crystal substrates, conventional methods of defect engineering previously derived from Si-based microelectronics may not be applicable for direct implementation. Nevertheless, the novel methods such as plasma doping or surface manipulation may well prove to be useful methods of defect engineering in metal oxides.

1.3. Titanium Dioxide Defect Engineering

Of the many metal oxide materials, titanium dioxide is one of the most studied materials [36]. It has potential as a photovoltaic material and also shows promise as a useful photocatalyst, which may be used for water splitting applications. Defects in TiO_2 can be thought to be in two categories: titanium defects and oxygen defects. Titanium dioxide in its natural state is partially reduced, denoted as TiO_{2-x}, where x is the degree of reduction. Hence, the main oxygen defect is known to be oxygen vacancies, typically with a +2 charge. However, some literature also suggest the possible existence of oxygen interstitials as well [37]. Titanium defects, on the other hand, are known to exist mainly as interstitials with charge states of +3 and +4. Evidence also exists of the presence of titanium vacancies [38], though, due to the extremely slow nature of their movement, they would only have effect at significantly long time scales (*i.e.*, on the order of hundreds to thousands of hours).

As with most oxide materials, most of the defect studies and manipulation attempts are focused on the oxygen atoms. Studies on the dependence of the ambient oxygen partial pressure have been carried out extensively, revealing the nature of the material at different oxidation states. While surface defects have also been taken into account in terms of their direct effects on applications, little attention has been given on their relation with regards to bulk defects. Previous studies in our lab have shown the effect of surface states on the behavior of bulk defects in Si [28,39,40]. The principles learned from these studies should be able to be extended to other classes of materials as well. Indeed, preliminary studies using isotopic oxygen diffusion reveal that surface states may well be a way to mediate defect behaviors [28].

Contrary to the case of oxygen, little investigation has been done with the focus on the behavior of titanium atoms. Only a number of isotopic tracer studies have been carried out

previously to study the properties of titanium defects [41,42]. As titanium atoms also constitute a large portion of the material, and with the possibility of the existence of interactions between titanium and oxygen atoms, it will also be worthwhile to focus on the behaviors of titanium atoms explicitly.

The focus of this work will be two-fold. First, Chapter 2 reviews the various aspects of defect engineering from Si microelectronics to metal oxides. The remainder of the work will focus on defect engineering methods regarding surface manipulation of titanium dioxide. Specifically, Chapter 3 will introduce the method of sulfur deposition, which has been used to manipulate the surface of TiO_2, while Chapter 4 will present experimental and computational studies on the behavior of titanium defects in TiO_2.

1.4. References

1 H. Bracht, *MRS Bull.* **25** (2000) 22-27.

2 N. Dasgupta, A. Dasgupta, *Semiconductor Devices: Modeling and Technology*, Prentice-Hall, New Delhi, 2004.

3 P. M. Fahey, P. B. Griffin, J. D. Plummer, *Rev. Mod. Phys.* **61** (1989) 289-384.

4 S. M. Hu, *Mater. Sci. Eng. R* **13** (1994) 105-192.

5 M. Y. L. Jung, C. T. M. Kwok, R. D. Braatz, E. G. Seebauer, *J. Appl. Phys.* **97** (2005) 063520.

6 J. W. Fergus, *J. Mater. Sci.* **38** (2003) 4259-4270.

7 W. Baiqi, J. Liqiang, Q. Yichun, L. Shudan, J. Baojiang, Y. Libin, X. Baifu, F. Honggang, *Appl. Surf. Sci.* **252** (2006) 2817-2825.

8 Y. Zhang, A. Kolmakov, S. Chretien, H. Metiu, M. Moskovits, *Nano Lett.* **4** (2004) 403-407.

9 W. W. Chow, S. W. Koch, *Semiconductor-Laser Fundamentals: Physics of the Gain Materials*, Springer, Berlin, 1999.

10 S. Guha, J. M. Depuydt, M. A. Haase, J. Qiu, H. Cheng, *Appl. Phys. Lett.* **63** (1993) 3107-3109.

11 G. Lutz, *Semiconductor Radiation Detectors: Device Physics*, Springer, Berlin, 1999.

12 S. R. Kurtz, A. A. Allerman, E. D. Jones, J. M. Gee, J. J. Banas, B. E. Hammons, *Appl. Phys. Lett.* **74** (1999) 729-731.

13 E. G. Seebauer, M. C. Kratzer, *Mater. Sci. Eng. R* **55** (2006) 57-149.

14 E. G. Seebauer, M. C. Kratzer, *Charged semiconductor defects: structure, thermodynamics and diffusion*, Springer, New York, 2008.

15 D. Hull, D. J. Bacon, *Introduction to dislocations*, Butterworth-Heinemann, Oxford, 2001.

16 K. Dev, M. Y. L. Jung, R. Gunawan, R. D. Braatz, E. G. Seebauer, *Phys. Rev. B* **68** (2003) 195311.

17 E. G. Seebauer, K. Dev, M. Y. L. Jung, R. Vaidyanathan, C. T. M. Kwok, J. W. Ager, E. E. Haller, R. D. Braatz, *Phys. Rev. Lett.* **97** (2006) 055503

18 W. Shockley, W. T. Read, *Phys. Rev.* **87** (1952) 835.

19 S. M. Sze, *Semiconductor devices, physics and technology*, Wiley, New York, 2002.

20 K. Vanheusden, W. L. Warren, C. H. Seager, D. R. Tallant, J. A. Voigt, B. E. Gnade, *J. Appl. Phys.* **79** (1996) 7983-7990.

21 B. A. Gillespie, H. N. G. Wadley, *J. Cryst. Growth* **311** (2009) 3195-3203.

22 S. Paul, W. Lerch, *Mater. Sci. Forum* **573-574** (2008) 207-228.

23 L. Pelaz, L. A. Marques, M. Aboy, P. Lopez, J. Barbolla, *Comput. Mater. Sci.* **33** (2005) 92-105.

24 N. G. Rudawski, K. S. Jones, S. Morarka, M. E. Law, R. G. Elliman, *J. Appl. Phys.* **105** (2009) 081101-081120.

25 N. E. B. Cowern, A. J. Smith, N. Bennett, B. J. Sealy, R. Gwilliam, R. P. Webb, B. Colombeau, S. Paul, W. Lerch, A. Pakfar, *Mater. Sci. Forum* **573-574** (2008) 295-304.

26 M. Y. L. Jung, E. G. Seebauer, in: Extended Abstracts of the 4th International Workshop on Junction Technology, IEEE, Shanghai, (2004) pp. 87-89.

27 E. G. Seebauer, in: Proceedings of the 8th International Conference on Solid-State and Integrated Circuits Technology, IEEE, Shanghai, (2007) pp. 450-453.

28 R. Vaidyanathan, Ph.D. thesis, University of Illinois at Urbana-Champaign, 2007.

29 S. Walther, R. Liebert, *J. Vac. Sci. Technol. B* **24** (2006) 482-488.

30 B. Beaumont, P. Vennéguès, P. Gibart, *Phys. Status Solidi B* **227** (2001) 1-43.

31 J. F. Geisz, S. Kurtz, M. W. Wanlass, J. S. Ward, A. Duda, D. J. Friedman, J. M. Olson, W. E. McMahon, T. E. Moriarty, J. T. Kiehl, *Appl. Phys. Lett.* **91** (2007) 023502.

32 E. Comini, C. Baratto, G. Faglia, M. Ferroni, A. Vomiero, G. Sberveglieri, *Prog. Mater. Sci.* **54** (2009) 1-67.

33 A. Fujishima, K. Honda, *Nature* **238** (1972) 37-38.

34 S. Sakthivel, B. Neppolian, M. V. Shankar, B. Arabindoo, M. Palanichamy, V. Murugesan, *Sol. Energy Mater. Sol. Cells* **77** (2003) 65-82.

35 G. Shen, P. C. Chen, K. Ryu, C. Zhou, *J. Mater. Chem.* **19** (2009) 828-839.

36 U. Diebold, *Surf. Sci. Rep.* **48** (2003) 53-229.

37 S. Na-Phattalung, M. F. Smith, K. Kim, M.-H. Du, S.-H. Wei, S. B. Zhang, S. Limpijumnong, *Phys. Rev. B* **73** (2006) 125205.

38 M. K. Nowotny, T. Bak, J. Nowotny, *J. Phys. Chem. B* **110** (2006) 16302-16308.

39 R. Gunawan, M. Y. L. Jung, E. G. Seebauer, R. D. Braatz, *AIChE J.* **49** (2003) 2114-2123.

40 C. T. M. Kwok, K. Dev, R. D. Braatz, E. G. Seebauer, *J. Appl. Phys.* **98** (2005) 013524.

41 M. A. Henderson, *Surf. Sci.* **419** (1999) 174-187.

42 K. Hoshino, N. L. Peterson, C. L. Wiley, *J. Phys. Chem. Solids* **46** (1985) 1397-1411.

2. NOVEL METHODS OF DEFECT ENGINEERING IN SEMICONDUCTORS

2.1. Introduction

Semiconductor materials are used in a variety of applications. One of the main aspects of semiconductors that enable such wide use is the capability of altering its electronic properties. This is done by moderating defects within the semiconductor material. The roles of defects may differ from application to application. In microelectronics, it is known that intrinsic defects, such as vacancies or interstitials, mediate the diffusion of dopant atoms [1-5]. Defects also play a role in the performance of sensors [6], catalysts [7,8], photo-active devices [9-11], and photovoltaic cells [12]. The importance of defects becomes even more pronounced as the feature size of devices become smaller. In nanometer scale structures, for example, the size of the structure is small enough that the effect of a single point defect cannot be ignored and must be taken into account. It is therefore clear that the ability to control defects is an important element to device development.

The microelectronics industry is one of the fields in which defect control was the main key to advancement. Microelectronic devices make use of the difference of electronic properties of various components embedded within the base semiconductor material, which is mainly silicon. These differences are due to the difference in defects, namely the substitutional defects, otherwise known as dopants. As the feature size of devices became smaller, controlling the behavior of dopants became more crucial which led to the development of advanced defect engineering techniques. These techniques include rapid thermal processing [13,14], ion implantation [2], solid phase epitaxial regrowth [13,15], etc. With the recent need for creating

ultra shallow junctions, the techniques have improved even further, giving rise to techniques such as flash/laser annealing [13,14,16], co-implantation [13,17,18], and molecular implantation [13,16]. In addition to the improved state-of-the-art techniques of defect engineering, other novel methods have also been studied. These include vacancy engineering [13,19], high energy light ion irradiation [20], and surface engineering [13,21,22].

While defect engineering has been mostly researched in the Si-based microelectronics industry, it may also be employed to other applications in which defects play an important role as well. To begin with, it is easily conceivable that these techniques may be readily employed to non-Si based microelectronics due to their similarities. Even for other systems, the knowledge and techniques acquired on defect engineering can provide insight into the control of defects. For example, with the increase of nanometer size applications where the surface effects begin to be more dominant, surface engineering can be a readily applied means of controlling the defects within these structures.

There are a few reports [13,23] that give a comprehensive review on the novel defect engineering methods for Si-based microelectronic device fabrication. Other reviews [24-27] can also be found that cover the subject comprehensively, but do not include the latest techniques. The vast majority of reviews with regards to Si-based technologies focus either on the overall manufacturing process of microelectronic devices [28-30] or on one particular method of choice. These include well established fields such as ion implantation [31-33] and rapid thermal processing [14,34,35], as well as the new methods including millisecond annealing [14,36,37], co-implantation [38], plasma doping [39-41], and vacancy engineering [42,43].

The literature base for applications outside of Si-based microelectronics is much less extensive. Some reviews on well established methods such as ion implantation can be found for

III-V compound semiconductors [44-46]. For metal oxides, the concept of defect engineering or control is relatively new and only a few reviews can be found [47,48]. There are, however, a variety of reviews on either the usage of ion implantation for photocatalysts [49,50] or the properties and roles of the defects themselves [51-53].

In this work, we review the novel methods of defect engineering techniques that have been mainly developed for the Si based microelectronics industry. Among these, our focus will not be on the advanced versions of the currently existing techniques. Rather, we will visit the newly arising methods that may not yet have been utilized in industry, but show potential to overcome the fast approaching limitations of current technology. We will then review defect engineering requirements in other applications and show how the new methods that have been originally designed for microelectronics may also provide an opportunity for improvement in these other fields.

2.2. Defect Characteristics

All crystalline materials above 0 K contain imperfections in their atomic structure called defects. These imperfections may be single atomic (point defects) or may involve multiple atoms or lattice sites (extended defects). Point defects consist of missing atoms in the lattice site (vacancies), additional atoms that are not occupying a lattice site (interstitials), and impurity atoms that are taking the place of native atoms (substitutional defects or dopants). Extended defects include linear or planar mismatches in the lattice (dislocations or stacking faults), clusters of point defects, and grain boundaries. The various types of defects are illustrated in Fig. 2.1. While extended defects can exist in a single material, they are also frequently generated at the interface between two different materials. Even if the adjacent materials are epitaxially grown, if

the native lattice constants of the two materials are different, there will be some degree of lattice mismatch which can result in the formation of dislocations in order to reduce the stress induced by such mismatch. These dislocations are also capable of penetrating multiple epitaxial layers, also known as threading dislocations.

Defects can alter the properties of the material in a variety of ways. In general, point defects typically affect the electronic properties such as carrier type, concentration, or mobility [54], while extended defects mainly affect the physical properties, *e.g.*, strength or toughness, of the material [55]. Most defects can act as sites where electrons and holes recombine with special facility [56-58], typically degrading the performance of the host material in applications ranging from optoelectronics to photocatalysis. Extended defects, on the other hand, have little influence on the electronic properties. However, they may also function as a source and/or sink of point defects and can consequently affect the electronic properties in an indirect way as well. It is also known that dislocations may serve as a non-radiative recombination centers, and their presence may degrade the performance of optoelectronic devices.

It has long been known that bulk defects in semiconductors can be electrically charged. Charging of surface defects has been identified and studied rather more recently. In either case, this charging can affect defect structure [59,60], thermal diffusion rates [61-63], trapping rates of electrons and holes [64,65], and luminescence quenching rates [66]. More interestingly, defect charging also introduces new phenomena such as nonthermally photostimulated diffusion [67-69]. Such phenomena offer completely new mechanisms for defect engineering, as well as new means to study the charging phenomenon itself.

Crystalline surfaces support native defects in the same way a bulk solid does [70], with many close analogies between the two cases. Understanding surface defects is becoming

increasingly important in practical applications – for example, as electronic devices shrink closer to the atomic scale (with the attendant increase in surface-to-volume ratios), and as molecular-level control of catalytic reactions becomes increasingly feasible. Of particular importance is defect-mediated surface diffusion, which plays an important role in crystal growth, heterogeneous catalysis, sintering, corrosion, and microelectronics fabrication. Considerably less is known about the behavior of surface defects than bulk defects. (Even less is known about defects at solid-solid interfaces, but some analogies with the bulk and free surface still hold.) Recent research has also indicated that surfaces or interfaces can directly influence point defect behavior in the bulk [21,71], and that bulk properties can couple directly into the behavior of surface defects [67,68].

For semiconductor materials, controlling the electronic properties to suit the needs of the various applications is the main point of interest. Hence, defect engineering in semiconductors is primarily focused on point defects. Following this argument, we will also focus our discussions on point defects and from here on, the word 'defect' will indicate point defects unless stated otherwise.

2.3. Si-based Microelectronics

Critical dimensions in Si-based integrated circuits have scaled down well into the range of a few tens of nanometers. Defect engineering in these applications focuses upon the initial creation of Si wafers by Czochralski growth or upon the later fabrication of *pn* junctions in field effect transistors (FETs) by ion implantation and annealing.

2.3.1. Czochralski Growth

Highly scaled microelectronic devices require Si wafer substrates that are exceptionally free of defects and impurities. Czochralski growth from the semiconductor melt is the most common manufacturing technique for producing such Si, and extensive efforts have been made to minimize defect formation or incorporation during the growth process. The most common defects that bedevil the grown material are microdefects such as aggregates of vacancies, self-interstitials and oxygen impurities. The resulting defects are often large enough to observe directly via light scattering or transmission electron microscopy (TEM) [72,73]. Yet these defects form by accretion of smaller point defects, which remain largely invisible yet still require control.

Early attempts at defect control were empirical methods involving specialized protocols for heat removal and crystal pulling from the melt to maintain spatial uniformity in temperature [72,74]. Oxygen dissolution within the Si was mitigated through crucible design. Such empiricism led to significant improvements. In recent years, however, detailed mathematical modeling of defect behavior within the high-temperature solid has augmented the experiments. The modeling of defect diffusion, reactions and equilibrium provides useful insights, reduces the number of experiments required to understand defect behavior, and has found direct connection to optimizing commercial processes [72,75-77].

For example, modeling coupled with experiments has shown that the majority defect that forms during growth depends upon the ratio of the pull rate v and the temperature gradient G [72,75,76]. At higher v/G ratios, vacancies dominate. Self-interstitials dominate at lower ratios. Recent models incorporate the effects of oxygen on the behaviors of intrinsic defects [78,79], and have extended to more complicated systems where intentional dopants such as nitrogen [79-

81] and germanium [82,83] are introduced. The same basic approach has also been applied to growth of germanium and metal oxide crystals [73,77,84].

2.3.2. Ion Implantation

For a semiconductor to function as an electronic device component, it must be doped properly to attain the necessary properties. In integrated circuits (IC), different regions of the wafer must be doped in different ways according to the circuit requirements, and thus doping must be done as a separate process. One of the most established ways of doping is ion implantation [31-33].

As the ICs became more integrated, the feature size of the nodes decreased accordingly. With this decrease, it became necessary to form shallower junctions, which posed challenges in the doping process as well. In order to achieve the necessary requirements, ions of various energies and components were used. Recently, new methods of doping have also began to become incorporated.

One such method is molecular doping [13,16]. For shallow junctions, the implanted dopants must not penetrate the substrate too deeply. Hence, a lower energy is necessary. This, however, leads to low throughput of doping as the flux of ions is proportional to the ion beam energy. Molecular doping is a method that attempts to overcome this predicament by using molecules or clusters that contain the target ion species instead of using single ion species as the source. The large size of the target molecules can provide high mass ratio and relax the ion beam energy, resulting in low energy ion bombardment. Since the ion beam energy is still high, a higher throughput is possible. Therefore, a high throughput of doping while maintaining small ion implantation energy becomes possible. Initial attempts were made by using decaborane

($B_{10}H_{14}$) as the implantation species [85-88]. However, limitations in the source stability and delivery systems retarded development of the technology. Improvements in the source enabled the use of octadecaborane ($B_{18}H_{22}$) as the new species for molecular doping which reignited interest [89-91]. Junctions with a depth of <10 nm have been successfully fabricated and shown to have similar performance as those obtained via B+ implants (Fig. 2.2). More recently, carborane ($C_2B_{10}H_{12}$) has gained interest as a new possible source for molecular implantation [92,93]. Its feasibility has been assessed for 65 nm high performance devices and the results show excellent performance, which shows potential for use in the 32 nm technology and beyond.

Co-implantation of other species concurrently with the main dopant is another promising method for achieving shallow junctions. This came about by studying the effects of F during BF_2 implantation processes. Ohyu et al. [94] found that by implanting F independently after B implantation, the redistribution of B after annealing was suppressed and the concentration of activated B increased, thus leading to a decrease in the leakage current of the p^+/n junction. The positive effects of F implantation have also been demonstrated in preamorphized Si by Huang et al. [95]. Since then, various studies have been carried out in order to find the role F [17,96-100]. Fluorine decreases the TED of boron by reducing the excess Si interstitials [97,98]. It has also been found that fluorine can deactivate boron under certain circumstances [17,97,100]. Carbon has also been found to be a useful co-implant. It was first demonstrated that epitaxially grown carbon rich silicon layers can reduce boron TED [101], which led to the co-implantation of carbon [102]. It was later found that combining C co-implantation with preamorphization or F co-implantation improves the boron TED and activation (Fig. 2.3) [103,104]. Similar effects were also found to exist for the case of P as well [105,106]. Lastly, N co-implantation has also

been studied and found to suppress boron TED and deactivation via similar mechanisms as that of C or F [107-109].

Plasma based doping/implantation is also being investigated as a suitable doping method for ultra shallow junction (USJ) fabrication [39-41]. Plasma sourced ion implantation was first implemented by Conrad et al. [110] followed by Mizuno et al. [111] who used this technique in doping. The use of plasma enables ultra-low energy implantation at a high beam current. This leads to high doping dose rate and throughput while keeping the penetration depth low. Using this method, junctions with ultra-shallow profiles, in the sub-10 nm range, and high doping concentration has been achieved [112,113]. Recent studies use plasma doping as a means to achieve doping in three-dimensional structures with large aspect ratios which are difficult to dope using conventional ion implantation [114,115].

2.3.3. Vacancy Engineering

This is a technique that introduces an excess of vacancies in the doping region via high energy co-implantation. Since the doping process creates a supersaturation of interstitials, the excess vacancies can annihilate these interstitials, thus reducing unwanted diffusion of the dopants. The introduction of the additional vacancies is done by a high energy co-implantation process, typically prior to the desired dopant implantation. The wafers are irradiated with high energy silicon. The main advantage of this method is that the wafers to not become amorphized, and thus the overall process may be reduced by one step. However, the gate electrode and dielectric are affected as they are implanted with high energy ions.

Raineri and coworkers [116] studied the effect of high energy co-implantation in relation to dopant enhanced diffusion. They applied a 1 MeV Si co-implant followed by a boron implant

in bulk substrate leading to reduction in transient enhanced diffusion (TED). Roth et al. [117] and Venezia et al. [118] used silicon on insulator (SOI) substrates to investigate a similar effect induced by high energy silicon co-implantation. They used a buried silicon oxide layer in the SOI substrate to isolate the deep interstitials-type extended defects of the MeV implant, thereby eliminating the possibility that these defects getter the interstitial excess induced by the keV Si implant. Through this decoupling, it was demonstrated that the MeV Si implant can completely eliminate the B TED even in the presence of the interstitial barrier. Other works [119,120] also showed that an improvement in sheet resistance was noticed at low temperature, in addition to the improvement in boron TED. Cowern and coworkers [19,121] have recently combined the concepts of vacancy engineering and proposed an advanced vacancy engineering implant method for ultra shallow junction formation. There are two key factors to which they propose. First, it is applied to semiconductor layers of finite thickness, *e.g.*, SOI, and the co-implant conditions are chosen to generate an excess vacancy profile throughout the layer under the implant window. Second, the co-implant species and dose/energy combination is chosen to generate an excess vacancy concentration that is very high close to the surface, but without amorphising the semiconductor crystal in the B implanted volume. Through simulation and physical experiments they have shown that this method has the potential to provide outstanding PMOS source-drain performance and scalability. Excellent USJ characteristics were achieved such as a "diffusionless" dopant profile and the associated dopant activation was greatly enhanced, and beyond the conventional boron solubility level (Fig. 2.4). More recent work by Bennett et al. [122] showed the possibility of applying this technique to bulk Si substrates as well, which further extends the potential of this defect engineering method.

2.3.4. Thermal Processing

Thermal processing is done in order to heal the damage done after doping of the substrate. By annealing after implantation of dopants, the damaged region will regain the crystallinity and the dopants will settle in to the lattice sites properly, thus becoming activated. This process is only enabled at higher temperatures as the diffusion of atoms only happens at a significant rate at elevated temperatures.

As the required feature size of devices became smaller, however, the diffusion aspect started to become a problem since the elevated temperatures also enabled the dopants to travel further into the substrate than what was desired. Thus the requirement of being able to heat the samples very quickly and maintain the heat for short times became crucial. This was done by using various lamps capable of achieving ramp rates of several hundred K/s. These types of rapidly heating processes are called rapid thermal processes (RTP) [16].

RTP is favorable for microelectronics fabrication in many ways. It is able to process wafers individually, relatively easy to cluster the system into other systems, and capable of heating just the target while maintaining the chamber walls cold. Of course, the capability of being able to keep the wafers at elevated temperatures for short periods of times and the ability to control the heating duration is the by far the most important. This enabled the fabrication of ultra shallow junctions (USJ), in which the diffusion of the dopants must be restricted to a very small range during dopant activation.

As device sizes scaled downward and junction depths became shallower (20 nm and below in present technology), techniques that enable annealing with durations in the millisecond region have emerged. Dopant activation can be improved greatly by annealing at temperatures just below the melting point of Si for millisecond durations (Fig. 2.5) [123]. Sources that can

deliver radiant energy in such short cycles have been used for annealing, which include the use of excimer lasers [124-126] and xenon flash lamps [37,124,127,128]. These methods are capable of heating cycles with the duration in the tens of milliseconds all the way down to nanoseconds. Computational studies on the effect of millisecond annealing have also been conducted [129,130]. Millisecond annealing methods reduce unwanted dopant spreading by greatly reducing the time for diffusion, which more than compensates for an increased concentration of Si interstitials that promote dopant spreading. In moving from conventional rapid thermal annealing to millisecond annealing of boron in Si, for example, the rate of interstitial-mediated dopant diffusion increases by almost 2 orders of magnitude due to the higher temperature, but the time scale is reduced by almost 3 orders of magnitude [131]. The net consequence is reduced profile spreading, as shown in Fig. 2.6. Millisecond annealing also favorably alters the relative balance of dopant interstitial sequestration by the crystal lattice vs. interstitial clusters, which leads to improved electrical activation at depths just short of the junction. Again, the key factor is the reduction in time scale, which significantly reduces the amount of re-accretion of dopant interstitials into interstitial clusters.

Proper device functioning requires the management of several kinds of defects during processing, ranging from native and dopant point defects to native and dopant defect clusters to extended structures such as end-of-range defects. Consequently, various combinations of millisecond annealing with more conventional thermal annealing have been developed [132,133]. With respect to interstitial clusters, for example, the rate of dissociation depends upon both peak temperature and ramp-rate. A higher ramp-rate reduces cluster dissociation, which keeps dopant atoms locked in an inactive state [127,134,135]. Annealing to higher temperatures can mitigate this problem to some extent. However, differential thermal expansion among the various

materials present in the device can lead to wafer warpage or breakage. The melting point of the underlying Si also imposes an obvious constraint. Thus, elevating the annealing temperature suffers limits in terms of dopant activation; removal of end-of-range defects suffers similarly [134,136,137]. Multiple exposures to the optical source (laser beam [137] or flashlamp [138,139]) are sometimes employed to circumvent these problems. Combination of millisecond processing with furnace annealing [132] or conventional rapid thermal annealing [140,141] seeks to accomplish similar goals. However, the optimal combination of laser (or flashlamp) pulse duration, number of pulses, and incorporation of standard annealing methods remains a subject of active research [142].

2.3.5. Surface Engineering

Recent studies have shown that modifying the surface can introduce new pathways to defect generation or annihilation [13,21,22]. The principle is that dangling bonds on the surface can be an easy pathway for interstitials to be generated. Likewise, vacancies can be relatively easily annihilated at dangling bonds. By creating an atomically clean surface, the amount of dangling bonds can be increased, thus initiating such processes.

Seebauer and coworkers have shown by experiments and simulations that the chemical state of the surface of Si has an influence on the defect concentration of the material [21,22,143,144]. It has first been shown that an atomically clean surface has a huge effect on the self diffusion of Si [21]. The adsorption of atomic nitrogen on Si(100) was capable of controlling the annihilation probability of self-interstitials in implanted material over at least two orders of magnitude (Fig. 2.7). It was further shown that even coverages as small as 0.01 monolayers (ML) have a significant effect. The atomically clean surface has the largest

annihilation probability (S=0.05) which leads to smaller concentrations of self-interstitials near the surface, thus reducing the spreading of implanted species. With increased surface coverage, however, some of the surface dangling bonds become saturated and reduces the probability of interstitial annihilation. This leaves more self-interstitials capable of profile spreading. In a following study [22], this basic principle was shown to apply to implanted dopants, arsenic in this case, as well. The atomically clean surface has a large number of dangling bonds, which are capable of acting as a large sink that removes Si interstitials selectively over dopant interstitials. Such selective removal has a favorable impact on dopant TED and activation.

The previous work pertained to crystalline Si without preamorphization implantation (PAI), however, and was unclear whether the concepts would be extended to amorphous surfaces. In addition, end of range (EOR) defect evolution was not addressed and the case of boron, the most technologically problematic dopant, was not examined. More recent studies by Yeong et al. [143] address these issues and show experimentally that surface effects can also be exploited for Ge-PAI Si with boron as the dopant (Fig.2.8). The results yield improvements in TED and boron activation as well as a substantial reduction of residual EOR damage. Dangling bonds at the surface open a major alternative pathway for annihilating the excess interstitials emitted from the EOR defect band. Also, the de-/reactivation of the dopants are significantly influenced.

The surface effects should take place regardless of the type and length of the annealing techniques that are to be employed. In addition, the benefits should not be interfered by the presence of substrate strain, and should be able to work along with other methods of defect engineering (*e.g.*, co-implantation or dopant cluster implantation). Along with these advantages, surface engineering can be used as a means to control the defect concentration within the substrate. It has been shown that such manipulation favorably impacts dopant diffusion and

activation. Such modification can show even more potential to nanometer size applications where the surface plays an increased role in the overall properties of the material.

There is another type of defect surface engineering in which surface treatment directly leads to the improvement of the electrical properties of the substrate. Jie et al. [145] have recently found that the surface state of Si nanowires (NWs) have an impact on its electrical properties. They compared the performance of Si NW field effect transistors (FETs) in air and vacuum, and found that the carrier mobility was higher when in vacuum environments. The performance was further improved when the NWs were embedded in SiO_2, which insulates the devices from atmosphere and passivates the surface defects. In other studies, organic molecules were use to passivate and functionalize the surface of materials which lead to huge improvements in device performance. Cui et al. [146] used 4-nitrophenyl octadecanoate to passivate the surface defects on the SiO_x coating around Si NWs. This surface treatment led to a significant increase in the Si NW FET performance with increases in the average transconductance and mobility.

2.3.6. Photostimulation Effects

It has recently been found that defects may be stimulated with irradiation. Due to the discontinuity of the crystalline periodicity at the surface, there exists a surface charge region near the surface, which creates an electrical field in this area. As the depth in question is on the order of several nanometers, this electrical field effect can be huge. Hence, if the defects within this region is stimulated by irradiation and their charge state changes, they will experience a significant change in their mobility which will influence the diffusion properties of species. Given that the main source of heat for the annealing process is in the form of light irradiation,

and the fact that the purpose of the thermal process is to control the diffusion of species, of which most can be in the charged state, the photostimulation effect of charged species must be taken into account.

Recent studies by Seebauer and coworkers [147,148] have shown that illumination can play a role in the self diffusion rates of Si. They used a novel experimental design employing a new heating configuration in which heating and illumination was largely decoupled. In n-type Si, the illuminated specimens showed an enhanced rate of diffusion, as shown in Fig. 2.9. On the other hand, the p-type Si showed no significant difference between the illuminated and unilluminated samples. The difference in behavior between n and p-type material gives strong evidence that the observed enhancement in n-Si is genuine, and not an artifact of some unknown heating or similar spurious effect. It is conjectured that this is due to the change of charged state of the Si interstitials, which is the species that is thought to dominate the mass transport at the temperature ranges of the experiments.

2.4. Non-Si Microelectronics

2.4.1. Germanium

Aside from Si, other semiconducting materials have been used for microelectonic devices as well. For single elements, Ge is the next potential candidate for extensive use. Especially with the limitations of Si being more pronounced in recent developments, Ge is gaining renewed interest as the alternative material. Ge possesses outstanding electrical properties, such as high carrier mobilities compared to Si, and also requires lower thermal budgets for dopant activation and implantation-induced defect anneal, which further enhances its potential [149]. The main

drawback that was keeping Ge from replacing Si was the absence of a stable native oxide. The physical properties also differ significantly from Si and pose a challenge in direct substitution with Si. For instance, the damage induced by ion bombardment is more substantial compared to that of Si [150]. Also, the mobility of defects is much lower, leading to reduced recombination and annihilation of these species. This also induces different diffusion characteristics of the widely used dopants such as phosphorus or boron. Fortunately, the current Si technology is shifting away from using the native oxide, SiO_2, to some other high-dielectric constant dielectric, *e.g.*, HfO_2. Thus, the oxide issue no longer poses a significant problem in employing Ge as the main semiconductor material.

Due to the many similarities of Ge and Si, most, if not all, of the defect engineering techniques that have been developed for the Si industry can be readily employed for the case of Ge. Several studies have already utilized methods such as flash lamp annealing [151], laser annealing [152,153], plasma doping [152], and vacancy engineering [154] to study the effect of dopant diffusion in Ge. While the related phenomena are similar with that of Si, the specific conditions and behaviors may vary, necessitating further characterization for the methods to be fully implemented. For example, boron is known to be a slow diffuser in Ge, while it has a low solid solubility [150,155-157]. On the other hand, the commonly used n-type dopants such as P, As and Sb have a high diffusivity at relatively low temperatures as 500 °C [158,159]. Hence, it is perceivable that investigation of the implantation and activation characteristics of n-type dopants in Ge would be more extensive compared to p-type – opposite to the case of Si. As the field develops further, other methods yet to be tried should also be able to reveal useful information of Ge and dopant properties. They may also be further utilized in the actual

fabrication of Ge-based microelectronic devices. This would lead to the introduction and development of more advanced components.

2.4.2. Compound Semiconductors

Compound semiconductors such as III-V and II-VI materials are another league of materials that is used as microelectronic components. The main advantage of the compound semiconductors is the fact that one may control the band gap of the material relatively easily by altering the composition of the components. This enables the fabrication of heterojunctions and high electron mobility transistors (HEMTs), also called heterostructure field effect transistors (HFETs), in addition to the metal oxide semiconductor field effect transistors (MOSFETs) that are commonly used in Si-based devices. In addition to electronic circuit components, compound semiconductors also find widespread use in optoelectronic devices such as light emitting diodes (LEDs) and laser diodes (LDs), as well as photovoltaic (PV) cells. In fact, some of the best PV cells with the highest efficiency in both terrestrial and space conditions have been fabricated using multiple layers of compound semiconductors [160,161].

The main challenge of fabricating these multi-layer devices is creating the multiple layers with a near-perfect crystal structure throughout the device. Unfortunately, altering the composition of the compound materials to achieve the required band gaps also change the lattice constant of the materials at the same time, making the task of creating perfect epitaxial layers a non-trivial matter. Lattice mismatch between the layers can lead to the formation of threading dislocations which are known to degrade the performance of devices significantly. Various methods, such as step grade growth of multiple layers [160,162] or epitaxial lateral overgrowth [163,164], have been employed to overcome these problems. Step grade growth makes use of

the fact that the lattice constant of compound semiconductors is proportional to the ratio of the constituting elements. By growing multiple layers with a gradually increasing ratio of components, it is possible to vary the lattice constant gradually through the layers. This gradation reduces the stress between layers and inhibits the formation of additional dislocations due to lattice mismatch. In epitaxial lateral overgrowth (Fig.2.10), the base material is grown on the substrate through a mask and eventually spreads laterally on top of the mask. The presence of the mask reduces the formation of dislocations, and any stress that was formed by the mask in reduced by the lateral overgrowth. The concentration of threading dislocations can be decreased significantly using this method.

In addition to these extended defects, other defects that form deep states within the band gap that can trap charge also degrade the performance of devices. For example, gate-lag effects, current collapse, and gate leakage currents in HMETs have been associated with the surface states of the material [165-169]. More recently, these phenomena have been attributed to surface charge states, surface defects and also nitrogen vacancies (for nitride semiconductors) [166,170,171]. By the use of proper surface treatment or surface passiviation, *e.g.*, H_2, N_2, or NH_3 plasma treatment, the leakage current has been found to decrease significantly [165,166,169]. Thus, the proper use of surface defect engineering can be utilized for the improvement of these devices, especially when the feature size decreases and the surface ratio increases. Currently, the compound semiconductors are mainly used in the undoped or uniformly doped form. There may come the time when shallow junctions are also required and the regional doping of compound semiconductors becomes necessary as well. In these cases, the other defect engineering methods may also be useful to achieve the goal more efficiently.

Recently, nanowires (NWs) have begun to be used as the channels on FETs. Several materials have been used for this application including Si, GaAs, ZnO, SnO_2, etc. The performance of these NW FETs depends on the doping state, size of the NW, surface states and defect states. As mentioned previously, various surface treatment methods can alter the electronic properties of the NWs significantly. Due to the size of these devices, other existing defect engineering methods have the likelihood of damaging the NWs directly. Hence, the surface will play the major role on its properties and will be the most accessible route for the control of their properties. For example, Keem et al. [172] observed an increase in the transconductance and mobility in ZnO NW FETs after being annealed in a H_2/Ar environment. This step reduced the surface trap charges and contaminants of the NWs. Chang and coworkers [173] found that passivating the surfaces of the ZnO NWs with a SiO_2/Si_3N_4 bilayer increases the performance of the FETs (Fig. 2.11). After passivation, the FETs exhibit improvement in the subthreshold swing, on/off ratio, and mobility. Lao and coworkers [174] used various types of carboxylic acid self-assembled molecules with different terminal groups (*e.g.*, stearic acid, lysine, dodecanedioic acid, mercapto-acetic acid, and perfluorotetradecanoic acid) to treat ZnO nanobelts. After treatment, the nanobelts exhibited an increase in conductance by 6 orders of magnitude, a change from a Schottky contact to an Ohmic contact, and greatly improved photoconductivity and gas sensing response. Fig. 2.12 shows a schematic of the mechanism.

2.5. Metal Oxide Semicondcutors

The science base for accomplishing defect engineering in metal oxide semiconductors is less well developed than for the semiconductors used for electronic devices. Metal oxides always contain at least two primary elements (as distinct from the elemental semiconductors Si

and Ge), and the oxides often lose oxygen to the gas phase upon heating. Defect chemistry is therefore more complicated. Electrical characterization of the defects (a primary tool in electronic devices) is more difficult to accomplish in metal oxides, especially those with large band gaps. Determination of carrier type and concentration are difficult for oxides because the contacts employed for four-point-probe or Hall Effect measurements need to obey Ohm's Law but actually behave as diodes. Alternative approaches by capacitance-voltage measurements should work in principle for thin film configurations. For a typical oxide such as TiO_2, however, the resulting values of carrier concentration vary widely and the data are often misinterpreted [175-178]. For polycrystalline material, electrically active states at grain boundaries can contribute to the carrier concentration at magnitudes that dominate the bulk crystallites (in some cases). Additionally, the bulk and/or grain boundary states whose energies lie deep within the band gap contribute to the carrier concentration in a way that depends upon applied voltage [179]. Despite these problems, attempts to engineer the defects in metal oxides continue to grow, especially in applications involving gas sensors and photocatalysis.

2.5.1. Gas Sensors

Several different gas sensors that can detect gases such as CO, NO_x, O_2, etc. have been made from various metal oxide materials [180-183]. The gases are detected by the change in electrical properties of the sensor material with reaction (adsorption) between the gas and metal oxide. As the gas molecules adsorb on the surface, electrons may be drawn to the surface or injected into the bulk depending on the property of the adsorbed species. This leads to a change in the carrier concentration of the sensor and induces a resistivity change which can be detected by the change of the current flowing through the sensor. Defects play an important role in this

process in that surface vacancies are frequently the adsorption sites for the gas molecules on the material. Also, charged defects and dopants provide the necessary base conductivity of the metal oxide. Initially, gas sensors were fabricated in the form of thick or thin films on a substrate. It was later found that sensors with smaller crystallite size and thus larger surface area had better sensing properties (Fig. 2.13) [184,185]. Following this argument, different types of nanostructures such as nanocrystals, nanowires and nanobelts began to be utilized in gas sensors. Moreover, nanowires are gaining additional interest as NW FETs became available [180,182,184,186]. These NW FETs are capable of enhanced sensitivity due to the ability to modify the electronic properties of the NW by controlling the applied gate voltage. Not only can the sensitivity be improved, but it is also possible to "reset" the surface by electron driven desorption (Fig. 2.14) [186]. This is especially important for operation at lower temperatures (*e.g.*, room temperature) where thermal desorption is impractical.

In order to achieve sensors with high sensitivity and good characteristics, it is important to be able to control the electrical properties of the sensor. This is mainly done by proper doping and defect control. Oxygen vacancies tend to be the dominant electrically active (*i.e.*, charged) defect in metal oxides. Oxygen vacancy control has been previously achieved by controlling the oxygen concentration during deposition or post-treatment in oxygen or reducing atmospheres [187,188]. For doping, the most commonly used method is to introduce the dopants concurrently during the growth of the sensor material [189,190]. The advantage of this approach is that it does not require a separate doping step, and that the resulting material can be uniformly doped. However, it provides little means of direct control over native defects within the material. Ion implantation has also been used as a post-deposition doping method [191-193]. In addition to introducing dopants, this method also induces point defects on the surface, which increase the

reactive sites, thus enhancing the sensitivity of the sensor. The downside is that the ion beam is directional, and it can be difficult to obtain uniform doping for configurations such as nanowires, where the structure is non-planar. A possible way to overcome this difficulty is by employing plasma based doping techniques. With this method, dopants may be implanted perpendicular to the surface regardless of its orientation and can ensure uniform doping of non-planar structures.

While the conductance method has been used extensively for gas sensing applications, it also has many difficulties in creating good contacts due to the possible formation of schottky barriers between the sensor material and the metal contacts, as well as difficulties in fabricating the accurate contacts due to the small size of the wires. In an attempt to overcome these difficulties, a completely different method of detection that utilizes the photoluminescence (PL) of the sensing material has been developed. Several wide band gap metal oxides have been found to have PL spectra in the visible light range. The exact mechanism of this visible PL is still unclear and under investigation. It is generally perceived that the oxygen vacancies play an important role in this phenomenon, whether directly or indirectly [194]. In addition, these effects become more pronounced for smaller sized structures, indicating that surface states may also play a role [180,195]. Under this premise, Faglia et al. [196] have found that NO_2 adsorption can quench the visible PL spectra in SnO_2 nanobelts. Furthermore, very low concentrations (in the ppm range) yield noticeable effects, pointing to the possibility of this being used as gas sensors (Fig. 2.15). Similar sensing properties have been found for NO_2 adsorbed on ZnO nanowires as well [195,197]. In this case, the response of the nanowires was not interfered by the presence of CO and only a little by humidity or ethanol (less than 5% difference for either 700% relative humidity or 1000 ppm of ethanol), as shown in Fig. 2.16.

The mechanism of gas detection using PL resembles the conductance method in some respects. Gas molecules adsorb on the surface which induces a change in the state of defects within the material, which in turn alters the PL property of the material. It is thought that NO_2 adsorption creates non-radiative recombination paths for electrons and holes, which reduces PL emission [180,194]. The advantage of this method is that the overall sensing apparatus can be very simple. Since the PL quenching does not invoke any shifts in the peak, a combination of an LED for excitation and a photodiode for detection is enough to create the gas sensor. It is also possible to combine both the conductive and PL methods for increased sensitivity and, more importantly, the selectivity of complex gas sensing devices.

2.5.2. Photocatalysts

Photocatalysis is capable of achieving a variety of reactions such as air pollutant reduction, bio degeneration, water purification and, most importantly, direct water splitting. Many different oxide materials such as TiO_2 [198-200], ZnO [201,202], SnO_2 [203,204] and In_2O_3 [205,206] have been utilized for this purpose and some have also been commercialized (known as advanced oxidation methods) [198-200]. Among these materials, TiO_2 has the highest potential as a photocatalyst due to its low cost and high stability against degradation by chemical attack or prolonged illumination [47,207].

Photocatalysis works in a similar way as a photovoltaic (PV) cell. Light irradiation, mostly provided by the sun, excites the electrons in the valance band or donor states into the conduction band or accepter states, generating electron-hole pairs. If the charge carriers generated this way is collected on either side of a p-n junction, the device becomes a PV cell. In photocatalysis, the generated carriers are transferred to the adsorbed reactant species, providing

the means for a redox reaction to take place. Metal oxides are the preferred material for this application due to the fact that the surface oxygen vacancies on these materials are capable of providing suitable adsorption sites necessary for the reactions to take place. Most metal oxides, however, have rather large band gaps (*e.g.*, 3.2 eV for anatase TiO_2) and can only absorb UV to near violet light, which is only a fraction of the total solar irradiation. Hence, in order to increase the efficiency of photocatalysis, various methods have been employed to reduce the band gap of the materials.

One of the methods to be used was transition metal doping. Elements such as Fe, V, Cr, Co, and others have been introduced into TiO_2 to extend the light absorbance to the visible region (Fig. 2.17) [208,209]. However, when it came to photocatalytic activity, the outcome was in mixed results. It was later found that while metal doping can indeed reduce the band gap and thus increase photoresponse, they may also provide non-radiative recombination centers and ultimately reduce the overall photocatalytic activity [209]. Metal doped TiO_2 is also unstable to heat treatment and can promote rutilization [209], which can further decrease photocatalytic activity due to the lower photoreactivity of rutile compared to anatase [210]. The metal dopants can exist as cations in the solid solution or form segregate clusters of metal oxides within the photocatalyst. The mechanisms by which these structures influence the photocatalyst is complex and can vary for different materials. Thus, the photoreactivity of doped TiO_2 appears to be a complex function of the dopant concentration, the energy level of dopants within the TiO_2 lattice, their electronic configuration, the distribution of dopants, the electron donor concentration, and the light intensity [208].

Due to the complexities of metal doping in photocatalytic activity, non-metal anion doping has also been investigated as an alternative. Nitrogen is among the first to be used, and

Asahi et al. [211] have shown by experiments and theoretical calculations that nitrogen doped TiO_2 is capable of visible-light photodegradation of methylene blue and gaseous acetaldehyde (Fig. 2.18). They found that the nitrogen atoms substitute lattice oxygen sites and can narrow the band gap by mixing the N2p and O2p states. Additional efforts have been made to introduce nitrogen using a variety of methods ranging from amination and nitration to ion implantation and sputtering [207,211-215]. In most cases the photocatalytic activity have increased, while there was some evidence that nitrogen may also function as recombination centers [215]. In addition to nitrogen, carbon has also been used as a promising anionic dopant element. Khan et al. [216] have used flame oxidation to treat Ti metal sheets and obtain carbon doped TiO_2 films. Some of the oxygen sites were substituted by the carbon atoms, reducing the band gap energy to 2.32 eV. The films were capable of obtaining a maximum photoconversion efficiency of ~8 % under the illumination of a xenon lamp (Fig. 2.19). Park et al. [217] synthesized vertical nanotube arrays of carbon doped TiO_2 with high aspect ratios by anodizing Ti metal followed by annealing in CO ambience. The measured photocurrent and water splitting efficiency under visible-light illumination (> 420 nm) far exceeded that of pure TiO_2 nanotube arrays. The mechanism of carbon in photocatalysis can be especially complex, and computational studies showed that carbon atoms can substitute either Ti or O sites depending on the conditions [218]. Nevertheless, carbon can be the most promising anion dopant due to a significant overlap between the O2p state and the carbon states near the valence band edge [219]. Other non-metals such as S, Br, Cl, etc. have also been used as dopants for TiO_2 and have succeeded in increasing the absorbance to the visible region, thus increasing photoactive reactivity [220-222]. Anionic doping to reduce the band gap has been carried out in other photocatalytic materials as well. Nitrogen has been introduced to ZnO photocatalytic degradation applications [223], and carbon and nitrogen doping

have found use in water splitting by In_2O_3 [205,206]. Although the exact mechanism may differ from material to material, the basic principle of reducing the band gap energy to increase photocatalytic activity holds.

In addition to introducing extrinsic impurities, controlling the intrinsic defect concentration is another method that has been used to enhance the photocatalytic reactions. For example, strongly reduced TiO_2 can gain absorbance in the visible region [224-227]. It has been reported that Ti^{3+}-V_O-Ti^{3+} centers may serve as catalytically active centers in photoassisted oxidation of water (where V_O represents oxygen vacancies) [228]. Hence, the introduction of oxygen vacancies can also play an important role in photocatalytic activities. However, high temperature annealing in reducing atmospheres to partially reduce TiO_2 leads to the formation of rutile phases, which is not favorable for photocatalytic reactions [210]. Thus, low temperature methods must be employed. Ihara and coworkers [226,227,229] have used radio-frequency H_2 plasma to reduce TiO_2 in lower temperatures and found an increase in the photocatalytic activity of benzoic acid, propanol, and NO_x oxidation. The effect on NO_x oxidation is shown in Fig. 2.20. They propose that the oxygen vacancy states lay 2.02-2.45 eV above the valance band, which lies in the visible region and thus electrons from the valance band may be excited to these vacancy states by absorbing visible light (Fig. 2.20) [227]. Recently, the role of oxygen vacancies in the enhancement of photocatalytic activity has also been shown in ZnO photocatalysts [230]. In this case, the oxygen vacancies were introduced by fast nucleation and growth of the nanoparticles by rapid heating using microwave irradiation and subsequent quenching during the precipitation reaction. It was found that this led to faster initial degradation rate of methylene blue as compared to the conventionally synthesized nanoparticles. In view of the fact that oxygen vacancy introduction can provide a pathway for photocatalytic activity

enhancement, the various surface treatment methods that have been mentioned in Section 2.3.5 may also be applied to introduce oxygen vacancies at lower temperatures.

2.6. Summary

Defect engineering is a key component of manufacturing various modern applications that utilize semiconductors. The Si-based microelectronics industry has been the primary work horse in the development of this field and several defect engineering techniques have been well established, such as ion implantation and rapid thermal processing. These methods continue to evolve as more advanced technology becomes necessary to keep up with the expectations of device development. With the feature size becoming ever smaller, the requirements of the ability to control the behavior of dopants and defects became more stringent. This gave rise to millisecond annealing techniques, which further decreased the amount of dopant diffusion while maintaining the amount of dopant activation. Co-implantation of other species was also used to further inhibit unnecessary dopant diffusion and point defect generation, while molecular doping methods emerged in order to decrease the dopant introduction depth more efficiently. In addition to the enhancement of previous methods, other novel techniques have also gained interest. Plasma doping is a method that is capable of uniformly introducing dopants with lower energy and thus shallower depths. The uniformity does not have any directional restrictions and can be extremely useful for the doping of three dimensional architectures which are on the rise. In vacancy engineering, vacancies are strategically introduced to junction regions in order to reduce dopant diffusion and also repair implantation damage by inducing defect annihilation. Lastly, surface engineering focuses on the ability of the surface to act as a sink or source of point defects. By appropriate modification of the surface states, the generation and annihilation rate of

defects can be controlled due to dangling bond effects. This can be even more important in nanoscale devices due to the increased surface area to volume ratio of such applications.

While most of the defect engineering methods have been focused on the Si-based microelectronics industry, other semiconductor applications ranging from non-Si microelectronics to various metal oxide applications have also emerged, which require defect engineering as well. The roles and effects of defects in these applications vary for each specific case and corresponding defect control methods have been developed in some of the mature fields. However, these methods are still in the beginning stages compared to the extensive investigation done in the Si-based microelectronics industry, and it can thus be advantageous to utilize what has been established in the Si industry where applicable. This is quite straightforward in the non-Si based microelectronics due to the many similarities. For the case of Ge, which has the potential to replace Si in the near future, most Si defect engineering methods can directly be applied. In the case of compound semiconductor devices, most of the attention is focused on obtaining high quality heterostructures, wherein extended defects are the primary concern. Nevertheless, point defect engineering may still be required as further applications become developed and the feature size of devices decreases. On the other hand, the advent of nanowire devices provides opportunities for the application of the newer defect engineering techniques. While the role of defects is very important in these small scale applications, the structures are no longer planar, which can be a challenge in applying the well established methods directly. In these cases, the novel techniques that utilize plasma or surface modification can be advantageous as they can be employed regardless of configuration.

Similar arguments hold for the various metal oxide applications as well. In gas sensors, appropriate defect control and doping is necessary to obtain the required electrical or optical

properties of the sensing material. Moreover, the materials are frequently in the form of nanowires, and defect engineering methods that can be applied to nanowire electronics (*e.g.*, plasma methods or surface engineering) can be directly applied. For photocatalysts, appropriate defect control is needed to gain the required photoresponse of the materials. At the same time, these applications require large scale fabrication, and the cost of the method to be used must also be taken into consideration. Hence, methods that enable the introduction of defect species during the actual fabrication of the materials would be the most favored, while relatively simple processes such as surface modification may also be employed.

2.7. Figures

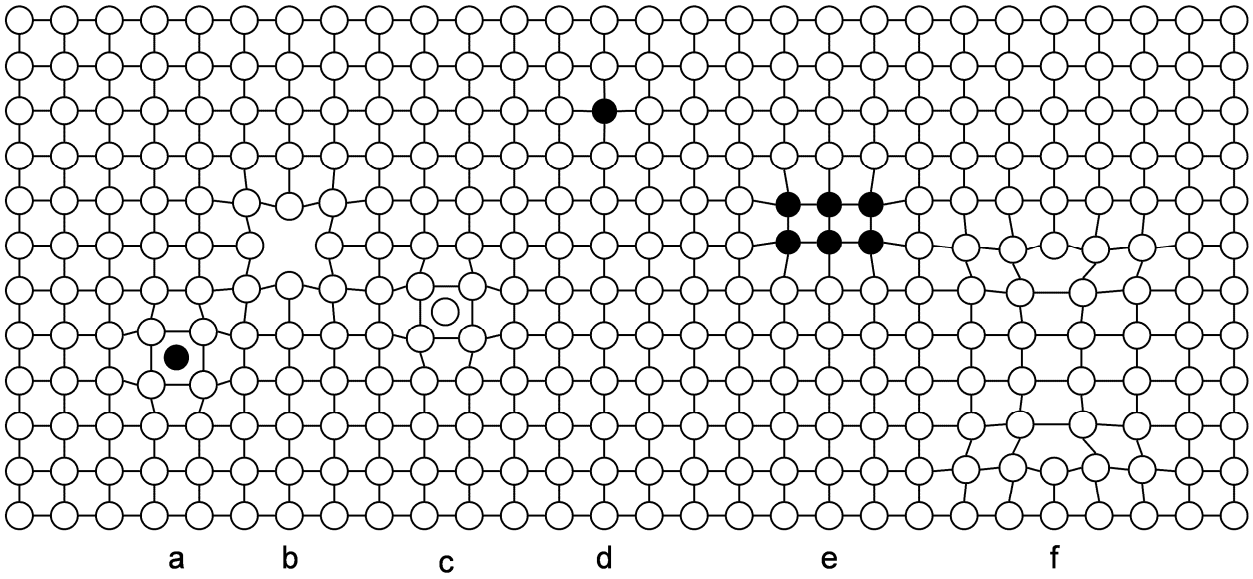

Fig. 2.1. Examples of common defects in semiconductors: a) Interstitial impurity atom, b) Vacancy, c) Self interstitial atom, d) Substitutional impurity atom (dopant), e) Precipitate of impurity atoms (clusters), f) Vacancy clusters.

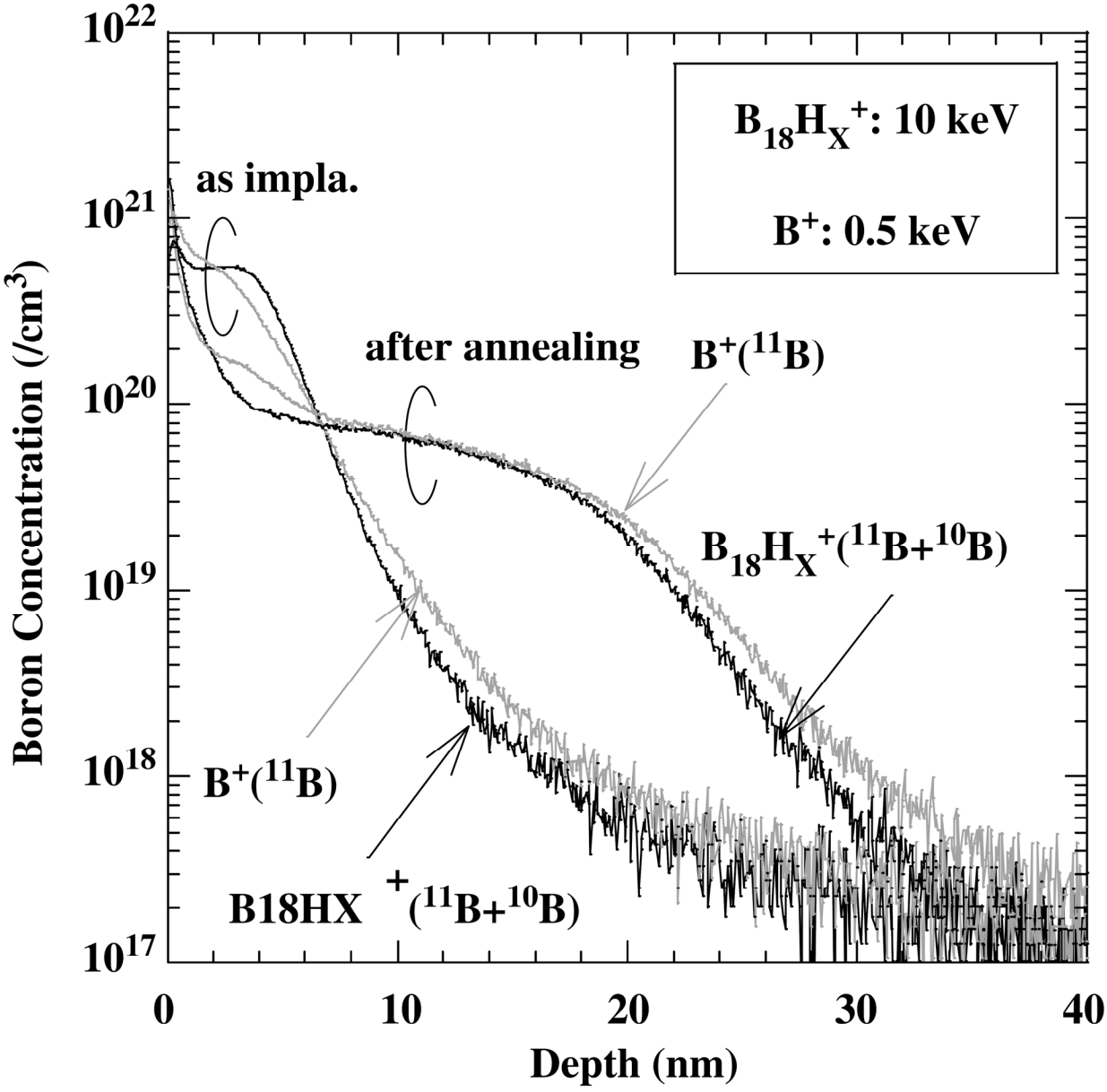

Fig. 2.2. Secondary ion mass spectroscopy (SIMS) profiles of B in Si, before and after annealing of $B_{18}H_X^+$ at 10 keV and B^+ at 0.5 keV. Reprinted from [90], Copyright 2005, with permission from Elsevier.

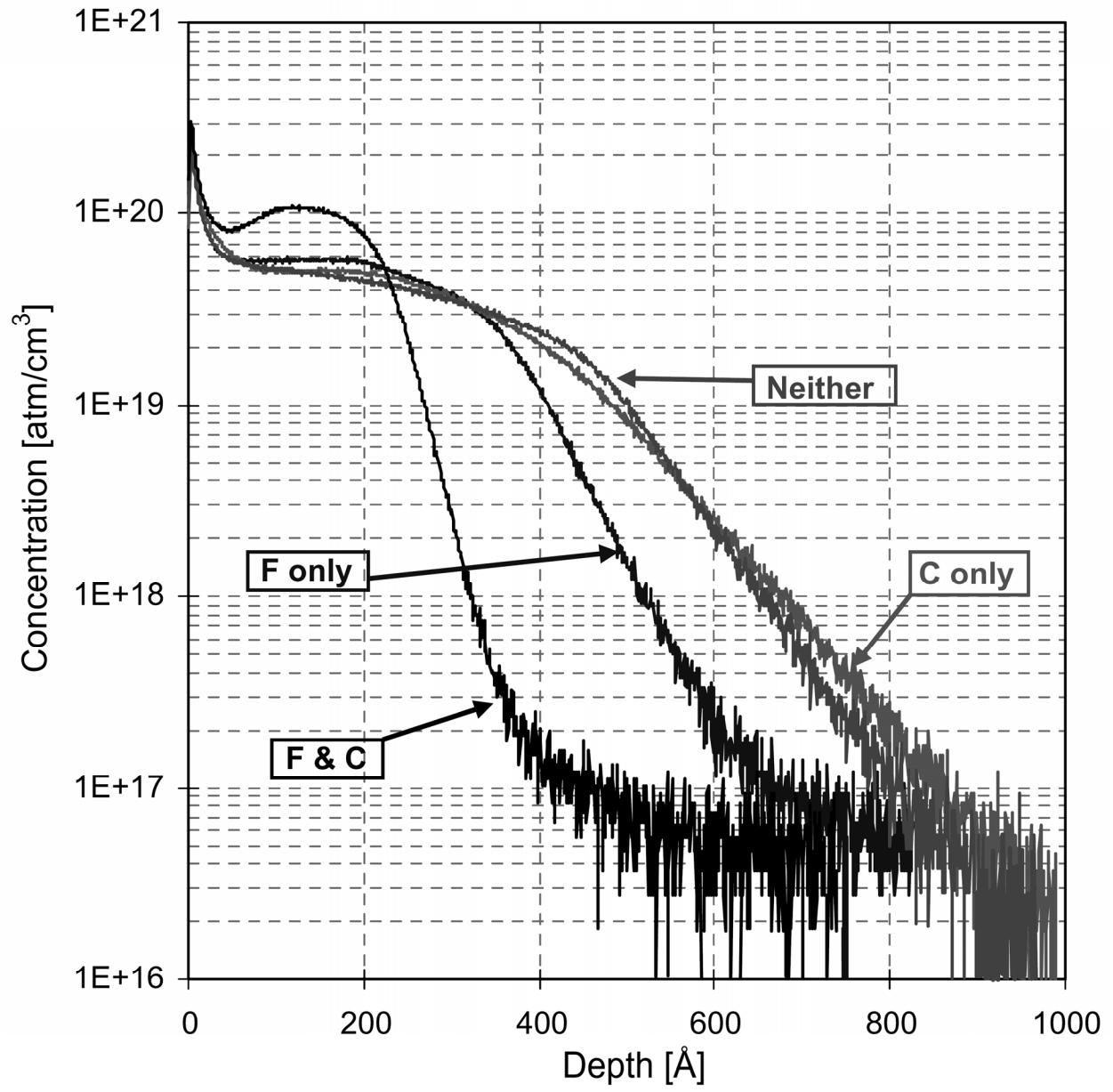

Fig. 2.3. Secondary ion mass spectroscopy (SIMS) profiles of B in Si after annealing with the co-implant conditions labeled. Note the dramatic boron diffusion reduction in the case where F and C co-implants are present. Reprinted from [104], Copyright 2005, with permission from Elsevier.

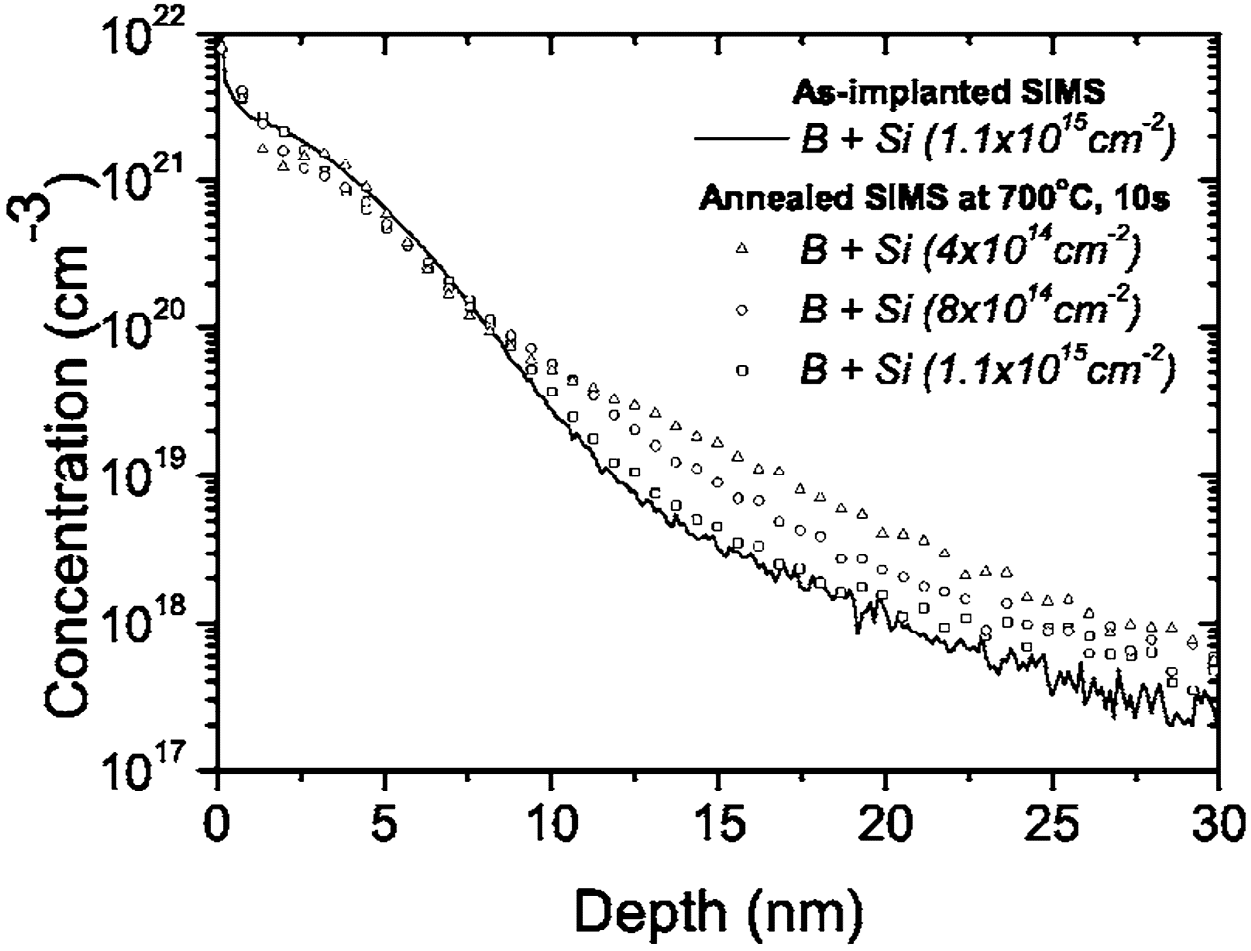

Fig. 2.4. Secondary ion mass spectroscopy (SIMS) analysis of 500 eV B implants in silicon after silicon co-implantation, before and after annealing. Symbols show data for three co-implant doses: 4×10^{14} cm^{-2} (△), 8×10^{14} cm^{-2} (○), and 1.1×10^{15} cm^{-2} (□), after annealing at 700 °C for 10 s. The solid line shows the as-implanted profile (taken from the sample implanted with 1.1×10^{15} cm^{-2} silicon). Reprinted with permission from [121], Copyright 2006 American Institute of Physics.

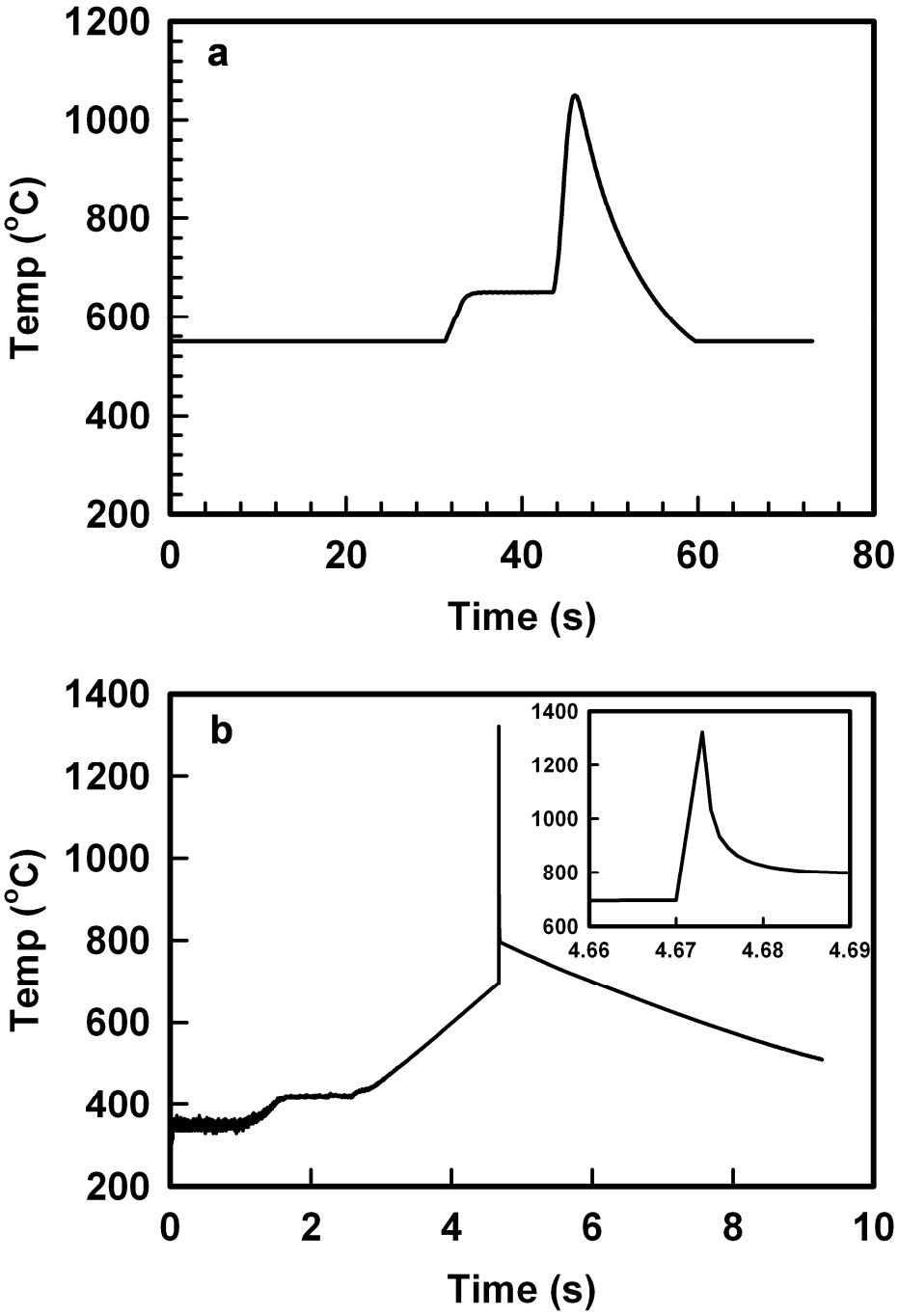

Fig. 2.5. (a) Temperature trajectory for rapid thermal annealing with a peak temperature of 1050 °C. (b) Annealing program for millisecond anneal experiment with a peak temperature of 1322 °C. Inset shows the detailed temperature trajectory. Reprinted with permission from [129], Copyright 2009 American Institute of Physics.

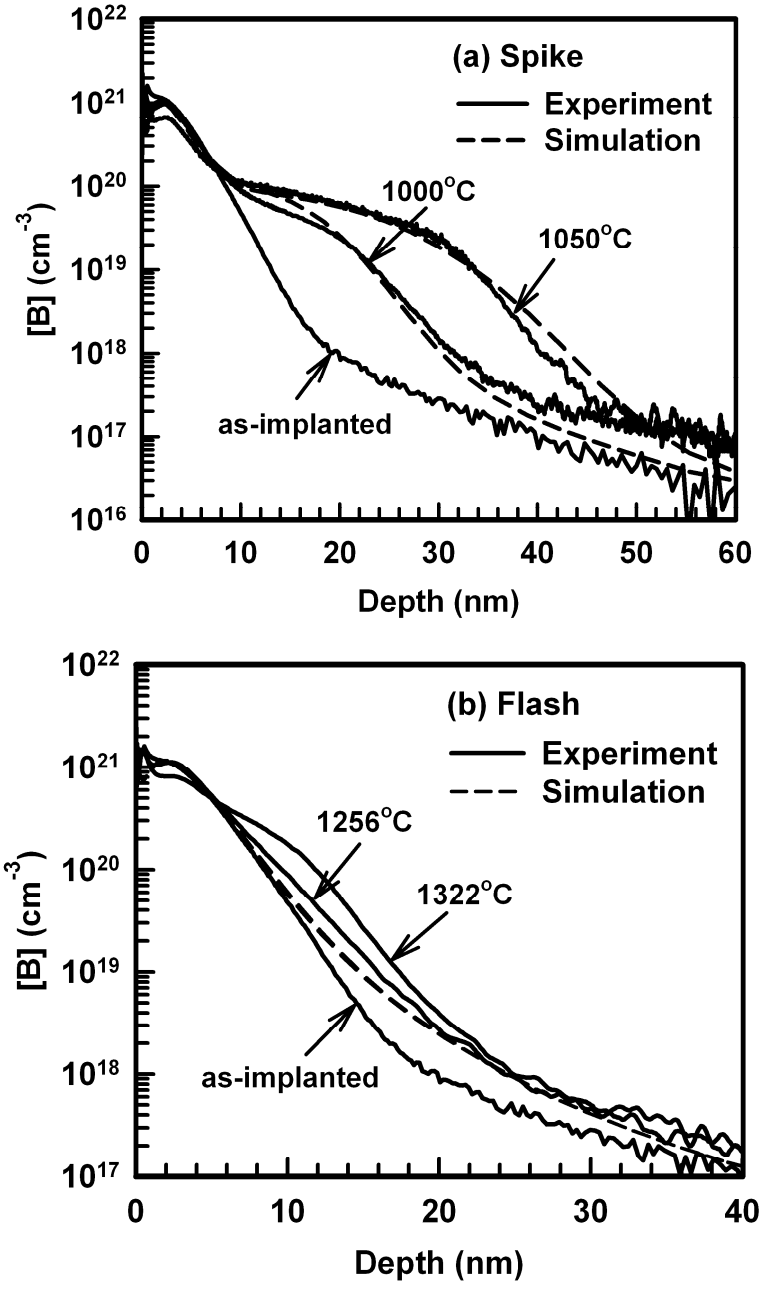

Fig. 2.6. Experimental and simulated boron profiles in silicon using *a priori* parameter estimates for (a) conventional rapid thermal annealing at 1000 °C and 1050 °C and (b) millisecond annealing to 1256 °C and 1322 °C. The millisecond annealing simulations essentially overlay each other and are indistinguishable from each other, in contrast to the experimental profiles. Reprinted with permission from [129], Copyright 2009 American Institute of Physics.

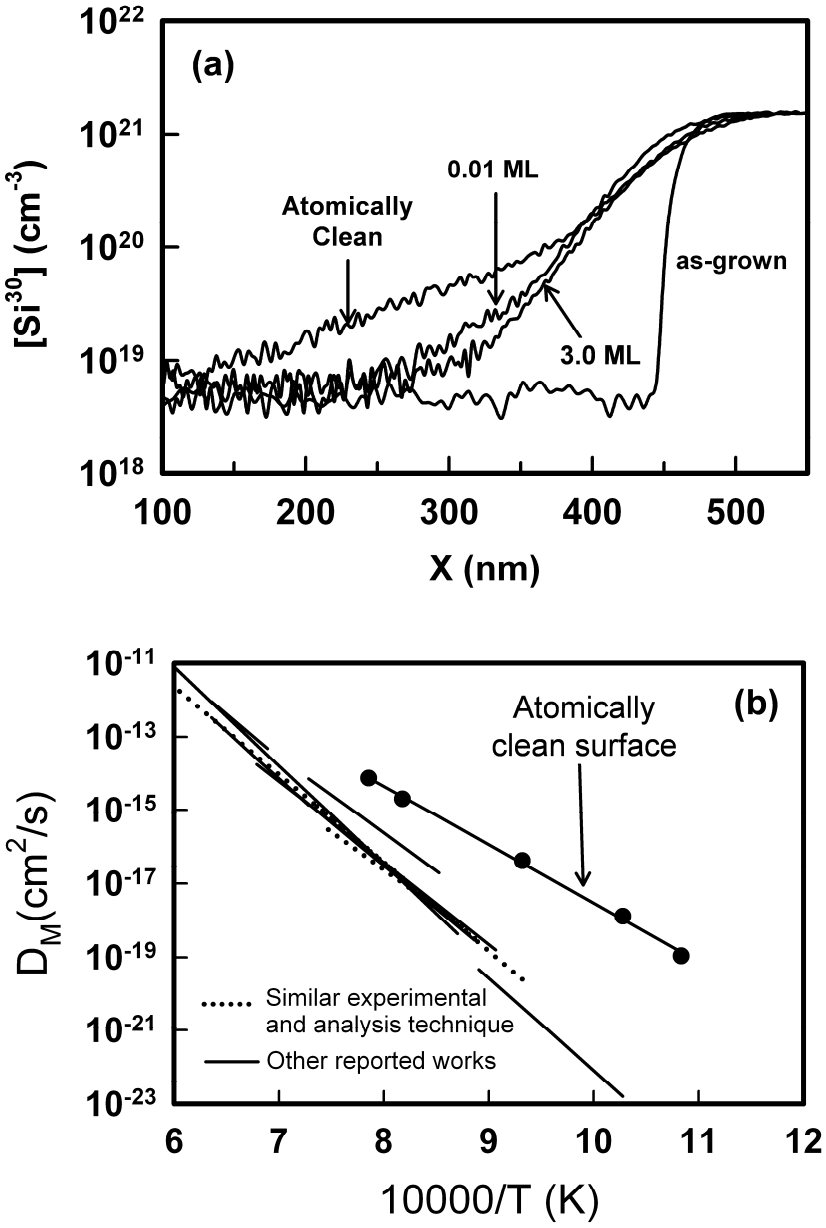

Fig. 2.7. (a) Profiles of ^{30}Si in isotopic heterostructures. Depth is measured with respect to the surface. Specimens (other than as-grown) supported various coverages of N, and were heated at 1100 °C for 60 min. (b) Self-diffusion coefficients in *n*-doped Si for the atomically clean (100) surface compared with literature reports with various methods and doping levels.

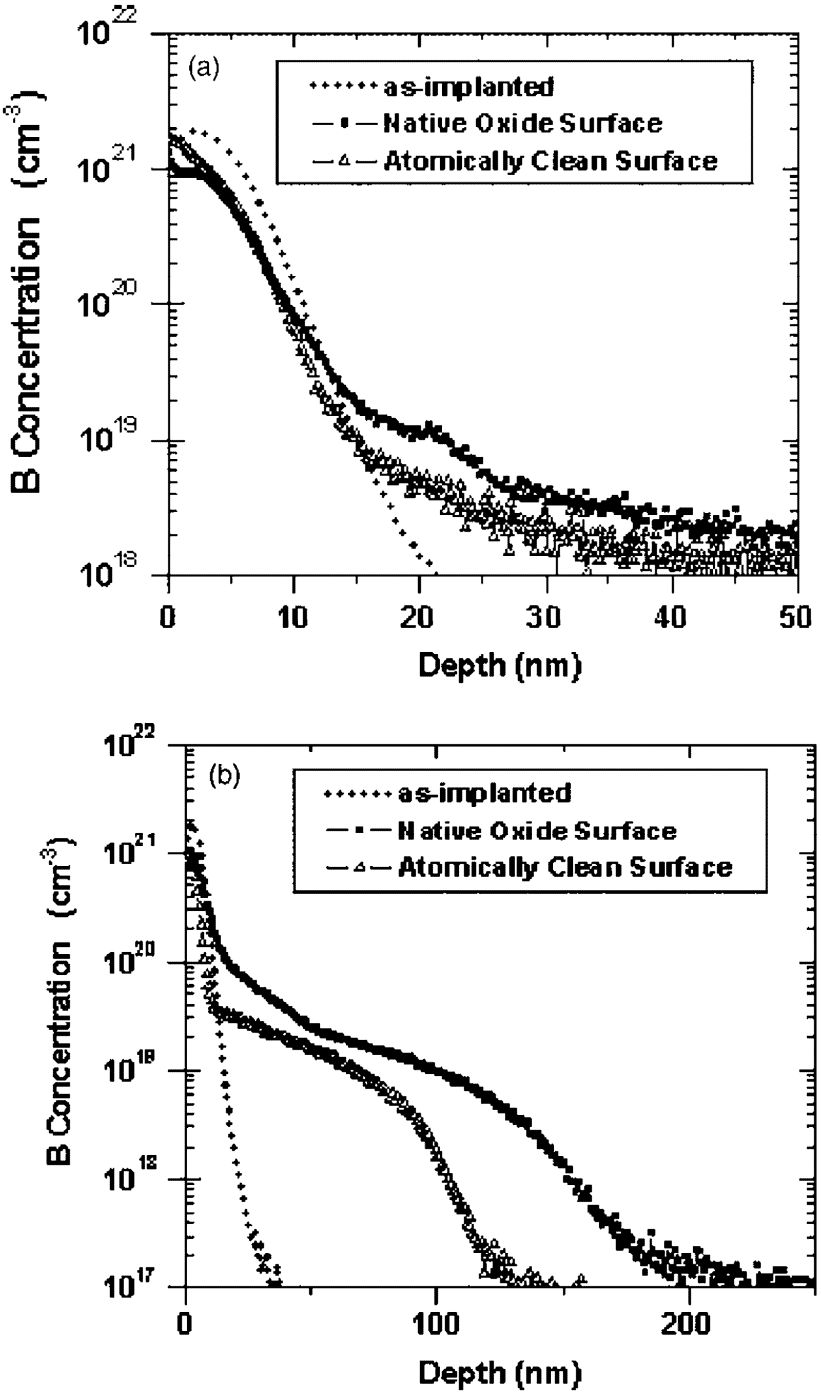

Fig. 2.8. Secondary ion mass spectroscopy (SIMS) profiles of 500 eV B implant in Si with prior 15 keV Ge preamorphizing implant. Annealing was performed at (a) 700 °C and (b) 800 °C for 60 min. The atomically clean surface leads to reduced diffusion in both cases. Reprinted with permission from [143], Copyright 2007 American Institute of Physics.

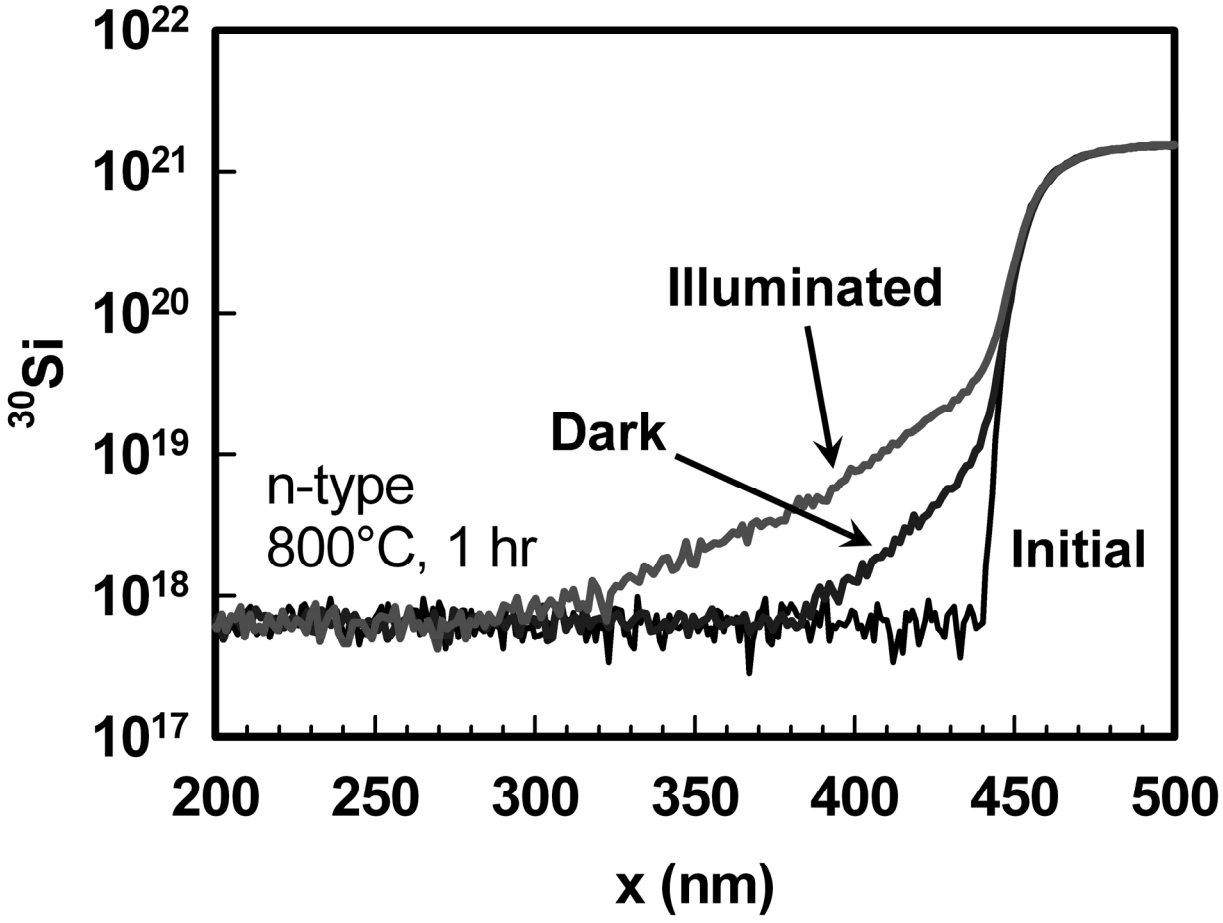

Fig. 2.9. Secondary ion mass spectroscopy (SIMS) profile of ^{30}Si in isotopic heterostructures showing illumination enhancement at 800 °C for 1 hr (*n*-type).

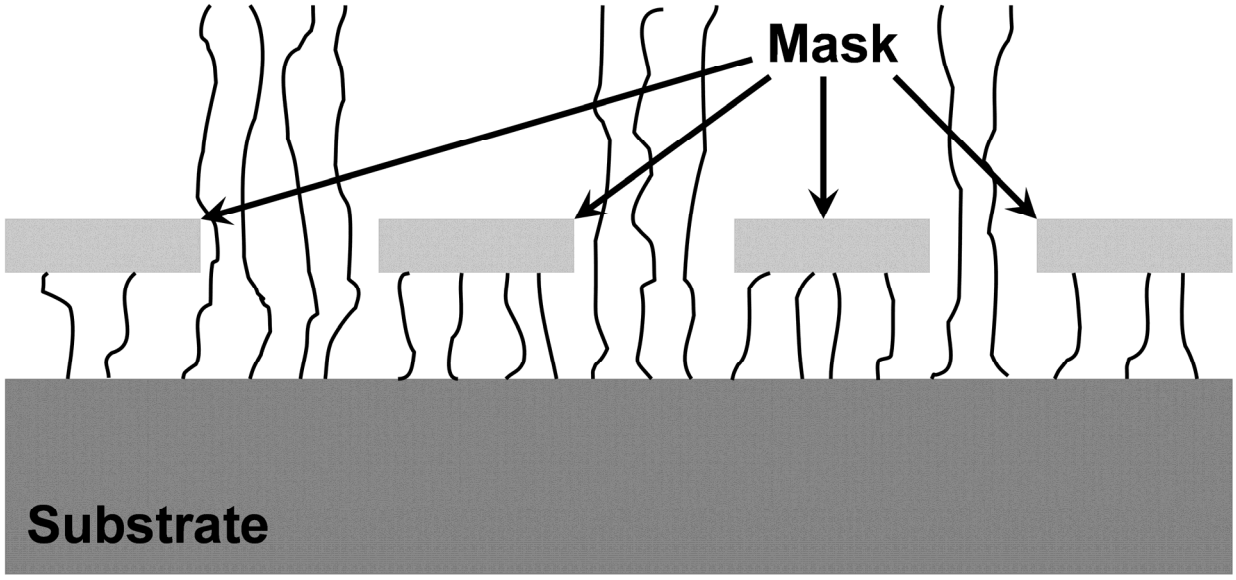

Fig. 2.10. Schematic of epitaxial lateral overgrowth. Black lines depict dislocations.

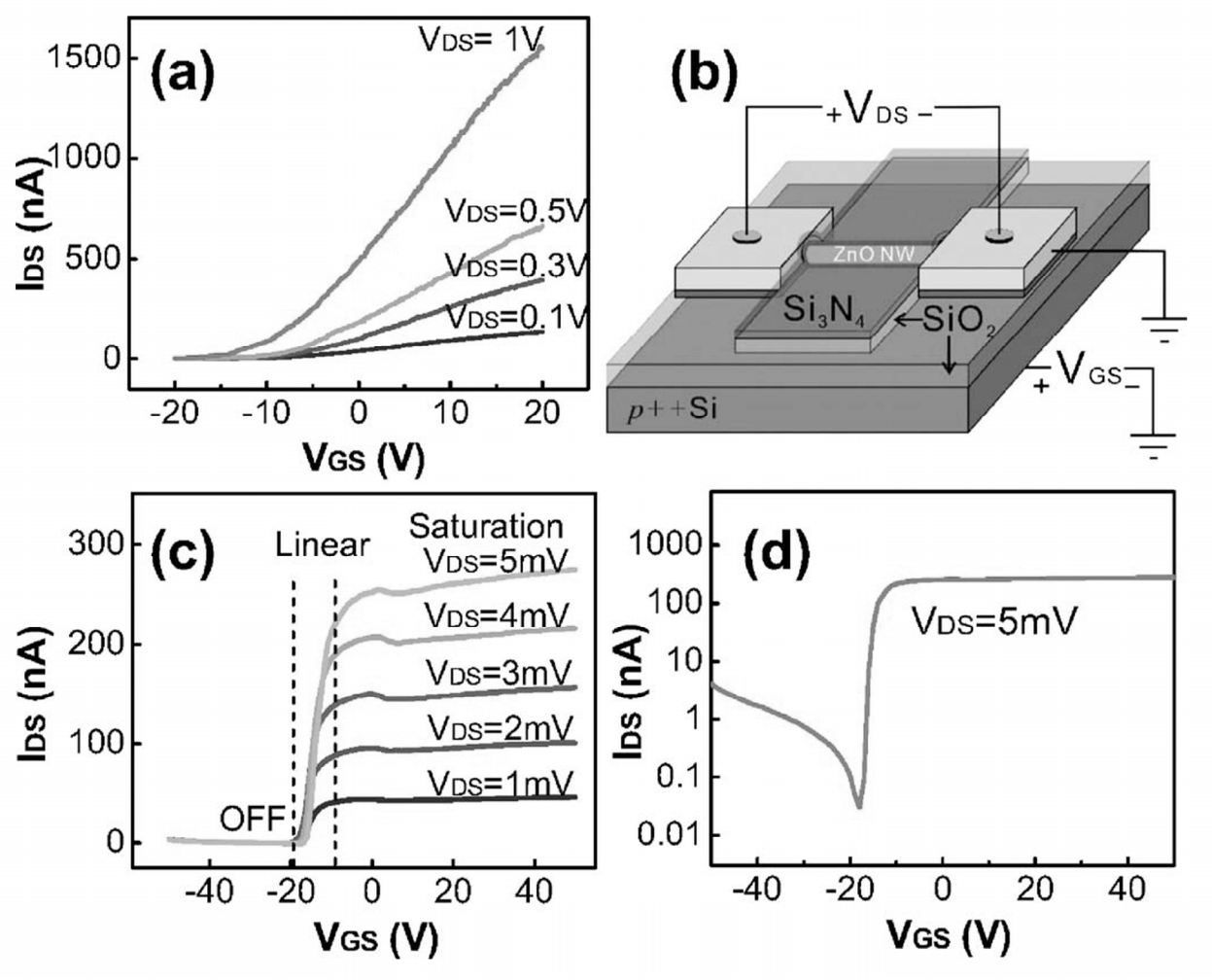

Fig. 2.11. Transport measurements present (a) I_{DS}-V_{GS} curves of a ZnO nanowire FET without surface treatments showing typical *n*-type semiconducting behavior. (b) Schematic of surface passivated ZnO nanowire FET with SiO_2/Si_3N_4 bilayer covering the nanowire channel. (c) I_{DS}-V_{GS} of a surface treated nanowire FET exhibits significantly enhanced on/off ratio and transconductance. (d) Semilog plot demonstrates a tenfold reduction in the subthreshold swing. At large negative gate voltages, band bending gives rise to hole conduction. Reprinted with permission from [173], Copyright 2006 American Institute of Physics.

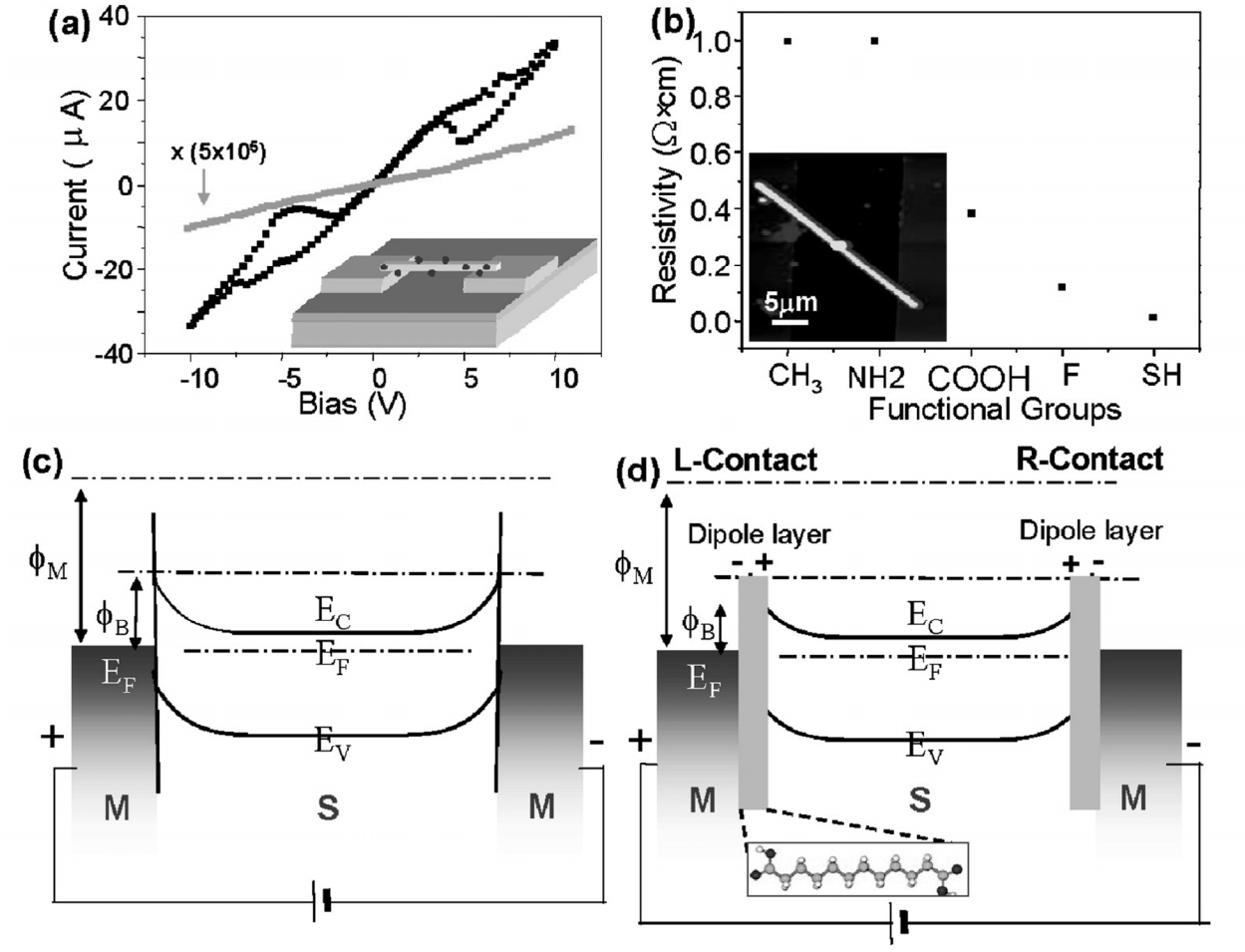

Fig. 2.12. (a) *I-V* characteristics of a ZnO nanobelt (NB) functionalized with the self-assembled thin molecule layer, $HOOC(CH_2)_{10}COOH$ (black line), and an untreated ZnO NB sample. The current of the untreated NB is magnified by 5×10^5 times for comparison purpose. Note: no Pt was deposited at the contacts so that the measured current for the untreated NB is low. Inset is a schematic view of the nanobelt device. (b) Resistivity of the NBs coated with different molecules. The lower inset image is an AFM image of a coated NB lying across two electrodes. (c) Energy-level diagram of metal/semiconductor/ metal interfaces; ϕ_M is the work function of the metal. There is an energy barrier ϕ_B between the metal contact and the untreated NB. (d) Energy-level diagram of the Au electrode and a ZnO NB with a thin molecular layer between. The molecules form an interface dipole layer, which helps to decrease the energy barrier between the NB and Au. Reprinted with permission from [174], Copyright 2007 American Chemical Society.

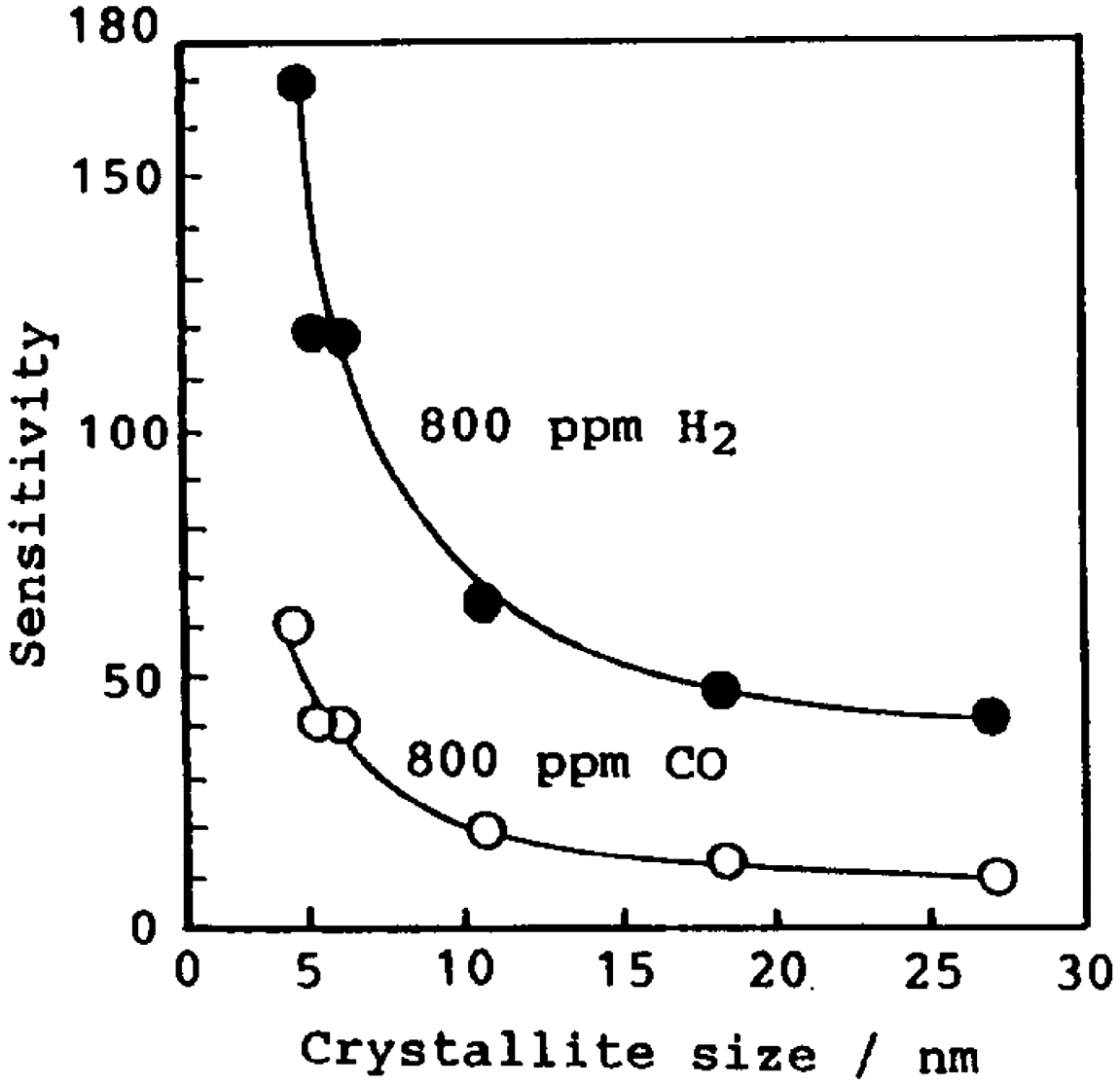

Fig. 2.13. Influence of crystallite size of SnO_2 on gas sensitivity to 800 ppm H_2 and 800 ppm CO in air at 300 °C (elements sintered at 400 °C). Reprinted from [185], Copyright 1991, with permission from Elsevier.

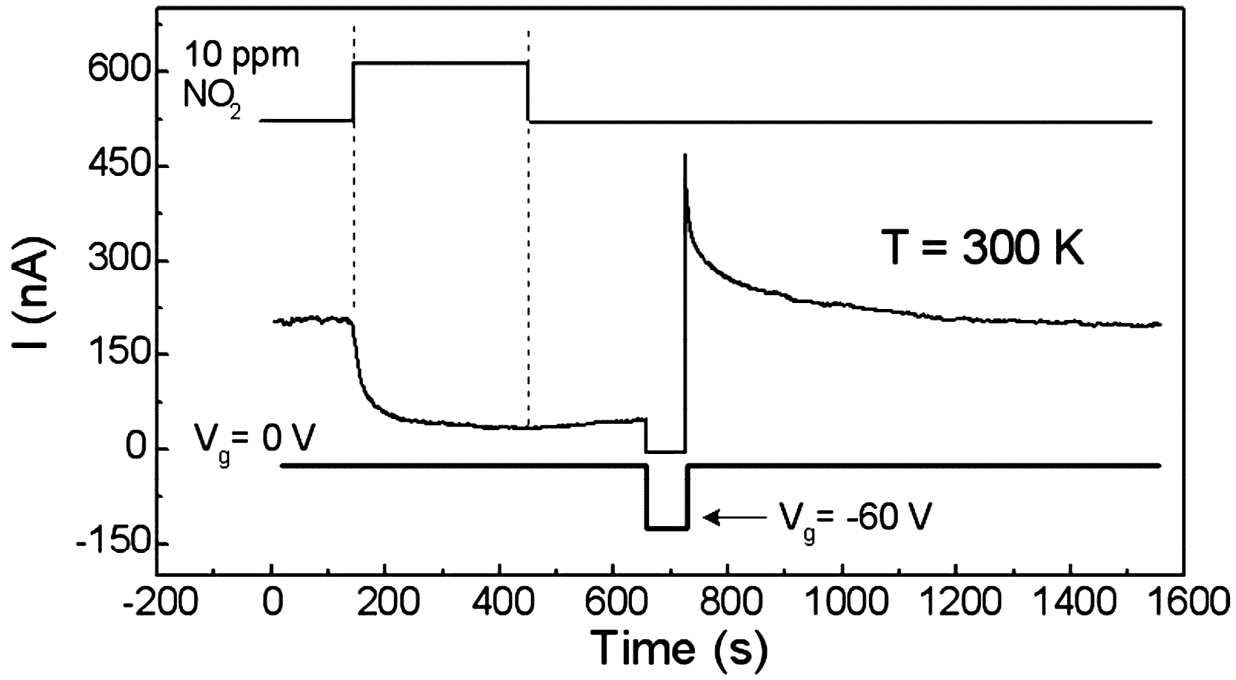

Fig. 2.14. ZnO nanowire FET sensing response to 10 ppm NO_2 and the conductance recovery process caused by a -60 V gate voltage pulse. Reprinted with permission from [186], Copyright 2005 American Institute of Physics.

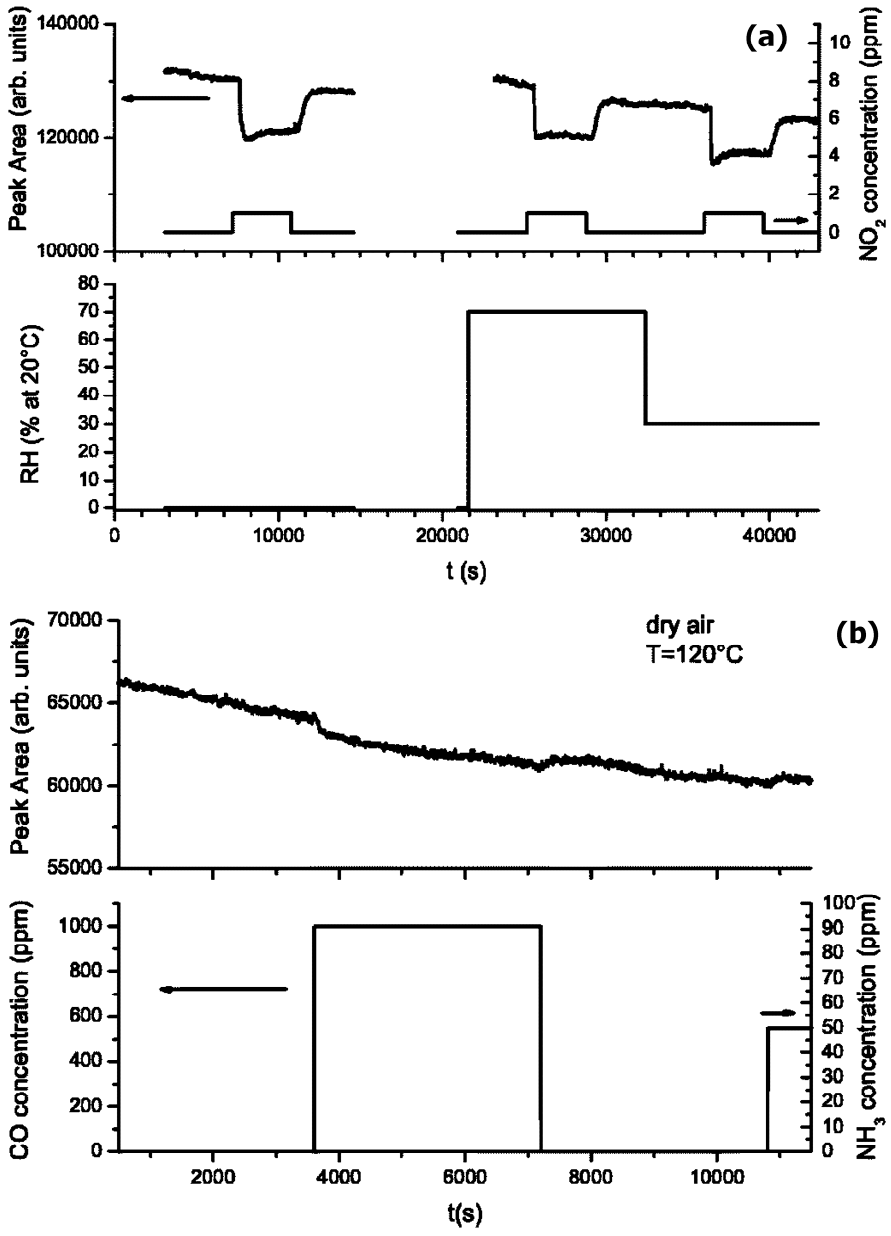

Fig. 2.15. Kinetic response (peak area intensity) of SnO_2 nanobelts toward (a) 1 ppm of NO_2 at 120 °C in dry air, in relative humidity (RH)=70% and at 20 °C in RH=30% and (b) 1000 ppm of CO and 50 ppm of NH_3 at 120 °C in dry air. Dynamic is fast, reversible, and unaffected by humidity changes. Reprinted with permission from [196], Copyright 2005 American Institute of Physics.

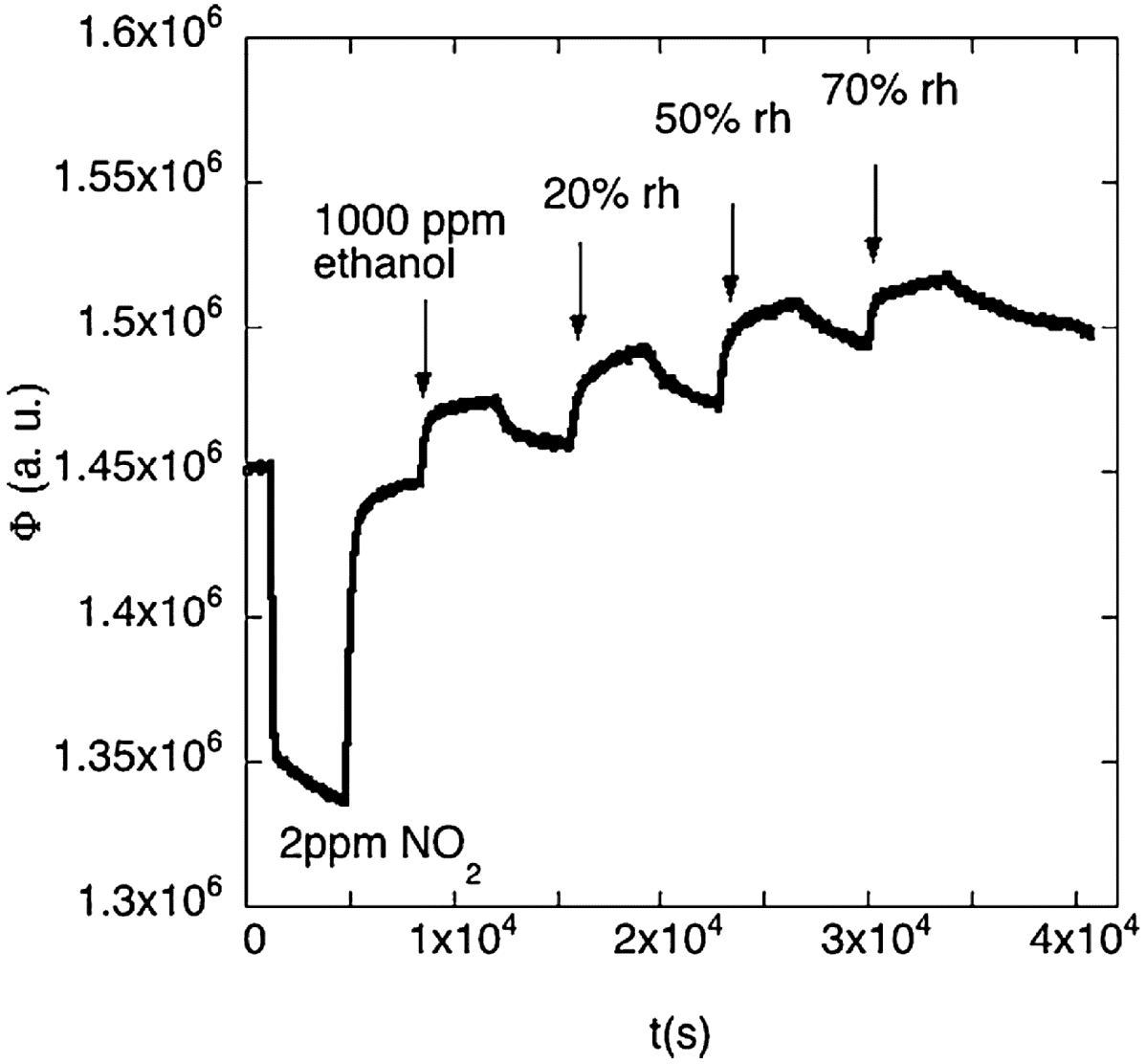

Fig. 2.16. Dynamic photoluminescence (PL) quenching versus time of ZnO nanowires as NO_2, ethanol and relative humidity (RH) are introduced into the test chamber. The nanowires were kept at room temperature. The relative response to ethanol concentration (1000 ppm) is 1.5% while the PL increase with RH gives relative response of 2.8%, 3.9% and 4.6% respectively to 20%, 50% and 70% RH. Reprinted from [195], Copyright 2009, with permission from Elsevier.

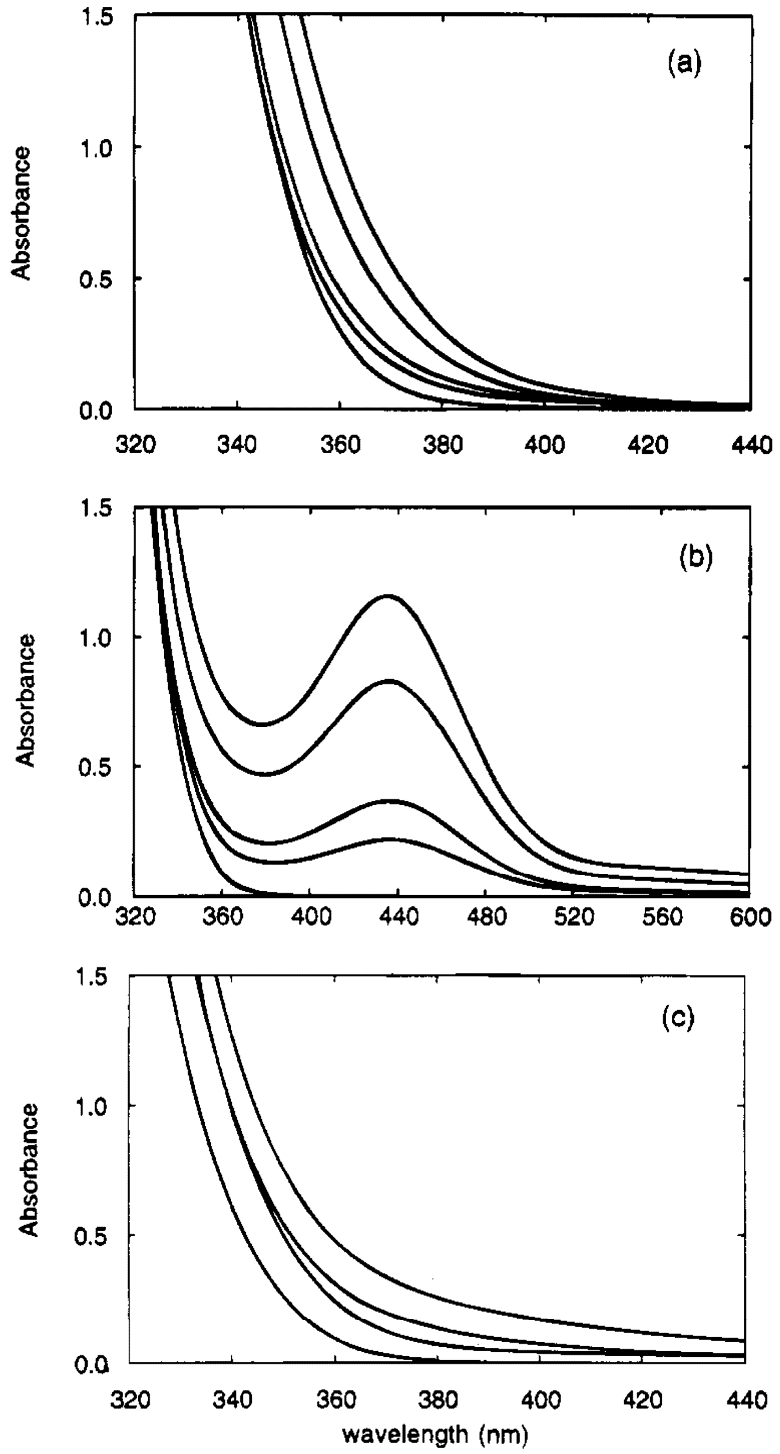

Fig. 2.17. Absorption spectra of (a) Fe^{3+} doped quantum (Q)-sized TiO_2 (1.34 g/L) at 0.0, 1.0, 2.0, 5.0, and 10.0% Fe^{3+} concentrations (from left to right), (b) Ru^{3+}-doped Q-sized TiO_2 (0.5 g/L) at 0.0, 0.5, 1.0, 2.0 and 3.0% Ru^{3+} concentrations (from bottom to up), and (c) undoped, Rh^{3+} (3.0%), V^{4+} (3.0%), and Mn^{3+} (3.0%) Q-sized TiO_2 at 0.5 g/L (from left to right). Reprinted with permission from [208], Copyright 1994 American Chemical Society.

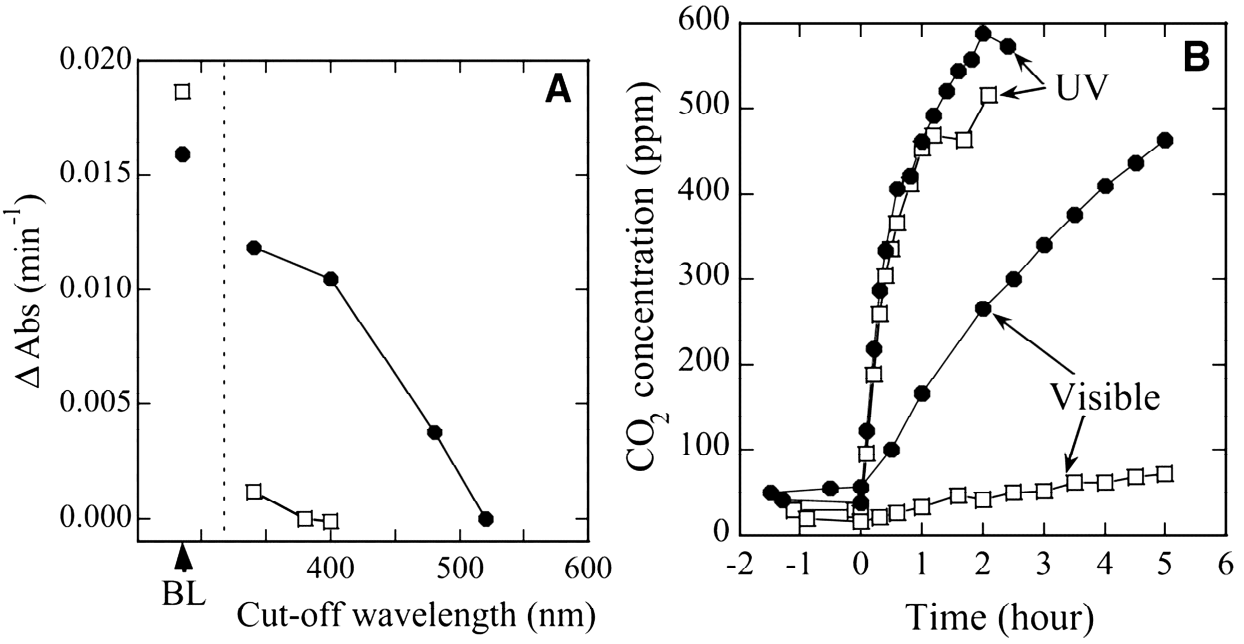

Fig. 2.18. Photocatalytic properties of $TiO_{2-x}N_x$ samples (solid circles) compared with TiO_2 samples (open squares). (A) Decomposition rates [measuring the change in absorption of the reference light (Δ_{abs})] of methylene blue as a function of the cutoff wavelength of the optical high-path filters under fluorescent light with the integrated photon flux of 2.45×10^{-9} einstein (E) s^{-1} cm^{-2} between 350 and 520 nm, compared with the results under black light (BL) illumination with the integrated photon flux of 3.51×10^{-9} E s^{-1} cm^{-2} in the UV range. (B) CO_2 evolution as a function of irradiation time (light on at zero) during the photodegradation of acetaldehyde gas [with an initial concentration of 485 parts per million (ppm)] under UV irradiation (BL with a peak at 351 nm and the light power of 5.4 mW cm^{-2}) and visible irradiation [fluorescent light cut by the optical high-path filter (SC42, Fuji Photo Film), with a peak intensity at 436 nm and a light power of 0.9 mW cm^{-2}]. From [211]. Reprinted with permission from AAAS.

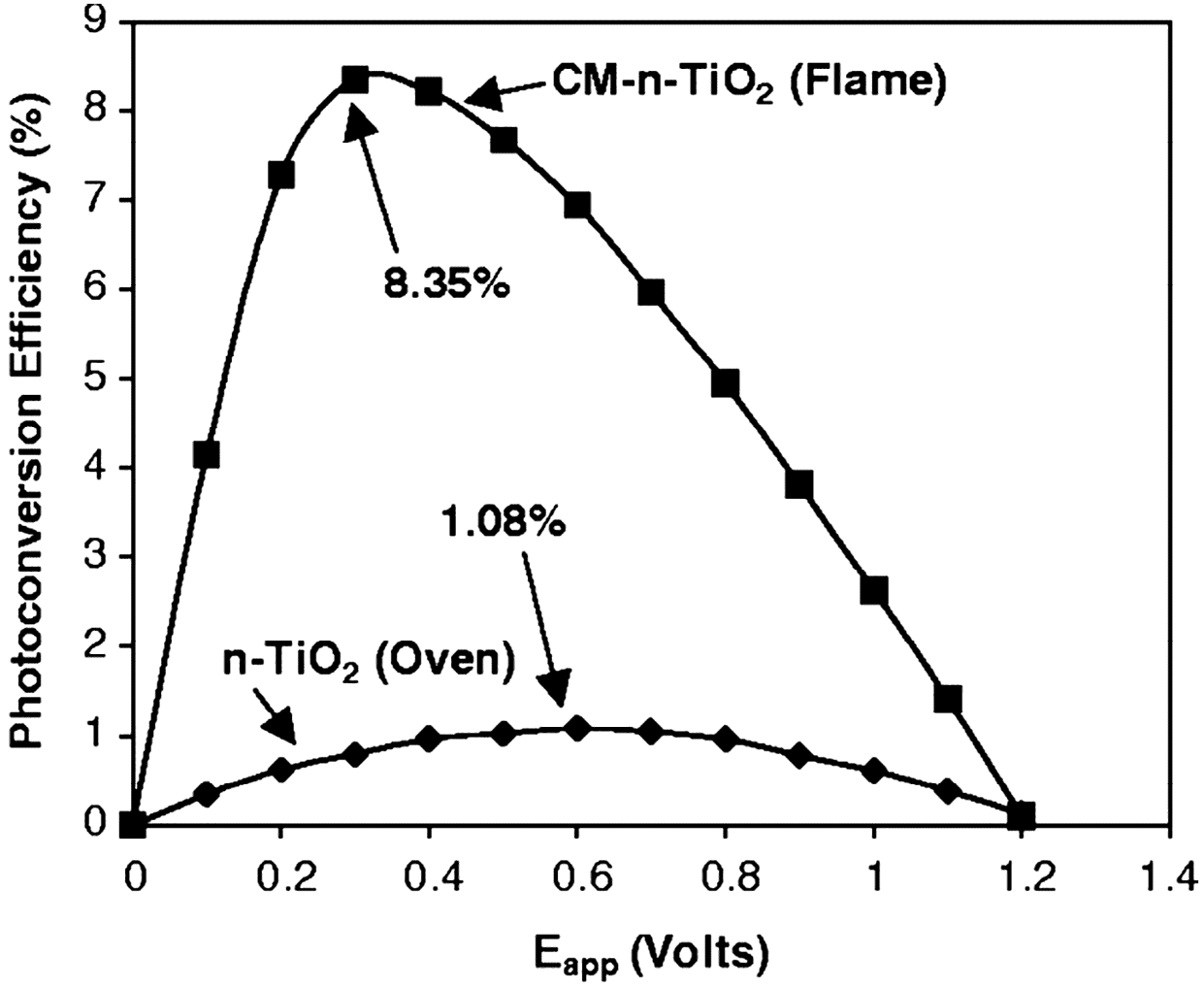

Fig. 2.19. Photoconversion efficiency as a function of applied potential E_{app} at chemically modified n-TiO_2 (flame-made) and the reference n-TiO_2 (electric tube furnace or oven-made) photoelectrodes under xenon lamp illumination at an intensity of 40 mW cm^{-2}. From [216]. Reprinted with permission from AAAS.

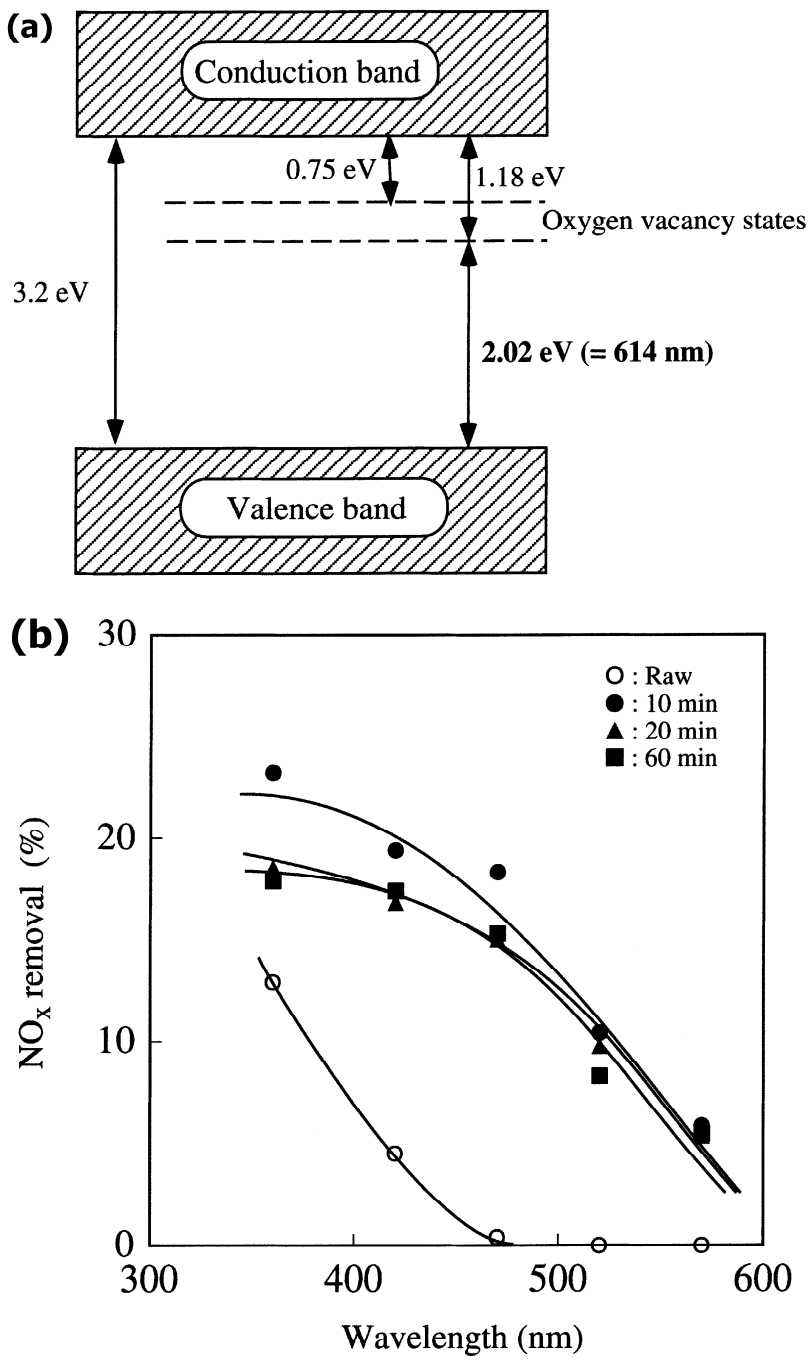

Fig. 2.20. (a) A proposed band structure model for anatase TiO_2 with oxygen vacancies. (b) NO_x removal percentage as a function of irradiation wavelength over the raw TiO_2 and the plasma-treated TiO_2 photocatalysts. Reprinted from [227], Copyright 2000, with permission from Elsevier.

2.8. References

1 H. Bracht, *MRS Bull.* **25** (2000) 22-27.

2 N. Dasgupta, A. Dasgupta, *Semiconductor Devices: Modeling and Technology*, Prentice-Hall, New Delhi, 2004.

3 P. M. Fahey, P. B. Griffin, J. D. Plummer, *Rev. Mod. Phys.* **61** (1989) 289-384.

4 S. M. Hu, *Mater. Sci. Eng. R* **13** (1994) 105-192.

5 M. Y. L. Jung, C. T. M. Kwok, R. D. Braatz, E. G. Seebauer, *J. Appl. Phys.* **97** (2005) 063520.

6 J. W. Fergus, *J. Mater. Sci.* **38** (2003) 4259-4270.

7 W. Baiqi, J. Liqiang, Q. Yichun, L. Shudan, J. Baojiang, Y. Libin, X. Baifu, F. Honggang, *Appl. Surf. Sci.* **252** (2006) 2817-2825.

8 Y. Zhang, A. Kolmakov, S. Chretien, H. Metiu, M. Moskovits, *Nano Lett.* **4** (2004) 403-407.

9 W. W. Chow, S. W. Koch, *Semiconductor-Laser Fundamentals: Physics of the Gain Materials*, Springer, Berlin, 1999.

10 S. Guha, J. M. Depuydt, M. A. Haase, J. Qiu, H. Cheng, *Appl. Phys. Lett.* **63** (1993) 3107-3109.

11 G. Lutz, *Semiconductor Radiation Detectors: Device Physics*, Springer, Berlin, 1999.

12 S. R. Kurtz, A. A. Allerman, E. D. Jones, J. M. Gee, J. J. Banas, B. E. Hammons, *Appl. Phys. Lett.* **74** (1999) 729-731.

13 B. Colombeau, S. H. Yeong, D. X. M. Tan, A. J. Smith, R. M. Gwilliam, C. M. Ng, K. R. C. Mok, F. Benistant, L. Chan, in: *Proceedings of the 17th International Conference on Ion Implantation Technology, AIP*, Monterey, CA, (2008) pp. 11-18.

14 S. Paul, W. Lerch, *Mater. Sci. Forum* **573-574** (2008) 207-228.

15 R. Lindsay, B. J. Pawlak, P. Stolk, K. Maex, *Mater. Res. Soc. Symp. Proc.* **717** (2002) 65-76.

16 J. Gelpey, S. McCoy, A. Kontos, L. Godet, C. Hatem, D. Camm, J. Chan, G. Papasouliotis, J. Scheuer, in: *Extended Abstracts of the 8th International Workshop on Junction Technology, IEEE*, Shanghai, (2008) pp. 82-86.

17 N. E. B. Cowern, B. Colombeau, J. Benson, A. J. Smith, W. Lerch, S. Paul, T. Graf, F. Cristiano, X. Hebras, D. Bolze, *Appl. Phys. Lett.* **86** (2005) 101905.

18 T. Murakami, T. Kuroi, Y. Kawasaki, M. Inuishi, Y. Matsui, A. Yasuoka, *Nucl. Instrum. Methods Phys. Res. B* **121** (1997) 257-261.

19 N. E. B. Cowern, A. J. Smith, B. Colombeau, R. Gwilliam, B. J. Sealy, E. J. H. Collart, in: *Technical Digest - International Electron Devices Meeting, IEEE*, Washington, DC, (2005) pp. 968-971.

20 D. Kabiraj, S. Ghosh, in: *Proceedings of the 14th International Workshop on the Physics of Semiconductor Devices, IEEE*, Bombay, (2007) pp. 926-929.

21 E. G. Seebauer, K. Dev, M. Y. L. Jung, R. Vaidyanathan, C. T. M. Kwok, J. W. Ager, E. E. Haller, R. D. Braatz, *Phys. Rev. Lett.* **97** (2006) 055503

22 R. Vaidyanathan, E. G. Seebauer, H. Graoui, M. A. Foad, *Appl. Phys. Lett.* **89** (2006) 152114.

23 H. J. L. Gossmann, *J. Vac. Sci. Technol. B* **26** (2008) 267-272.

24 S. A. Campbell, *The science and engineering of microelectronic fabrication*, Oxford University Press, New York, 2001.

25 R. Doering, Y. Nishi, *Handbook of semiconductor manufacturing technology*, CRC Press, Boca Raton, 2008.

26 P. Siffert, E. F. Krimmel, *Silicon: evolution and future of a technology*, Springer, Berlin, 2004.

27 E. C. Jones, E. Ishida, *Mater. Sci. Eng. R* **24** (1998) 1-80.

28 M. Orlowski, in: *RTP 2005 - 13th IEEE International Conference on Advanced Thermal Processing of Semiconductors, IEEE*, Santa Barbara, CA, (2005) pp. 3-21.

29 W. Vandervorst, *AIP Conference Proceedings* **931** (2007) 233-245.

30 G. Wang, H. Wu, in: *Proceedings of the 9th International Conference on Solid-State and Integrated Circuits Technology, IEEE*, Beijing, (2008) pp. 1134-1137.

31 E. Chason, S. T. Picraux, J. M. Poate, J. O. Borland, M. I. Current, T. D. delaRubia, D. J. Eaglesham, O. W. Holland, M. E. Law, C. W. Magee, J. W. Mayer, J. Melngailis, A. F. Tasch, *J. Appl. Phys.* **81** (1997) 6513-6561.

32 A. Claverie, B. Colombeau, B. De Mauduit, C. Bonafos, X. Hebras, G. Ben Assayag, F. Cristiano, *Appl. Phys. A* **76** (2003) 1025-1033.

33 L. Pelaz, L. A. Marques, M. Aboy, P. Lopez, J. Barbolla, *Comput. Mater. Sci.* **33** (2005) 92-105.

34 A. Bratschun, *J. Electron. Mater.* **28** (1999) 1328-1332.

35 J. Nakos, J. Shepard, *Mater. Sci. Forum* **573-574** (2008) 3-19.

36 J. Foggiato, W. S. Yoo, *Mater. Sci. Eng. B* **124** (2005) 219-222.

37 W. Skorupa, R. A. Yankov, M. Voelskow, W. Anwand, D. Panknin, R. A. McMahon, M. Smith, T. Gebel, L. Rebohle, R. Fendler, W. Hentsch, in: *RTP 2005 - 13th IEEE*

International Conference on Advanced Thermal Processing of Semiconductors, IEEE, Santa Barbara, CA, (2005) pp. 53-71.

38 L. Shao, J. R. Liu, Q. Y. Chen, W. K. Chu, *Mater. Sci. Eng. R* **42** (2003) 65-114.

39 P. K. Chu, *Plasma Phys. Control. Fusion* **45** (2003) 555-570.

40 J. Pelletier, A. Anders, *IEEE Trans. Plasma Sci.* **33** (2005) 1944-1959.

41 S. Walther, R. Liebert, *J. Vac. Sci. Technol. B* **24** (2006) 482-488.

42 N. E. B. Cowern, A. J. Smith, N. Bennett, B. J. Sealy, R. Gwilliam, R. P. Webb, B. Colombeau, S. Paul, W. Lerch, A. Pakfar, *Mater. Sci. Forum* **573-574** (2008) 295-304.

43 R. M. Gwilliam, N. E. B. Cowern, B. Colombeau, B. Sealy, A. J. Smith, *AIP Conference Proceedings* **876** (2006) 181-190.

44 S. O. Kucheyev, J. S. Williams, C. Jagadish, *Vacuum* **73** (2004) 93-104.

45 C. Ronning, E. P. Carlson, R. F. Davis, *Phys. Rep.* **351** (2001) 349-385.

46 W. Wesch, *Nucl. Instrum. Methods Phys. Res. B* **68** (1992) 342-354.

47 M. K. Nowotny, L. R. Sheppard, T. Bak, J. Nowotny, *J. Phys. Chem. C* **112** (2008) 5275-5300.

48 C. G. Van de Walle, *Physica B* **308** (2001) 899-903.

49 M. Anpo, S. Dohshi, M. Kitano, Y. Hu, M. Takeuchi, M. Matsuoka, *Annu. Rev. Mater. Res.* **35** (2005) 1-27.

50 M. Ni, M. K. H. Leung, D. Y. C. Leung, K. Sumathy, *Renew. Sust. Energ. Rev.* **11** (2007) 401-425.

51 S. Dutta, S. Chattopadhyay, A. Sarkar, M. Chakrabarti, D. Sanyal, D. Jana, *Prog. Mater. Sci.* **54** (2009) 89-136.

52 J. Liqiang, Q. Yichun, W. Baiqi, L. Shudan, J. Baojiang, Y. Libin, F. Wei, F. Honggang, S. Jiazhong, *Sol. Energy Mater. Sol. Cells* **90** (2006) 1773-1787.

53 L. Schmidt-Mende, J. L. MacManus-Driscoll, *Mater. Today* **10** (2007) 40-48.

54 E. G. Seebauer, M. C. Kratzer, *Mater. Sci. Eng. R* **55** (2006) 57-149.

55 D. Hull, D. J. Bacon, *Introduction to dislocations*, Butterworth-Heinemann, Oxford, 2001.

56 W. Shockley, W. T. Read, *Phys. Rev.* **87** (1952) 835.

57 S. M. Sze, *Semiconductor devices, physics and technology*, Wiley, New York, 2002.

58 K. Vanheusden, W. L. Warren, C. H. Seager, D. R. Tallant, J. A. Voigt, B. E. Gnade, *J. Appl. Phys.* **79** (1996) 7983-7990.

59 S. A. Centoni, B. Sadigh, G. H. Gilmer, T. J. Lenosky, T. D. de la Rubia, C. B. Musgrave, *Phys. Rev. B* **72** (2005) 195206.

60 H. Y. H. Chan, K. Dev, E. G. Seebauer, *Phys. Rev. B* **67** (2003) 035311.

61 C. E. Allen, R. Ditchfield, E. G. Seebauer, *J. Vac. Sci. Technol. A* **14** (1996) 22-29.

62 W. C. Lee, S. G. Lee, K. J. Chang, *J. Phys.: Condes. Mat.* **10** (1998) 995-1002.

63 J. Tersoff, *Phys. Rev. Lett.* **65** (1990) 887-890.

64 P. Mascher, S. Dannefaer, D. Kerr, *Phys. Rev. B* **40** (1989) 11764-11771.

65 M. J. Puska, C. Corbel, R. M. Nieminen, *Phys. Rev. B* **41** (1990) 9980-9993.

66 P. W. Tasker, A. M. Stoneham, *J. Phys. C: Solid State Phys.* **10** (1977) 5131-5140.

67 R. Ditchfield, D. Llera-Rodriguez, E. G. Seebauer, *Phys. Rev. Lett.* **81** (1998) 1259-1262.

68 R. Ditchfield, D. Llera-Rodriguez, E. G. Seebauer, *Phys. Rev. B* **61** (2000) 13710-13720.

69 E. G. Seebauer, in: *Proceedings of the 7th International Conference on Solid-State and Integrated Circuits Technology, IEEE*, Beijing, (2004) pp. 1032-1037.

70 S. P. Wilks, *J. Phys. D: Appl. Phys.* **35** (2002) R77-R90.

71 K. Dev, M. Y. L. Jung, R. Gunawan, R. D. Braatz, E. G. Seebauer, *Phys. Rev. B* **68** (2003) 195311.

72 T. Sinno, E. Dornberger, W. von Ammon, R. A. Brown, F. Dupret, *Mater. Sci. Eng. R* **28** (2000) 149-198.

73 J. Vanhellemont, J. Van Steenbergen, F. Holsteyns, P. Roussel, M. Meuris, K. Młynarczyk, P. Śpiewak, W. Geens, I. Romandic, *J. Mater. Sci.: Mater. Electron.* **19** (2008) 24-31.

74 G. Müller, in: *Perspectives on Inorganic, Organic, and Biological Crystal Growth: From Fundamentals to Applications: Based on the lectures presented at the 13th International Summer School on Crystal Growth*, Park City, Utah (USA), (2007) pp. 3-33.

75 E. Dornberger, W. von Ammon, J. Virbulis, B. Hanna, T. Sinno, *J. Cryst. Growth* **230** (2001) 291-299.

76 M. S. Kulkarni, *Ind. Eng. Chem. Res.* **44** (2005) 6246-6263.

77 G. Müller, *Cryst. Res. Technol.* **42** (2007) 1150-1161.

78 M. S. Kulkarni, *J. Cryst. Growth* **303** (2007) 438-448.

79 M. S. Kulkarni, *J. Cryst. Growth* **310** (2008) 324-335.

80 A. Taguchi, H. Kageshima, K. Wada, *J. Appl. Phys.* **97** (2005) 053514.

81 X. Yu, D. Yang, X. Ma, J. Yang, L. Li, D. Que, *J. Appl. Phys.* **92** (2002) 188-194.

82 D. Yang, J. Chen, H. Li, X. Ma, D. Tian, L. Li, D. Que, *J. Cryst. Growth* **292** (2006) 266-271.

83 D. Yang, J. Chen, H. Li, X. Ma, D. Tian, L. Li, D. Que, *Phys. Status Solidi A* **203** (2006) 685-695.

84 J. Vanhellemont, P. Spiewak, K. Sueoka, I. Romandic, *Phys. Status Solidi C* **6** (2009) 1906-1911.

85 A. Agarwal, H. J. Gossmann, D. C. Jacobson, D. J. Eaglesham, M. Sosnowski, J. M. Poate, I. Yamada, J. Matsuo, T. E. Haynes, *Appl. Phys. Lett.* **73** (1998) 2015-2017.

86 K. Goto, J. Matsuo, T. Sugii, H. Minakata, I. Yamada, T. Hisatsugu, in: *Technical Digest - International Electron Devices Meeting, IEEE*, (1996) pp. 435-438.

87 D. Takeuchi, N. Shimada, J. Matsuo, I. Yamada, *Nucl. Instrum. Methods Phys. Res. B* **121** (1997) 345-348.

88 R. Smith, M. Shaw, R. P. Webb, M. A. Foad, *J. Appl. Phys.* **83** (1998) 3148-3152.

89 S. Heo, H. Hwang, H. T. Cho, W. A. Krull, *Appl. Phys. Lett.* **89** (2006) 243516.

90 Y. Kawasaki, T. Kuroi, T. Yamashita, K. Horita, T. Hayashi, M. Ishibashi, M. Togawa, Y. Ohno, M. Yoneda, T. Horsky, D. Jacobson, W. Krull, *Nucl. Instrum. Methods Phys. Res. B* **237** (2005) 25-29.

91 L. A. Marques, L. Pelaz, I. Santos, V. C. Venezia, *Phys. Rev. B* **74** (2006) 201201.

92 A. Renau, in: *Extended Abstracts of the 7th International Workshop on Junction Technology, IEEE*, Kyoto, (2007) pp. 107-112.

93 C. F. Tan, L. W. Teo, C. S. Yin, J. G. Lee, J. Liu, A. See, M. S. Zhou, E. Quek, S. Chu, C. Hatem, N. Variam, E. Arevalo, A. Gupta, S. Mehta, *Mater. Res. Soc. Symp. Proc.* **1070** (2008) 99-104.

94 K. Ohyu, T. Itoga, N. Natsuaki, *Jpn. J. Appl. Phys.* **29** (1990) 457-462.

95 T. H. Huang, H. Kinoshita, D. L. Kwong, *Appl. Phys. Lett.* **65** (1994) 1829-1831.

96 R. Duffy, V. C. Venezia, A. Heringa, B. J. Pawlak, M. J. P. Hopstaken, G. C. J. Maas, Y. Tamminga, T. Dao, F. Roozeboom, L. Pelaz, *Appl. Phys. Lett.* **84** (2004) 4283-4285.

97 D. Girginoudi, C. Tsiarapas, *Nucl. Instrum. Methods Phys. Res. B* **266** (2008) 3565-3576.

98 G. Impellizzeri, J. H. R. Dos Santos, S. Mirabella, F. Priolo, E. Napolitani, A. Camera, *Appl. Phys. Lett.* **84** (2004) 1862-1864.

99 J. M. Jacques, L. S. Robertson, K. S. Jones, M. E. Law, M. Rendon, J. Bennett, *Appl. Phys. Lett.* **82** (2003) 3469-3471.

100 B. J. Pawlak, R. Surdeanu, B. Colombeau, A. J. Smith, N. E. B. Cowern, R. Lindsay, W. Vandervorst, B. Brijs, O. Richard, F. Cristiano, *Appl. Phys. Lett.* **84** (2004) 2055-2057.

101 E. Napolitani, A. Coati, D. De Salvador, A. Carnera, S. Mirabella, S. Scalese, F. Priolo, *Appl. Phys. Lett.* **79** (2001) 4145-4147.

102 V. Moroz, Y. S. Oh, D. Pramanik, H. Graoui, M. A. Foad, *Appl. Phys. Lett.* **87** (2005) 051908.

103 B. J. Pawlak, T. Janssens, B. Brijs, W. Vandervorst, E. J. H. Collart, S. B. Felch, N. E. B. Cowern, *Appl. Phys. Lett.* **89** (2006) 062110.

104 A. Vanderpool, M. Taylor, *Nucl. Instrum. Methods Phys. Res. B* **237** (2005) 142-147.

105 K. C. Ku, C. F. Nieh, J. Gong, L. P. Huang, Y. M. Sheu, C. C. Wang, C. H. Chen, H. Chang, L. T. Wang, T. L. Lee, S. C. Chen, M. S. Liang, *Appl. Phys. Lett.* **89** (2006) 112104.

106 B. J. Pawlak, R. Duffy, T. Janssens, W. Vandervorst, S. B. Felch, E. J. H. Collart, N. E. B. Cowern, *Appl. Phys. Lett.* **89** (2006) 062102.

107 N. Auriac, C. Laviron, N. Cagnat, J. Singer, B. Duriez, R. Gwoziecki, G. Chabanne, C. Rando, in: *Extended Abstracts of the 7th International Workshop on Junction Technology, IEEE*, Kyoto, (2007) pp. 13-16.

108 C. T. Liu, E. J. Lloyd, Y. Ma, M. Du, R. L. Opila, S. J. Hillenius, in: *Technical Digest - International Electron Devices Meeting, IEEE*, (1996) pp. 499-502.

109 S. H. Yeong, B. Colombeau, K. R. C. Mok, F. Benistant, C. J. Liu, A. T. S. Wee, G. Dong, L. Chan, M. P. Srinivasan, *Mater. Sci. Eng. B* **154-155** (2008) 43-48.

110 J. R. Conrad, J. L. Radtke, R. A. Dodd, F. J. Worzala, N. C. Tran, *J. Appl. Phys.* **62** (1987) 4591-4596.

111 B. Mizuno, I. Nakayama, N. Aoi, M. Kubota, T. Komeda, *Appl. Phys. Lett.* **53** (1988) 2059-2061.

112 S. B. Felch, Z. Fang, B. W. Koo, R. B. Liebert, S. R. Walther, D. Hacker, *Surf. Coat. Technol.* **156** (2002) 229-236.

113 D. Lenoble, A. Grouillet, *Surf. Coat. Technol.* **156** (2002) 262-266.

114 B. Mizuno, K. Okashita, K. Nakamoto, C. G. Jin, Y. Sasaki, K. Tsutsui, H. A. Sauddin, H. Iwai, in: *Extended Abstracts of the 8th International Workshop on Junction Technology, IEEE*, Shanghai, (2008) pp. 20-24.

115 B. Mizuno, Y. Sasaki, C. G. Jin, K. Okashita, K. Nakamoto, T. Kitaoka, K. Tsutsui, H. A. Sauddin, H. Iwai, in: *Proceedings of the 9th International Conference on Solid-State and Integrated Circuits Technology, IEEE*, Beijing, (2008) pp. 1288-1291.

116 V. Raineri, R. J. Schreutelkamp, F. W. Saris, K. T. F. Janssen, R. E. Kaim, *Appl. Phys. Lett.* **58** (1991) 922-924.

117 E. G. Roth, O. W. Holland, V. C. Venezia, B. Nielsen, *J. Electron. Mater.* **26** (1997) 1349-1354.

118 V. C. Venezia, T. E. Haynes, A. Agarwal, L. Pelaz, H. J. Gossmann, D. C. Jacobson, D. J. Eaglesham, *Appl. Phys. Lett.* **74** (1999) 1299-1301.

119 S. Saito, M. Kumagai, T. Kondo, *Appl. Phys. Lett.* **63** (1993) 197-199.

120 L. Shao, J. M. Zhang, J. Chen, D. Tang, P. E. Thompson, S. Patel, X. M. Wang, H. Chen, J. K. Liu, W. K. Chu, *Appl. Phys. Lett.* **84** (2004) 3325-3327.

121 A. J. Smith, N. E. B. Cowern, R. Gwilliam, B. J. Sealy, B. Colombeau, E. J. H. Collart, S. Gennaro, D. Giubertoni, M. Bersani, M. Barozzi, *Appl. Phys. Lett.* **88** (2006) 082112.

122 N. S. Bennett, N. E. B. Cowern, H. Kheyrandish, S. Paul, W. Lerch, A. J. Smith, R. Gwilliam, B. J. Sealy, in: *Proceedings of the 38th European Solid-State Device Research Conference, IEEE*, Edinburgh, (2008) pp. 290-293.

123 P. Timans, J. Gelpey, S. McCoy, W. Lerch, S. Paul, in: *Materials Research Society Symposium Proceedings*, (2006) pp. 3-14.

124 K. Adachi, K. Ohuchi, N. Aoki, H. Tsujii, T. Ito, H. Itokawa, K. Matsuo, K. Suguro, Y. Honguh, N. Tamaoki, K. Ishimaru, H. Ishiuchi, in: *Digest of Technical Papers - Symposium on VLSI Technology, IEEE*, Kyoto, (2005) pp. 142-143.

125 Y. F. Chong, K. L. Pey, A. T. S. Wee, A. See, L. Chan, Y. F. Lu, W. D. Song, L. H. Chua, *Appl. Phys. Lett.* **76** (2000) 3197-3199.

126 Y. Takamura, S. H. Jain, P. B. Griffin, J. D. Plummer, *J. Appl. Phys.* **92** (2002) 230.

127 T. Ito, T. Iinuma, A. Murakoshi, H. Akutsu, K. Suguro, T. Arikado, K. Okumura, M. Yoshioka, T. Owada, Y. Imaoka, H. Murayama, T. Kusuda, *Jpn. J. Appl. Phys.* **41** (2002) 2394-2398.

128 W. Skorupa, T. Gebel, R. A. Yankov, S. Paul, W. Lerch, D. F. Downey, E. A. Arevalo, *J. Electrochem. Soc.* **152** (2005) G436-G440

129 C. T. M. Kwok, R. D. Braatz, S. Paul, W. Lerch, E. G. Seebauer, *J. Appl. Phys.* **105** (2009) 063514.

130 L. Wang, P. Clancy, M. O. Thompson, C. S. Murthy, *J. Appl. Phys.* **92** (2002) 2412.

131 T. M. Kwok, Ph.D. thesis, University of Illinois at Urbana-Champaign, 2007.

132 S. Baek, S. Heo, H. Choi, H. Hwang, *J. Vac. Sci. Technol. B* **23** (2005) 257-261.

133 W. Lerch, S. Paul, J. Niess, S. McCoy, T. Selinger, J. Gelpey, F. Cristiano, F. Severac, M. Gavelle, S. Boninelli, P. Pichler, D. Bolze, *Mater. Sci. Eng. B* **124-125** (2005) 24-31.

134 J. Borland, A. Mineji, W. Krull, M. Tanjyo, R. Hillard, T. Walker, *Solid State Technol.* **49-5** (2006) 47-54.

135 W. S. Yoo, K. Kang, *Nucl. Instrum. Methods Phys. Res. B* **237** (2005) 12-17.

136 C. H. Poon, L. S. Tan, B. J. Cho, A. See, M. Bhat, *J. Electrochem. Soc.* **151** (2004) G80-G83.

137 J. A. Sharp, N. E. B. Cowern, R. P. Webb, K. J. Kirkby, D. Giubertoni, S. Gennaro, M. Bersani, M. A. Foad, F. Cristiano, P. F. Fazzini, *Appl. Phys. Lett.* **89** (2006) 192105.

138 A. Florakis, D. Tsoukalas, I. Zergioti, K. Giannakopoulos, P. Dimitrakis, D. G. Papazoglou, G. Bennassayag, H. Bourdon, A. Halimaoui, *Nucl. Instrum. Methods Phys. Res. B* **253** (2006) 13-17.

139 F. Torregrosa, C. Laviron, F. Milesi, M. Hernandez, H. Faïk, J. Venturini, *Nucl. Instrum. Methods Phys. Res. B* **237** (2005) 18-24.

140 S. Earles, M. Law, R. Brindos, K. Jones, S. Talwar, S. Corcoran, *IEEE Trans. Electron Devices* **49** (2002) 1118-1123.

141 E. V. Monakhov, B. G. Svensson, M. K. Linnarsson, A. La Magna, M. Italia, V. Privitera, G. Fortunato, M. Cuscuna, L. Mariucci, *Appl. Phys. Lett.* **87** (2005) 192109.

142 J. Venturini, M. Hernandez, G. Kerrien, C. Laviron, D. Camel, J. L. Santailler, T. Sarnet, J. Boulmer, *Thin Solid Films* **453-454** (2004) 145-149.

143 S. H. Yeong, M. P. Srinivasan, B. Colombeau, L. Chan, R. Akkipeddi, C. T. M. Kwok, R. Vaidyanathan, E. G. Seebauer, *Appl. Phys. Lett.* **91** (2007) 102112.

144 X. Zhang, M. Yu, C. T. M. Kwok, R. Vaidyanathan, R. D. Braatz, E. G. Seebauer, *Phys. Rev. B* **74** (2006) 235301.

145 J. Jie, W. Zhang, K. Peng, G. Yuan, C. S. Lee, S. T. Lee, *Adv. Funct. Mater.* **18** (2008) 3251-3257.

146 Y. Cui, Z. Zhong, D. Wang, W. U. Wang, C. M. Lieber, *Nano Lett.* **3** (2003) 149-152.

147 E. G. Seebauer, in: *Proceedings of the 8th International Conference on Solid-State and Integrated Circuits Technology, IEEE*, Shanghai, (2007) pp. 450-453.

148 M. Y. L. Jung, E. G. Seebauer, in: *Extended Abstracts of the 4th International Workshop on Junction Technology, IEEE*, Shanghai, (2004) pp. 87-89.

149 C. Claeys, E. Simoen, K. Opsomer, D. P. Brunco, M. Meuris, *Mater. Sci. Eng. B* **154-155** (2008) 49-55.

150 G. Impellizzeri, S. Mirabella, E. Bruno, A. M. Piro, M. G. Grimaldi, *J. Appl. Phys.* **105** (2009) 063533.

151 A. Satta, A. D'Amore, E. Simoen, W. Anwand, W. Skorupa, T. Clarysse, B. Van Daele, T. Janssens, *Nucl. Instrum. Methods Phys. Res. B* **257** (2007) 157-160.

152 S. Heo, S. Baek, D. Lee, M. Hasan, H. Jung, J. Lee, H. Hwang, *Electrochem. Solid-State Lett.* **9** (2006) 136-137.

153 J. Huang, N. Wu, Q. Zhang, C. Zhu, A. A. O. Tay, G. Chen, M. Hong, *Appl. Phys. Lett.* **87** (2005) 173507.

154 E. Simoen, A. Satta, A. D'Amore, T. Janssens, T. Clarysse, K. Martens, B. De Jaeger, A. Benedetti, I. Hoflijk, B. Brijs, M. Meuris, W. Vandervorst, *Mater. Sci. Semicond. Process.* **9** (2006) 634-639.

155 W. C. Dunlap Jr, *Phys. Rev.* **94** (1954) 1531-1540.

156 S. Uppal, A. F. W. Willoughby, J. M. Bonar, A. G. R. Evans, N. E. B. Cowern, R. Morris, M. G. Dowsett, *J. Appl. Phys.* **90** (2001) 4293-4295.

157 A. Satta, E. Simoen, T. Clarysse, T. Janssens, A. Benedetti, B. De Jaeger, M. Meuris, W. Vandervorst, *Appl. Phys. Lett.* **87** (2005) 172109.

158 A. Axmann, M. Schulz, C. R. Fritzsche, *Appl. Phys.* **12** (1977) 173-178.

159 A. Satta, T. Janssens, T. Clarysse, E. Simoen, M. Meuris, A. Benedetti, I. Hoflijk, B. De Jaeger, C. Demeurisse, W. Vandervorst, *J. Vac. Sci. Technol. B* **24** (2006) 494-498.

160 J. F. Geisz, S. Kurtz, M. W. Wanlass, J. S. Ward, A. Duda, D. J. Friedman, J. M. Olson, W. E. McMahon, T. E. Moriarty, J. T. Kiehl, *Appl. Phys. Lett.* **91** (2007) 023502.

161 R. R. King, D. C. Law, K. M. Edmondson, C. M. Fetzer, G. S. Kinsey, H. Yoon, R. A. Sherif, N. H. Karam, *Appl. Phys. Lett.* **90** (2007) 183516.

162 F. D. Newman, M. A. Stan, S. L. Murray, C. S. Murray, *J. Cryst. Growth* **272** (2004) 650-657.

163 B. Beaumont, P. Vennéguès, P. Gibart, *Phys. Status Solidi B* **227** (2001) 1-43.

164 A. Sakai, H. Sunakawa, A. Usui, *Appl. Phys. Lett.* **73** (1998) 481-483.

165 A. P. Edwards, J. A. Mittereder, S. C. Binari, D. S. Katzer, D. F. Storm, J. A. Roussos, *IEEE Electron Device Lett.* **26** (2005) 225-227.

166 H. Hasegawa, T. Inagaki, S. Ootomo, T. Hashizume, *J. Vac. Sci. Technol. B* **21** (2003) 1844-1855.

167 G. Verzellesi, A. Mazzanti, A. F. Basile, A. Boni, E. Zanoni, C. Canali, *IEEE Trans. Electron Devices* **50** (2003) 1733-1740.

168 R. Yeats, D. C. D'Avanzo, K. Chan, N. Fernandez, T. W. Taylor, C. Vogel, in: *Technical Digest - International Electron Devices Meeting, IEEE*, (1988) pp. 842-845.

169 S. C. Binari, P. B. Klein, T. E. Kazior, *Proc. IEEE* **90** (2002) 1048-1058.

170 T. Hashizume, J. Kotani, H. Hasegawa, *Appl. Phys. Lett.* **84** (2004) 4884-4886.

171 W. Saito, M. Kuraguchi, Y. Takada, K. Tsuda, I. Omura, T. Ogura, *IEEE Trans. Electron Devices* **52** (2005) 159-164.

172 K. Keem, J. Kang, C. Yoon, D. Y. Jeong, B. M. Moon, S. Kim, *Jpn. J. Appl. Phys.* **46** (2007) 6230-6232.

173 P. C. Chang, Z. Fan, C. J. Chien, D. Stichtenoth, C. Ronning, J. G. Lu, *Appl. Phys. Lett.* **89** (2006) 133113.

174 C. Lao, Y. Li, C. P. Wong, Z. L. Wang, *Nano Lett.* **7** (2007) 1323-1328.

175 C. S. Enache, J. Schoonman, R. Van De Krol, *Journal of Electroceramics* **13** (2004) 177-182.

176 H. Matsui, H. Tabata, N. Hasuike, H. Harima, B. Mizobuchi, *Journal of Applied Physics* **97** (2005) 1-8.

177 C. S. Enache, J. Schoonman, R. V. Krol, *J. Electroceram.* **13** (2004) 177-182.

178 H. Matsui, H. Tabata, N. Hasuike, H. Harima, B. Mizobuchi, *J. Appl. Phys.* **97** (2005) 123511.

179 E.-J. Lee, S.-I. Pyun, *J. Appl. Electrochem.* **22** (1992) 156-160.

180 E. Comini, C. Baratto, G. Faglia, M. Ferroni, A. Vomiero, G. Sberveglieri, *Prog. Mater. Sci.* **54** (2009) 1-67.

181 X. J. Huang, Y. K. Choi, *Sens. Actuators, B* **122** (2007) 659-671.

182 A. Kolmakov, M. Moskovits, *Annu. Rev. Mater. Res.* **34** (2004) 151-180.

183 G. Shen, P. C. Chen, K. Ryu, C. Zhou, *J. Mater. Chem.* **19** (2009) 828-839.

184 E. Comini, *Anal. Chim. Acta* **568** (2006) 28-40.

185 N. Yamazoe, *Sens. Actuators, B* **5** (1991) 7-19.

186 Z. Fan, J. G. Lu, *Appl. Phys. Lett.* **86** (2005) 123510.

187 M. W. Ahn, K. S. Park, J. H. Heo, J. G. Park, D. W. Kim, K. J. Choi, J. H. Lee, S. H. Hong, *Appl. Phys. Lett.* **93** (2008) 263103.

188 B. Lei, C. Li, D. Zhang, T. Tang, C. Zhou, *Appl. Phys. A* **79** (2004) 439-442.

189 P. Nguyen, H. T. Ng, J. Kong, A. M. Cassell, R. Quinn, J. Li, J. Han, M. McNeil, M. Meyyappan, *Nano Lett.* **3** (2003) 925-928.

190 N. Wang, Y. Cai, R. Q. Zhang, *Mater. Sci. Eng. R* **60** (2008) 1-51.

191 S. Geburt, D. Stichtenoth, S. Muller, W. Dewald, C. Ronning, J. Wang, Y. Jiao, Y. Y. Rao, S. K. Hark, Q. Li, *J. Nanosci. Nanotechnol.* **8** (2008) 244-251.

192 B. Guo, A. Bermak, P. C. H. Chan, G. Z. Yan, *IEEE Sens. J.* **8** (2008) 1397-1398.

193 L. Liao, H. B. Lu, J. C. Li, C. Liu, D. J. Fu, Y. L. Liu, *Appl. Phys. Lett.* **91** (2007) 173110.

194 S. Lettieri, A. Setaro, C. Baratto, E. Comini, G. Faglia, G. Sberveglieri, P. Maddalena, *New J. Phys.* **10** (2008) 043013.

195 C. Baratto, S. Todros, G. Faglia, E. Comini, G. Sberveglieri, S. Lettieri, L. Santamaria, P. Maddalena, *Sens. Actuators, B* **140** (2009) 461-466.

196 G. Faglia, C. Baratto, G. Sberveglieri, M. Zha, A. Zappettini, *Appl. Phys. Lett.* **86** (2005) 011923.

197 E. Comini, C. Baratto, G. Faglia, M. Ferroni, G. Sberveglieri, *J. Phys. D: Appl. Phys.* **40** (2007) 7255-7259.

198 A. Fujishima, K. Hashimoto, T. Watanabe, *TiO2 photocatalysis : fundamentals and applications*, Bkc, Tokyo, 1999.

199 A. Fujishima, K. Honda, *Nature* **238** (1972) 37-38.

200 A. Fujishima, T. N. Rao, D. A. Tryk, *J. Photochem. Photobiol. C* **1** (2000) 1-21.

201 D. Li, H. Haneda, *J. Photochem. Photobiol. A* **155** (2003) 171-178.

202 S. Sakthivel, B. Neppolian, M. V. Shankar, B. Arabindoo, M. Palanichamy, V. Murugesan, *Sol. Energy Mater. Sol. Cells* **77** (2003) 65-82.

203 S. K. Kansal, M. Singh, D. Sud, *J. Hazard. Mater.* **141** (2007) 581-590.

204 M. Miyauchi, A. Nakajima, T. Watanabe, K. Hashimoto, *Chem. Mater.* **14** (2002) 2812-2816.

205 K. R. Reyes-Gil, E. A. Reyes-García, D. Raftery, *J. Phys. Chem. C* **111** (2007) 14579-14588.

206 Y. Sun, C. J. Murphy, K. R. Reyes-Gil, E. A. Reyes-Garcia, J. P. Lilly, D. Raftery, *Int. J. Hydrogen Energy* **33** (2008) 5967-5974.

207 C. Burda, Y. Lou, X. Chen, A. C. S. Samia, J. Stout, J. L. Gole, *Nano Lett.* **3** (2003) 1049-1051.

208 W. Choi, A. Termin, M. R. Hoffmann, *J. Phys. Chem.* **98** (1994) 13669-13679.

209 F. Gracia, J. P. Holgado, A. Caballero, A. R. Gonzalez-Elipe, *J. Phys. Chem. B* **108** (2004) 17466-17476.

210 J. Augustynski, *Electrochim. Acta* **38** (1993) 43-46.

211 R. Asahi, T. Morikawa, T. Ohwaki, K. Aoki, Y. Taga, *Science* **293** (2001) 269-271.

212 O. Diwald, T. L. Thompson, E. G. Goralski, S. D. Walck, J. T. Yates Jr, *J. Phys. Chem. B* **108** (2004) 52-57.

213 A. Ghicov, J. M. Macak, H. Tsuchiya, J. Kunze, V. Haeublein, L. Frey, P. Schmuki, *Nano Lett.* **6** (2006) 1080-1082.

214 J. L. Gole, J. D. Stout, C. Burda, Y. Lou, X. Chen, *J. Phys. Chem. B* **108** (2004) 1230-1240.

215 H. Irie, Y. Watanabe, K. Hashimoto, *J. Phys. Chem. B* **107** (2003) 5483-5486.

216 S. U. M. Khan, M. Al-Shahry, W. B. Ingler Jr, *Science* **297** (2002) 2243-2245.

217 J. H. Park, S. Kim, A. J. Bard, *Nano Lett.* **6** (2006) 24-28.

218 C. Di Valentin, G. Pacchioni, A. Selloni, *Chem. Mater.* **17** (2005) 6656-6665.

219 H. Wang, J. P. Lewis, *J. Phys.: Condens. Matter* **18** (2006) 421-434.

220 H. Luo, T. Takata, Y. Lee, J. Zhao, K. Domen, Y. Yan, *Chem. Mater.* **16** (2004) 846-849.

221 T. Ohno, T. Mitsui, M. Matsumura, *Chem. Lett.* **32** (2003) 364-365.

222 J. C. Yu, W. Ho, J. Yu, H. Yip, K. W. Po, J. Zhao, *Environ. Sci. Technol.* **39** (2005) 1175-1179.

223 M. Zheng, J. Wu, *Appl. Surf. Sci.* **255** (2009) 5656-5661.

224 R. G. Breckenridge, W. R. Hosler, *Phys. Rev.* **91** (1953) 793-802.

225 D. C. Cronemeyer, *Phys. Rev.* **113** (1959) 1222-1226.

226 T. Ihara, M. Miyoshi, M. Ando, S. Sugihara, Y. Iriyama, *J. Mater. Sci.* **36** (2001) 4201-4207.

227 I. Nakamura, N. Negishi, S. Kutsuna, T. Ihara, S. Sugihara, K. Takeuchi, *J. Mol. Catal. A: Chem.* **161** (2000) 205-212.

228 P. Salvador, M. L. G. González, F. Muñoz, *J. Phys. Chem.* **96** (1992) 10349-10353.

229 K. Takeuchi, I. Nakamura, O. Matsumoto, S. Sugihara, M. Ando, T. Ihara, *Chem. Lett.* (2000) 1354-1355.

230 S. Baruah, S. S. Sinha, B. Ghosh, S. K. Pal, A. K. Raychaudhuri, J. Dutta, *J. Appl. Phys.* **105** (2009) 074308.

3. SULFUR DEPOSITION ON TiO_2

3.1. Introduction

Defects play the key role in altering and controlling the electrical properties of semiconductors, which enables the use of these materials in the various applications from microelectronics and photovoltaics to gas sensors and photocatalysts [1-7]. Hence, the ability to control the defects in semiconductor materials has been the focus of ongoing research for many decades. Of the many approaches to this task, it has been found in our lab that the surface chemical state can open new pathways of defect generation and annihilation [8-10]. It has been shown for silicon that atomically clean surfaces leads to enhanced self-diffusion, which is the evidence of additional concentrations of defects created at the clean surface. To further ascertain these effects, the same experiments were carried out under identical conditions, only with the surface covered with nitrogen atoms. The results showed there is indeed an enhancement for clean surfaces compared to adsorbed ones. The same principles are thought to hold true for metal oxide semiconductors as well.

Titanium dioxide is a well studied material due to its wide variety of applications such as photovoltaics, gas sensors, coatings and microelectronics [11]. The discovery of the potential to be used as a phtocatalyst for water-splitting applications has promoted the interest of this material even further [12]. In all cases, defects play the main role to gain the special properties that make such applications possible. For these reasons, the group has chosen titanium dioxide as a candidate to show the effects of the surface on defect concentrations. Preliminary experiments of monitoring the self-diffusion of oxygen atoms showed that atomically clean

surfaces exhibit enhanced self-diffusion and have opened new pathways for metal oxides as well [13].

In order to further verify the effects of the surface, control experiments where only the surface pathways are blocked must be carried out. To accomplish this, a suitable adsorbate must be used. In this work, we discuss possible elements that can be used as adsorbates. A successful method of producing the element that suits our experimental conditions is also provided.

3.2. Sulfur as an Adsorbate

There are several properties that the adsorbate must have in order to be suitable for the purpose of surface effect studies. First and foremost, it has to have good adherence to the substrate. What is more, it should be able to stay adsorbed at elevated temperatures (~700 C). This is important as the role of the adsorbate is to block surface pathways of defect generation/annihilation during self-diffusion experiments. In view of the fact that these experiments are done at high temperatures, the adsorbate must also be able to withstand these conditions and remain adsorbed to the substrate to sufficiently function as desired. In addition to preferable adsorption characteristics, it is also crucial that the adsorbate does not diffuse into the bulk substrate itself. Diffusion of the adsorbate into the material will reduce the amount of adsorbate on the surface, thereby defeating the purpose of surface adsorption altogether. Lastly, it would be preferable if the adsorbate adsorbs on sites that are likely to be the source of defect generation and annihilation. These sites include surface defects and dangling bonds on the surface. Also, for the diatomic substrates, it is necessary to find the adsorbate that will likely influence the defect generation of the atom of interest more than the other.

Several candidates ranging from metals to halogens to organic molecules have been considered for use in the studies of titanium oxide defect engineering. Our main focus is on the behavior of oxygen atoms and, therefore, elements that would preferably adsorb on oxygen sites were reviewed first. Among the many elements, halogens and sulfur were found to have most of the properties mentioned above. Due to the unfavorable properties of halogens when handled in vacuum chambers (*e.g.*, contamination of the components and eventual increase in base pressure of the chamber), sulfur became the most likely element of choice for our studies. Sulfur is reported to preferably adsorb on the bridge oxygen vacancies and at the cross section of planar oxygen atoms of the (110) surface of rutile titanium dioxide [11]. The desorption temperature is not as high as initially hoped for (only ~0.2 monolayers survive at 700°C) but nevertheless was higher than most other elements. Since sulfur preferably occupies surface oxygen vacancies, a low coverage may still be sufficient. It was also found in previous studies on silicon that the transition between adsorbed and clean surface behavior happens at rather low coverages (on the order of 0.01 monolayers) [9]. In addition, while surface atom exchange has been observed at high temperature adsorption, no significant diffusion into the bulk material was observed. Thus, sulfur became the element of choice.

3.3. Experimental Methods

An electrochemcial method was used to produce and deposit sulfur onto the titanium dioxide substrates *in situ*. Diffusion was to be carried out in high vacuum (~10^{-7} Torr), necessitating the need for a dry, vacuum compatible method of deposition. The electrochemical cell was based on what has been previously reported in the literature [14]. A schematic diagram of the cell is shown in Fig. 3.1. The cell construction is a two electrode cell, Ag|AgI|Ag_2S|Pt,

with Ag|AgI serving as the reference and counter electrode. The working electrode was a Pt film of thickness 0.1 mm and the counter/reference electrode was a 2 mm Ag disk. AgI (99%) and Ag_2S (99.9%) powder was used as the reagents. All reagents, including the electrode materials, were purchased from Sigma Aldrich. The reagents were put inside a glass piston assembly fabricated with a glass tube ending with a glass to Kovar seal. Lead wires were then attached to the electrodes. The leads were copper wires, while nickel chromium wire was used for the connection between the Pt electrode and copper wires in order to spot weld the lead wire to the Pt electrode. Chromel A wire (AWG 26) was wrapped around the glass piston to serve as the heating element. The entire assembly was mounted on a 2.75 in./1.63 in. zero-length reducer flange using TorrSeal. A 1.63 in. 4-pin feedthrough was attached to the flange to deliver power to the heating element and the cell. A thermocouple (type K) was attached close to the heating element to monitor the operation temperature. This came through a separate thermocouple feedthrough on the chamber. Direct current (DC) power supplies were used to provide power for the heating element and the electrochemical cell. Operation of the cell was carried out by applying a working potential of 0.15 - 0.3 V, which produced a current ranging from 0.01 - 10 mA. Heat was applied to the cell via the heating wires, and the operational temperature was varied from 65 °C to 200 °C, read from the attached thermocouple. The cell was tested on silicon substrates and single crystal rutile ((110) and (001) surfaces) substrates. The resulting adsorption of sulfur was characterized using X-ray Photoelectron Spectroscopy (XPS, PEI5400) and Auger Electron Spectroscopy (AES, Perkin Elmer). AES was carried out *in situ*, while XPS was *ex situ*.

3.4. Results and Discussion

Sulfur has successfully been deposited on Si substrates, verified by XPS (Fig. 3.2). Some additional artifacts can also be seen, such as the presence of chromium, which may have come from the heating wires. In an effort to eliminate this extra contamination, the heating was reduced to lower temperatures of ~100°C. As a result, the contamination has gone but the amount of sulfur deposited has also been reduced (Fig. 3.3). Fig. 3.3 shows the result on a rutile TiO_2 substrate. The amount of sulfur present is quite low but it turns out that it is enough for the purpose of surface effect studies on TiO_2 as evidenced in ref. [15]. Due to the uncontrollable nature of external contaminants (mainly carbon), *ex situ* XPS could not be used as a reliable method for detailed characterization of the deposited sulfur and its correlations with deposition conditions.

In an attempt to overcome these difficulties and provide a reliable method of adsorbate characterization, *in situ* analysis using AES was also performed. Fig. 3.4 shows the AES spectra before and after deposition of sulfur on a rutile TiO_2 substrate. It can be seen clearly that the sulfur peak at ~2100-2200 eV has appeared after deposition, indicating the successful deposition of sulfur. Unfortunately, many technical difficulties arose in the operation of AES, hindering the ability to obtain coherent results at times. Moreover, the device failed to operate eventually, and no further data could be obtained. Thus, further characterization of the deposition details could not be carried out.

3.5. Summary

It had been found previously for Si that surfaces can play a role in the control of defect concentration within the bulk material. Preliminary experiments have shown this effect may also be present in metal oxide semiconductors as well, namely TiO_2. To completely verify the existence of such surface pathways, control experiments with the surface covered with an appropriate adsorbate must be carried out. Sulfur was chosen as a suitable element to be used for titanium oxide. An electrochemical method was utilized for sulfur deposition onto the surface, and a working device has been fabricated. Results show the device is fully functional and sulfur can be readily deposited onto silicon and rutile TiO_2 substrates. This sulfur deposition device has been used to verify the surface effects on defect manipulation of rutile TiO_2; detailed results can be found in ref. [15].

3.6. Figures

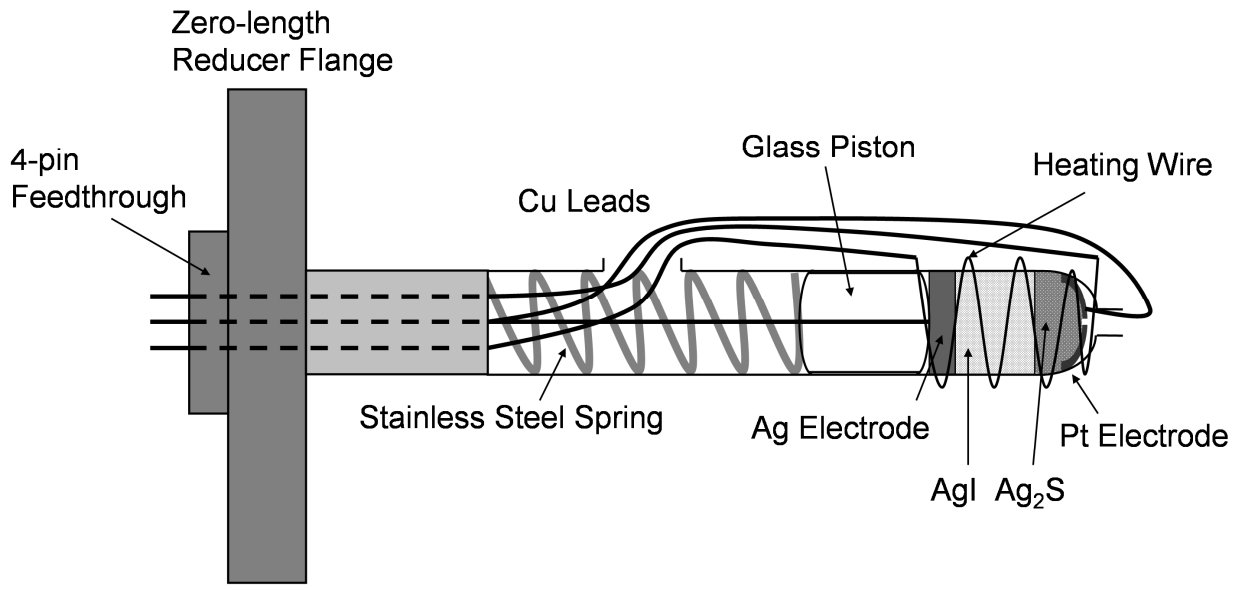

Fig. 3.1. Schematic diagram of the sulfur deposition electrochemical cell.

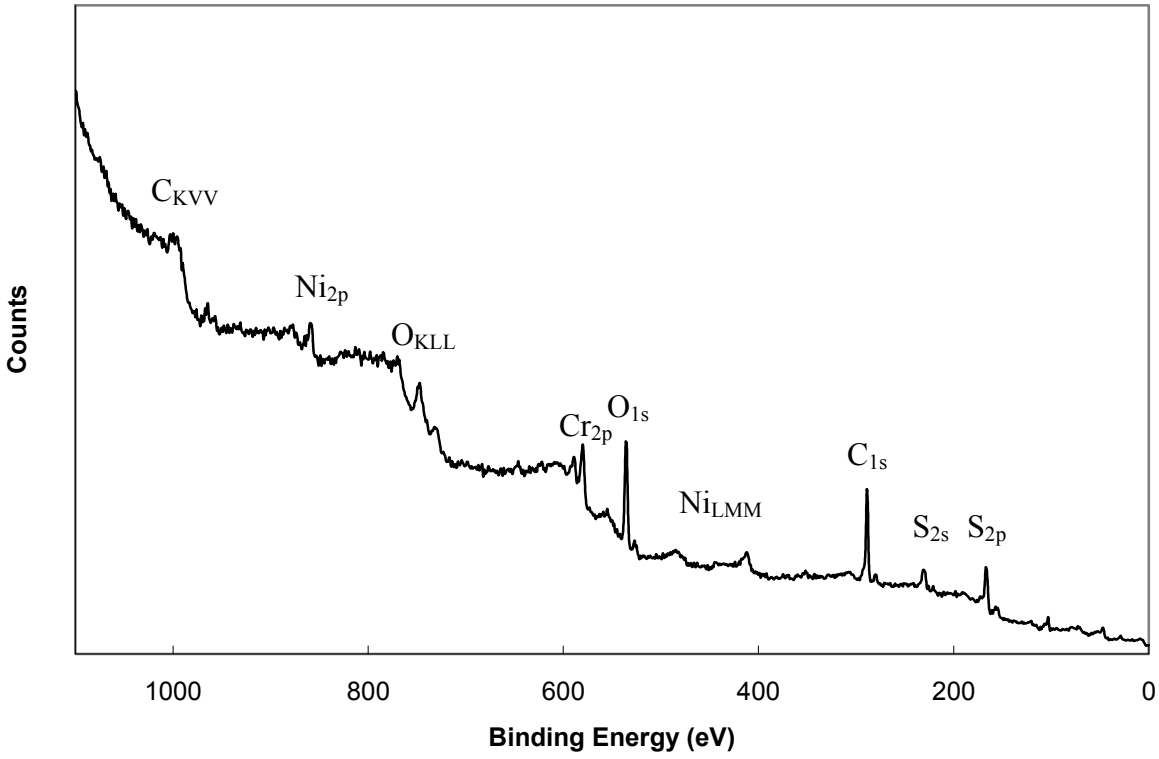

Fig. 3.2. XPS spectra of sulfur deposited on silicon.

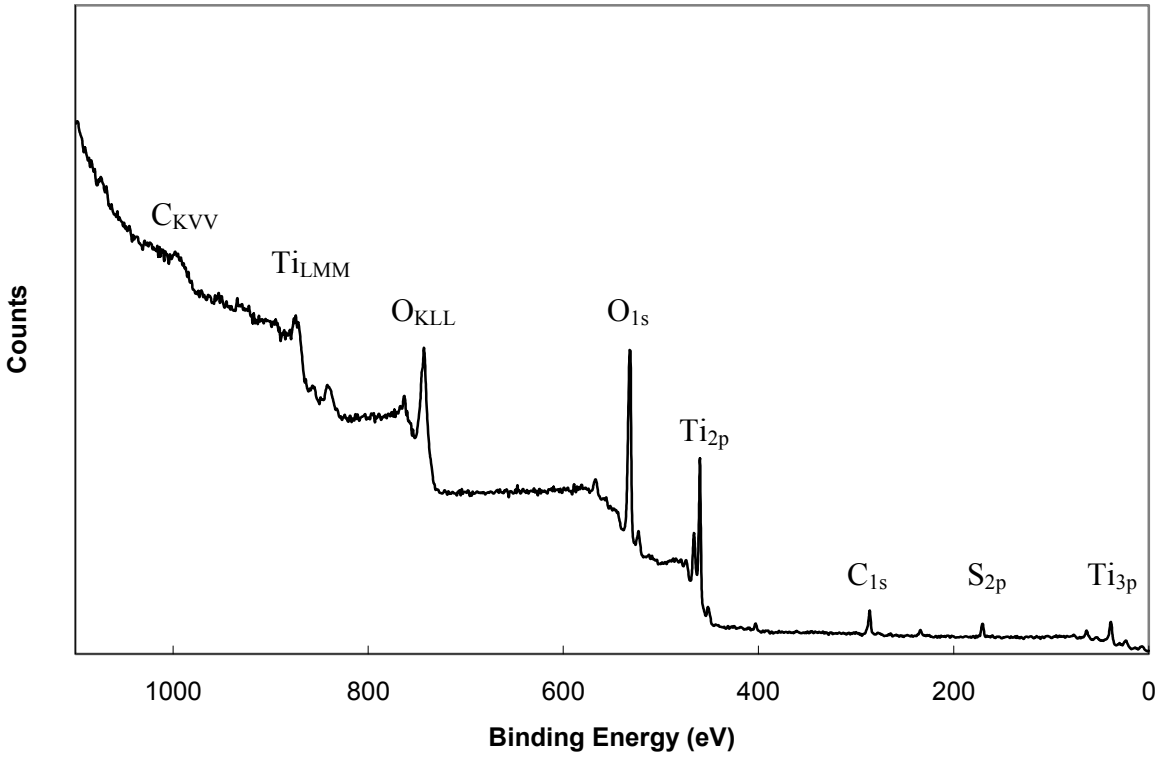

Fig. 3.3. XPS spectra of sulfur deposited on TiO_2 rutile.

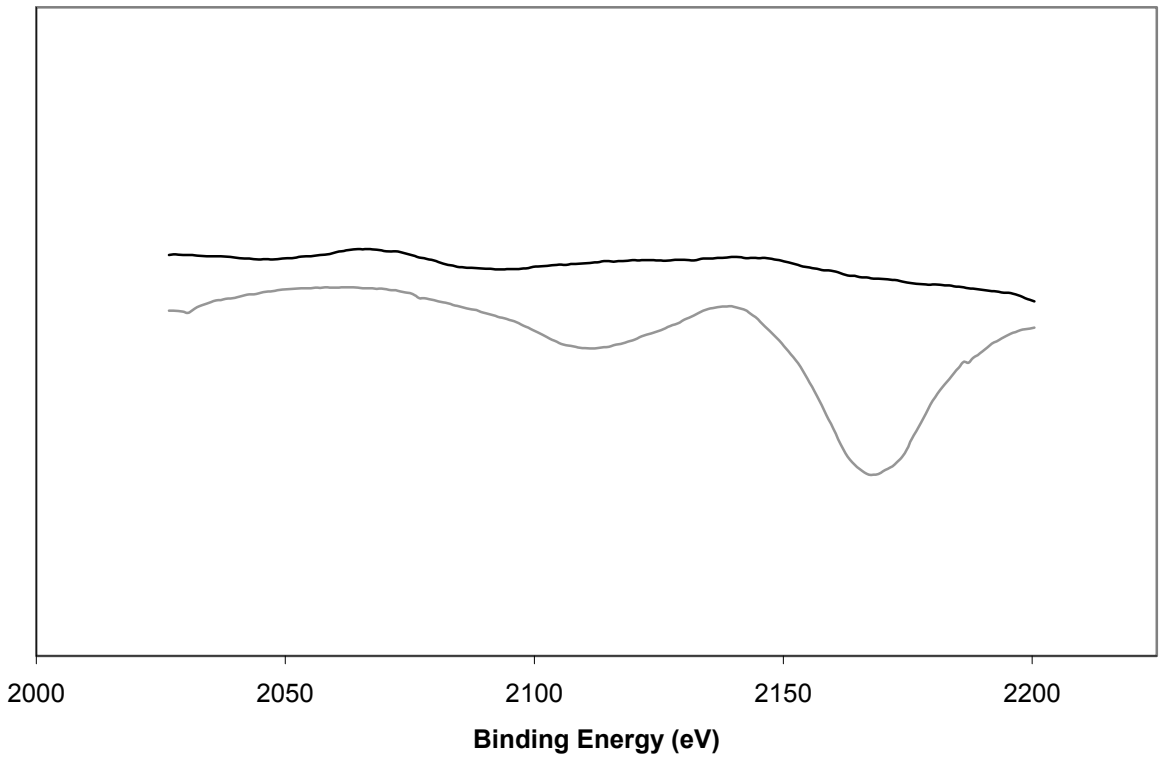

Fig. 3.4. AES spectra of TiO_2 rutile, before (black line) and after (gray line) deposition of sulfur. Data taken by A. Hollister.

3.7. References

1 W. Baiqi, J. Liqiang, Q. Yichun, L. Shudan, J. Baojiang, Y. Libin, X. Baifu, F. Honggang, *Appl. Surf. Sci.* **252** (2006) 2817-2825.

2 W. W. Chow, S. W. Koch, *Semiconductor-Laser Fundamentals: Physics of the Gain Materials*, Springer, Berlin, 1999.

3 J. W. Fergus, *J. Mater. Sci.* **38** (2003) 4259-4270.

4 S. Guha, J. M. Depuydt, M. A. Haase, J. Qiu, H. Cheng, *Appl. Phys. Lett.* **63** (1993) 3107-3109.

5 S. R. Kurtz, A. A. Allerman, E. D. Jones, J. M. Gee, J. J. Banas, B. E. Hammons, *Appl. Phys. Lett.* **74** (1999) 729-731.

6 G. Lutz, *Semiconductor Radiation Detectors: Device Physics*, Springer, Berlin, 1999.

7 Y. Zhang, A. Kolmakov, S. Chretien, H. Metiu, M. Moskovits, *Nano Lett.* **4** (2004) 403-407.

8 K. Dev, E. G. Seebauer, *Surf. Sci.* **550** (2004) 185-191.

9 E. G. Seebauer, K. Dev, M. Y. L. Jung, R. Vaidyanathan, C. T. M. Kwok, J. W. Ager, E. E. Haller, R. D. Braatz, *Phys. Rev. Lett.* **97** (2006) 055503

10 R. Vaidyanathan, E. G. Seebauer, H. Graoui, M. A. Foad, *Appl. Phys. Lett.* **89** (2006) 152114.

11 U. Diebold, *Surf. Sci. Rep.* **48** (2003) 53-229.

12 A. Fujishima, K. Honda, *Nature* **238** (1972) 37-38.

13 R. Vaidyanathan, Ph.D. thesis, University of Illinois at Urbana-Champaign, 2007.

14 W. Heegemann, K. H. Meister, E. Bechtold, K. Hayek, *Surf. Sci.* **49** (1975) 161-180.

15 A. Hollister, Ph.D. thesis, University of Illinois at Urbana-Champaign, 2010.

4. Ti SELF DIFFUSION IN TiO_2

4.1. Introduction

Since the discovery of its potential as a photocatalyst [1], titanium dioxide has become the focus of intense research. The key components of interest are the various defects in the material as these species are what gives rise to the many different special properties. Defect chemistry studies using galvanoelectric and conductivity studies [2-4] revealed that the dominant intrinsic defects are either titanium interstitials or oxygen vacancies, depending on the conditions. Recent studies also report that titanium vacancies begin to show during annealing in much longer time frames (~thousands of hours) [3]. While there have been much research in this area, there still is debate as to what species is dominant in specific conditions.

Many of the defect studies have been focused on the oxygen constituent for multiple reasons. As an oxide, many properties of the material depend on the oxygen behavior and the oxidation state. Moreover, under annealing conditions, titanium dioxide readily exchanges oxygen atoms with gaseous O_2 in a temperature- and pressure-dependent way. Also, implementing methods to study oxygen is much easily achieved. For example, introducing isotopic oxygen can be done simply by introducing $^{18}O_2$ gas as the ambient. Hence, studies have been mainly focused on the oxygen behavior. Recently in our lab, for example, it has been found that the surface can play an important role in opening new mechanisms for oxygen diffusion [5].

Studies on the cation side have also been carried out previously if not extensively. For example, isotopic ^{44}Ti and ^{46}Ti was used to measure the diffusivity of Ti interstitials [6,7]. The difficulty in studying the cation behavior, however, has lead to significantly less research compared to oxygen. Nevertheless, cation studies can give insight to the overall properties of

titanium oxide, as well as additional details of the behaviors of oxygen. For instance, it is proposed that oxygen vacancies may travel by forming complexes with titanium interstitials [8]. Monitoring the cation behavior can verify the existence of such interactions. This work aims at shedding light into the behavior of Ti defects via experimental and computational methods.

4.2. Experimental Setup

Titanium diffusion was investigated via tracer diffusion using ^{46}Ti (natural occurrence 8.0%) available in the oxide form. $^{46}TiO_2$ (enhanced at 72.40%, from Chemgas) was evaporated onto rutile single crystal substrates with orientation (001) (from MTI corp.) in order to form isotopic heterostructures. Evaporation was done in high vacuum (~1×10^{-6} torr) by introducing the $^{46}TiO_2$ powder in a boat made of Ta foil, which was resistively heated via W wires. A thermocouple (type-K) was attached to the boat in order to monitor the temperature. The boat was heated to 900 - 1000 °C for 30 - 60 min. The substrate was also resistively heated through a silicon wafer backing to ~400 °C. After deposition, the samples were to be annealed at various temperatures (700 - 1000 °C) for varying times (2 - 4 hrs). The results would be analyzed with secondary ion mass spectroscopy (SIMS).

4.3. Model Setup

4.3.1. Diffusion Mechanisms

The system is an isotopic heterostructure with $^{46}TiO_2$ deposited on a natural TiO_2 substrate. Ti has five stable isotopes, the most naturally abundant being ^{48}Ti (natural occurrence 73.8%). For simplicity, we assume that only Ti isotopes of mass 46 and 48 exist in the system.

The model for this system uses continuum equations to describe the reaction and diffusion of the various intrinsic defects, namely titanium interstitials and vacancies. These equations have the general form for species *i*,

$$\frac{\partial C_i}{\partial t} = -\frac{\partial J_i}{\partial x} + G_i \tag{4.1}$$

where C_i, J_i, and G_i are concentration, flux, and net generation rate of species *i*, respectively. The flux J_i comprises terms due to both Fickian diffusion and electric drift motion,

$$J_i = -D_i \frac{\partial^2 C_i}{\partial x^2} + \gamma_i \mu_i C_i \xi(x) \tag{4.2}$$

where μ is the mobility of diffusing species calculated by the Einstein equation and γ_i is the net charge of species *i*, which is the sum of all possible charge states, z_j weighted by the corresponding fraction, γ_{zj}:

$$\gamma_i = \sum_j z_j \gamma_{z_j} \tag{4.3}$$

The electric field (ξ) is obtained as the solution to Poisson's equation, with the charge density (ρ) incorporating terms due to the concentrations of electrons, holes, charged defects and background doping:

$$\frac{dE(x)}{dx} = \frac{\rho(x)}{\varepsilon} \tag{4.4}$$

The titanium interstitials are known to have two charge states, +3 and +4. The population of the two charged states is determined by Fermi-Dirac statistics [9],

$$f(E) = \frac{1}{1 + \frac{g_0}{g_1} \exp \frac{E - E_i}{kT}} \tag{4.5}$$

where $f(E)$ is the probability that an available energy state at E will be occupied by an electron, E_i is the ionization level, g_0 and g_1 are the degeneracy of the unoccupied and occupied centers, respectively. For Ti interstitials with possible charge states of +3 and +4, $g_0 = 1$ and $g_1 = 2$.

There are two mechanisms that are incorporated in the net generation term G_i in Eq. (4.1). First is the bulk generation of defects, represented as:

$$\mathrm{Ti_{Ti}} \underset{k_2}{\overset{k_1}{\rightleftarrows}} \mathrm{Ti_{int}} + \mathrm{Ti_{vac}} \tag{4.6}$$

The reaction rate constant of generation follows the Arrhenius relation. The activation energy of k_1 is approximated by the formation energy of bulk Frenkel pairs. Maximum likelihood estimates from literature give a value of 6.06 eV (Table 4.1). On the other hand, the annihilation process is thought to be diffusion limited rather than reaction limited. Hence, the reaction constant for annihilation is given by

$$k_2 = 4\pi a\left(D_{\mathrm{Ti_{int}}} + D_{\mathrm{Ti_{vac}}}\right) \tag{4.7}$$

where a is the capture radius (a = 2.95 Å) and $D_{\mathrm{Ti_{int}}}$, $D_{\mathrm{Ti_{vac}}}$ are the diffusivities of titanium interstitials and vacancies, respectively.

The second mechanism is the kick-in/ kick-out mechanism.

$$^{46}\mathrm{Ti_{Ti}} + {}^{48}\mathrm{Ti_{int}} \underset{k_3}{\overset{k_3}{\rightleftarrows}} {}^{46}\mathrm{Ti_{int}} + {}^{48}\mathrm{Ti_{Ti}} \tag{4.8}$$

As can be seen, the mechanism involves the exchange of lattice atoms with interstitial atoms and would not show in normal circumstances. For isotopic heterostructures, however, this mechanism can lead to different diffusion behaviors, as can be seen in the results (Section 4.5). Naturally, the reaction constants are the same for the forward and reverse reactions, and would also follow the Arrhenius relation. As this mechanism is virtually unobservable in natural materials, there are no previous estimates to the activation energy of the reaction. Hence, various

values have been tried out, and an approximate value of 12.3 eV was found and implemented. Details will be discussed in Section 4.5.

4.3.2. Boundary Conditions

As Ti interstitials are also known to equilibrate with oxygen gas, there must be surface generation and annihilation occurring as well. A proposed mechanism is as follows.

$$O_2(g) \underset{k_{des}}{\overset{k_{ads}}{\rightleftarrows}} 2O(ad) \tag{4.9}$$

$$Ti_{Ti} + 2O_O \underset{k_5}{\overset{k_4}{\rightleftarrows}} Ti_{int} + 2O(ad) \tag{4.10}$$

The oxygen adsorption phase, Eq. (4.9), can be explained by the dissociative Langmuir isotherm. Hence, the amount of adsorbed oxygen can be estimated from the oxygen partial pressure by

$$\theta = \frac{\sqrt{bP}}{1+\sqrt{bP}} \tag{4.11}$$

where θ is the fraction of occupied adsorption sites, P is the oxygen partial pressure and b is a factor that is a function of temperature and follows the Arrhenius relation. The activation energy term for b can be obtained by the difference of the activation energies of the rate constants of adsorption and desorption. Literature gives a value of -0.58 eV for this quantity [10].

The generation reaction can be approximated as a zeroth order reaction since only a fraction of the surface atoms will participate and also because the surface site will still be available for generation after a reaction occurs. As an initial estimate, the activation energy of the reaction rate constant is approximated to be the formation energy of Ti interstitials in equilibrium with oxygen gas. Maximum likelihood estimation of previous literature values gives 9.673 eV for this quantity (Table 4.1). The rate of surface annihilation, on the other hand, is

represented in terms of an annihilation probability *S*, as formulated previously in this laboratory for the case of Si [11,12]. The rate constant for annihilation is then given by

$$k_5 = \frac{3D_{\mathrm{Ti_{int}}}S}{a} \tag{4.12}$$

where *a* is the nearest neighbor distance (*a* = 2.95 Å). As these reactions happen only at the surface, they are implemented as boundary conditions given as

$$-D_{\mathrm{Ti_{int}}}\left.\frac{\partial C_{\mathrm{Ti_{int}}}}{\partial x}\right|_{x=0} = k_4 - k_5 C_{\mathrm{Ti_{int}}}\theta \tag{4.13}$$

The model was implemented using the profile simulator FLOOPS 2002 (by Mark E. Law of the University of Florida and Al Tasch of the University of Texas at Austin) [13]. The simulator solves a set of coupled differential equations for the motion and/or reaction of interstitials, vacancies, and lattice sites.

4.4. Systems-Based Tools

4.4.1. Maximum Likelihood

The parameters to be used were obtained by maximum likelihood (ML) estimation based on previously reported literature values. ML estimation is a useful method for quantifying errors in rate parameters extracted from data sets that have complicated error structures and are described by models incorporating numerous elementary kinetic steps [14,15]. A simplified ML method was used to calculate the weighted average of previously reported parameters. The average is given by

$$\bar{x} = \frac{\sum_{i=1}^{n} w_i x_i}{\sum_{i=1}^{n} w_i} \tag{4.14}$$

where the weighing factor w_i equals the inverse of the error variance,

$$w_i = \frac{1}{\sigma_i^2} \tag{4.15}$$

for each report. The variance of the weighted mean is

$$\bar{\sigma}_{\bar{x}}^2 = \frac{1}{\sum_{i=1}^{n} w_i} \tag{4.16}$$

Table 4.1 summarizes the parameters used in this work that has been obtained by this method.

4.4.2. Parameter Sensitivity Analysis

Parameter sensitivity analysis studies the influence of perturbations in model parameters on the process outputs. This technique has been widely applied in the analysis and design of chemical systems [16,17]. The analysis determines which model parameters need to be estimated or calculated most accurately in order give high predictability. The matrix F of sensitivity coefficients includes the partial derivatives of the variables β_j with respect to the dependent variables P_i [18,19],

$$F_{i,j} = F\left(P_i; \beta_j\right) = \frac{\partial P_i\left(\beta_j\right)}{\partial \beta_j} \tag{4.17}$$

The sensitivity coefficients are estimated by the finite difference method [12],

$$F\left(P_i; \beta_j\right) = \frac{\Delta P_i}{\Delta \beta_j} = \frac{P_i\left(\beta_j + \Delta\beta_j\right) - P_i\left(\beta_j - \Delta\beta_j\right)}{2\Delta\beta_j} \tag{4.18}$$

where $F(P_i; \beta_j)$ denotes the sensitivity coefficient of the i^{th} measurement (*i.e.*, the depth within the profile) to the j^{th} parameter. The total sensitivity for the j^{th} parameter, Φ_j, is given by the sum of the normalized absolute values of this approximated partial derivative over the entire depth of the profile (^{46}Ti in the case of this study),

$$\Phi_j = \sum_{i=1}^{N_d} \left| \frac{C^{^{46}\mathrm{Ti}}_{i,\beta_j+\Delta\beta_j} - C^{^{46}\mathrm{Ti}}_{i,\beta_j-\Delta\beta_j}}{2\Delta\beta_j} \cdot \frac{\beta_j}{C^{^{46}\mathrm{Ti}}_{i,\beta_j}} \right| \tag{4.19}$$

where N_d is the total number of data points in the profile, $C^{^{46}\mathrm{Ti}}$ is the concentration of ^{46}Ti at the corresponding depth and parameter, and $\Delta\beta_j = 0.05\beta_j$. A higher value of the total sensitivity Φ_j implies a stronger influence of the corresponding model parameter β_j on the final profile.

4.5. Results and Discussion

4.5.1. Experimental Results

The evaporation of TiO_2 was first tested on silicon wafer pieces of size 1 × 0.5 cm. The surface was then analyzed with x-ray photoelectron spectroscopy (XPS) to verify the presence of TiO_2. Fig. 4.1 shows the result of successfully deposited TiO_2 on silicon. This, unfortunately, was unable to be reproduced routinely. One of the first obstacles was copper/ copper oxide contamination. This was first thought to have come from the copper lead and feedthrough wires which were used to carry the high current (~8-9 A) for heating the Ta boat containing the TiO_2 powder. However, copper contamination was still observed even after changing the feedthrough to Ni wires and replacing the main lead wires to Ta wires. Fortunately, the contamination was found to decrease after a few runs following the assembly of a new boat. It is thus hypothesized the source may be from the copper spot welding leads which are used during the assembly of the

boat. The next contamination issue was tungsten, which can also be seen to exist in Fig. 4.1. The source of this is obviously the tungsten wire that was used to heat the boat. This is clearly seen from the control experiments where an empty boat was heated in order to isolate the source of contamination (Fig. 4.2). Fortunately, it was also observed that a properly filled boat has significantly less to even negligible tungsten contamination (Fig. 4.3). Hence, it was decided that if the tungsten wires are not directly exposed to the substrate, tungsten contamination can be minimized to a degree that is negligible for our purposes. Lastly, potassium contamination was found to happen extensively in some cases. The source of this is unknown. Some control of experiments using an empty boat followed by a filled boat (Figs. 4.2 and 4.3) show that the source is from the powder itself or at least introduced during the loading of the boat. Various efforts have been made to successfully deposit TiO_2 on the Si sample, but turned out unsuccessful in achieving reproducible results. Hence, the following results will be solely based on computational analysis.

4.5.2. Simulated Effects of Temperature

Fig. 4.4 shows the diffusion profiles at different temperatures. As can be seen, the overall diffusion of Ti atoms is on the slow side. Temperatures of ~1400 °C or higher are required to observe any significant amount of travel of ^{46}Ti. There can be a number of possible reasons for this behavior. First of all, the only mobile species of Ti is the interstitials. The lattice atoms would be stationary, and Ti vacancies have been shown to have very slow diffusion times (~ thousands of hours) [3], and can thus be assumed to be stationary in the current time frame (3 hr). Since the fraction of atoms that are in the form of interstitials (*i.e.*, mobile species) is small, a spread in the mobile species will have very little effect on the overall spread of atoms. Hence,

in order for the mobile species to have an influence in the travel of the overall population of atoms, the number of mobile species must increase to a significant amount and/or the mobile species must actively interact with the lattice atoms. Both of these mechanisms require high temperatures to be effective, thus leading to high temperature requirements in observing noticeable diffusion of the entire species.

In order to view the role of mobile species more explicitly, the profile of ^{46}Ti interstitials was also monitored separately (Fig. 4.5). Notice that the amount of spread of interstitials decreases with increasing temperature, which is contrary to the behavior of the overall concentration of ^{46}Ti. This implies that the interaction of mobile species with the lattice is more important than the amount of mobile species present in achieving greater amounts of ^{46}Ti diffusion.

4.5.3. Comparison of Mechanisms

The two different methods for the small fraction of mobile species to achieve global movement can be linked with the three different mechanisms that are incorporated in the model. The total amount (fraction) of mobile species is governed by the bulk and surface generation mechanism. The interaction between the mobile species and the lattice atoms is governed by the kick-in/ kick-out mechanism and the bulk generation mechanism. Parameter sensitivity analysis (with all mechanisms present) of the activation energy of each mechanism shows that the model is most sensitive to the bulk generation mechanism (Table 4.2). Fig. 4.6 illustrates the effect of each mechanism when they are present alone. First to notice is the fact that the presence of surface reaction alone has almost no effect on the overall diffusion of ^{46}Ti. It thus follows that the amount of mobile species can be less important than the interaction of mobile and stationary

species on the overall diffusion; as was seen in the previous section. The bulk generation and kick-in/ kick-out mechanism both induce noticeable amounts of ^{46}Ti diffusion. The resulting behavior is quite different, however. It can be seen that the kick-in/ kick-out induces more spread, while the bulk generation increases the total amount of displaced ^{46}Ti atoms.

The effective diffusivity of ^{46}Ti was calculated using the method previously derived in our lab [5,20] to quantify the difference in profiles. From a normalized semilog plot of the profile at short time scales, the parameters λ and K_{gen} can be extracted, which is the mean path length between generation and annihilation events and the generation rate of mobile species, respectively. These can be combined to give the effective diffusivity by the relation [5,21]

$$D_{eff} = K_{gen}\lambda^2 \tag{4.20}$$

The resulting D_{eff} for the bulk generation only case and kick-in/ kick-out only case is 1.13×10^{-15} cm^2/s and 7.51×10^{-16} cm^2/s, respectively. This indicates that the bulk generation induces more diffusion compared to kick-out/ kick-in. However, λ is larger for kick-in/ kick-out (46.08 nm verses 34.97 nm, for kick-in/ kick-out and bulk generation, respectively), which means the spreading is indeed larger than bulk generation.

While the surface reaction does not influence the overall diffusion of ^{46}Ti on its own, it can have a dramatic effect when combined with other mechanisms. As can be seen in Fig 4.7, adding the surface reaction mechanism to either one or both of the other two mechanisms alters the profiles significantly. The main effect is an increase in the amount of spreading, which also leads to increased effective diffusivities. Namely, a significant increase in λ can be observed, followed by an increase in D_{eff}. The most dramatic change comes for the combination of kick-in/ kick-out and surface reaction, where D_{eff} sees almost an order of magnitude increase with the

introduction of surface reaction. The obtained diffusivity values for the profiles presented in Fig. 4.7 are tabulated in Table 4.3.

Overall, the addition of each mechanism increases the effective diffusivity, albeit in different manners. Bulk generation increases the interaction between mobile and lattice atoms, thereby increasing the total amount of atoms traveling. Surface reaction, on the other hand, increases the amount of traveling of the atoms. Kick-in/ kick-out achieves a combination of both. It can thus be concluded that each mechanism plays a separate but significant role in the diffusion of ^{46}Ti under the given conditions.

4.5.5. Surface Effects

Surface coverage effects were analyzed by multiplying a coverage factor φ to the boundary condition in Eq. (4.13). The coverage was varied from clean surfaces ($\varphi = 1$) to 90% coverage ($\varphi = 0.1$), and the diffusion profiles were obtained (Fig. 4.8). As expected, clean surfaces induce increased diffusion. The effective diffusivities and corresponding parameters were also obtained for each case (Table 4.4). It can be seen that the results reflect the discussions in Section 4.5.4 regarding surface reactions. Increasing the surface coverage has the effect of reducing the surface reaction mechanism. This reduction leads to a reduction in the amount of spreading, represented by a decrease in λ and an increase in K_{gen} values. It thus follows that along with influencing the total diffusivity, the surface reaction affects the spreading factor as well.

4.6. Conclusion

Computational studies of the cation diffusion in TiO_2 have been carried out, revealing the effects of the various governing mechanisms and the surface. The ^{46}Ti diffusion was found to be relatively slow and higher temperatures (~1400 °C or above) were required to observe noticeable diffusion. Examination of the effects of the three main mechanisms implemented – bulk generation, kick-in/ kick-out, and surface reactions – show that the interaction of mobile species (*i.e.*, Ti interstitials) with lattice atoms is necessary to induce the overall diffusion of species. While increased amounts of mobile species have little impact on the overall diffusion on its own, it can greatly enhance the amount of diffusion, especially the amount of spreading, when suitable interaction mechanisms are present. It is through this method that clean surfaces can bring enhanced diffusion of species.

For more accurate results to be obtained, the simulated profiles must be compared with experimental results to extract refined parameters. Nevertheless, the computational analysis revealed some insight into the behaviors of cations in TiO_2. These results should provide a good starting point for future attempts of unveiling the fundamentals of cation and related defect behaviors.

4.7. Tables and Figures

Table 4.1. Maximum likelihood estimation of parameters

Parameter	Maximum Likelihood Estimate ($\bar{x}$)	Error ($\bar{\sigma}_{\bar{x}}^2$)	References
E_1, Bulk Generation	6.06	0.103	Tomlinson et al., 1989 [22] Dawson et al., 1997 [23] Ikeda et al., 1993 [24] Smyth, 2000 [25] He and Sinnott, 2005 [26] He et al., 2007 [27] Li et al., 2009 [28]
E_4, Surface Generation	9.67	0.175	Blumenthal et al., 1966 [29] Alcock et al., 1967 [30] Kofstad, 1967 [2] Picard and Gardanian, 1975 [31] Baumard and Tani, 1977 [32,33] Marucco et al., 1981 [34] Lee et al., 2005 [35]
$E_{D_{Ti_{int}}}$, Ti Interstitial Diffusivity	2.84	0.022	Venkatu and Poteat, 1970 [36] Lundy et al., 1973 [37] Akse and Whitehurst, 1978 [38] Hoshino and Peterson, 1985 [7] Henderson, [6] Lee and Yoo, 2006 [39]

Table 4.2. Parameter sensitivity analysis

Parameter	Value (eV)	Sensitivity (Φ_j)
E_1, Bulk Generation	6.06	3.9697×10^3
E_3, Kick-in/ Kick-out	12.3	3.3078×10^3
E_4, Surface Generation	9.67	3.0414×10^3
$E_{D_{Ti_{int}}}$, Ti Interstitial Diffusivity	2.84	4.1115×10^2

Table 4.3. Effective diffusivities of various combinations of mechanisms

Mechanism	λ (nm)	K_{gen} (s^{-1})	D_{eff} (cm^2/s)
All	51.81347	1.5667×10^{-4}	4.2061×10^{-15}
Bulk Generation	34.96503	9.2696×10^{-5}	1.1333×10^{-15}
Bulk Generation + Surface Reaction	77.51938	3.6034×10^{-5}	2.1654×10^{-15}
Kick-in/ Kick-out	46.08295	3.5372×10^{-5}	7.5118×10^{-16}
Kick-in/ Kick-out + Surface Reaction	56.81818	1.2687×10^{-4}	4.0957×10^{-15}
Bulk Generation + Kick-in/ Kick-out	29.67359	1.6676×10^{-4}	1.4683×10^{-15}

Table 4.4. Effective diffusivities of various surface coverages

Coverage	λ (nm)	K_{gen} (s^{-1})	D_{eff} (cm^2/s)
Clean	51.81347	1.5667×10^{-4}	4.2061×10^{-15}
10%	50.00000	1.5885×10^{-4}	3.9712×10^{-15}
25%	47.39336	1.6040×10^{-4}	3.6027×10^{-15}
50%	42.01681	1.6668×10^{-4}	2.9425×10^{-15}
75%	36.49635	1.7143×10^{-4}	2.2834×10^{-15}
90%	31.84713	1.8611×10^{-4}	1.8876×10^{-15}

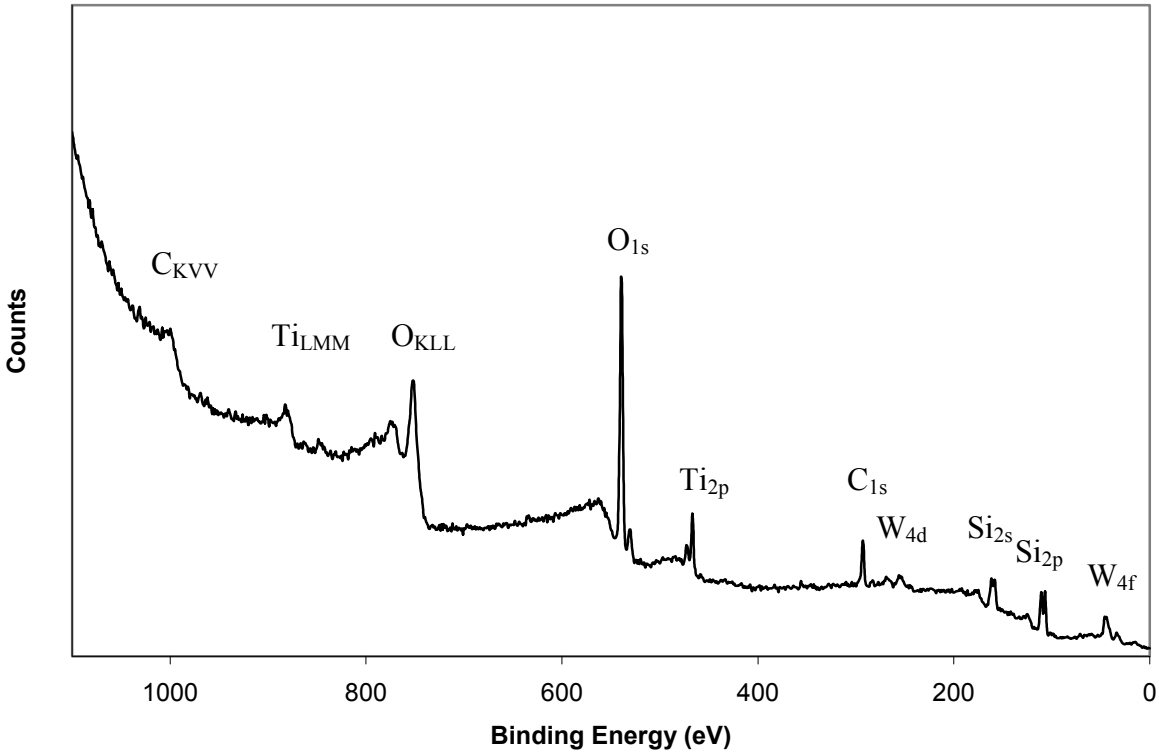

Fig. 4.1. XPS spectra of TiO_2 deposited on Si. Deposition was done for 25 min at 900 °C.

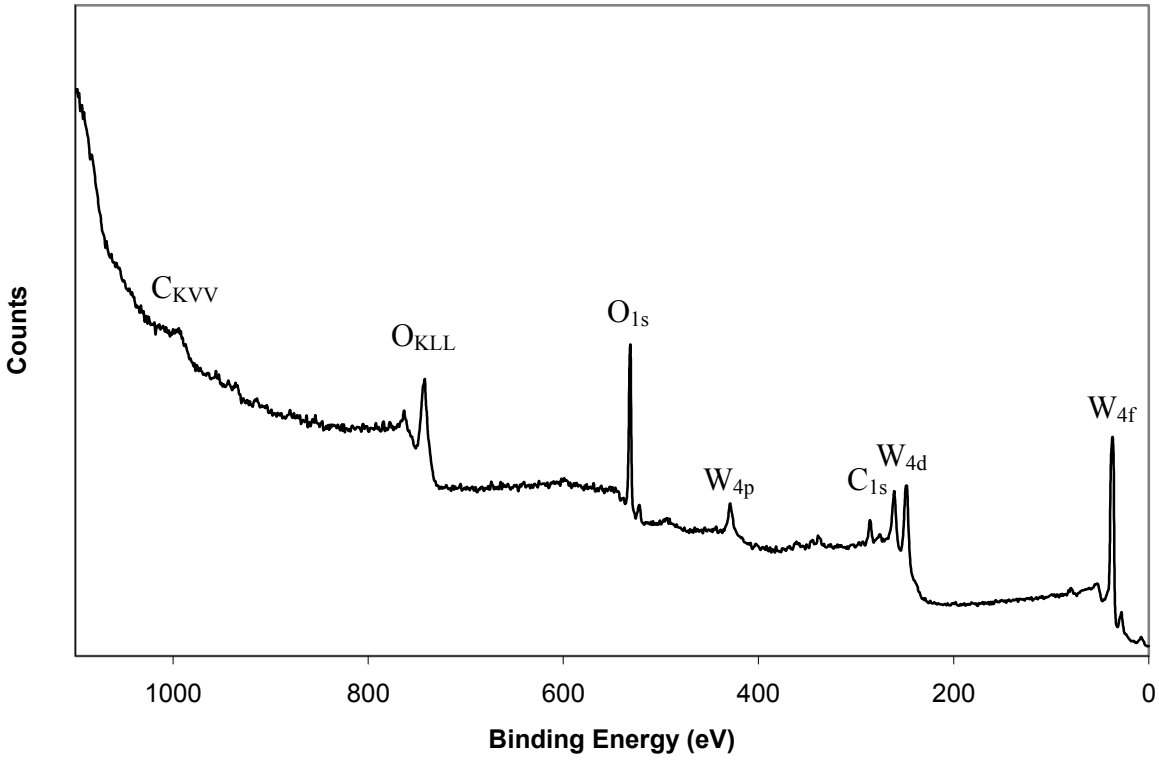

Fig. 4.2. XPS spectra of Si after exposure to the heated empty boat at 900 °C for 40 min.

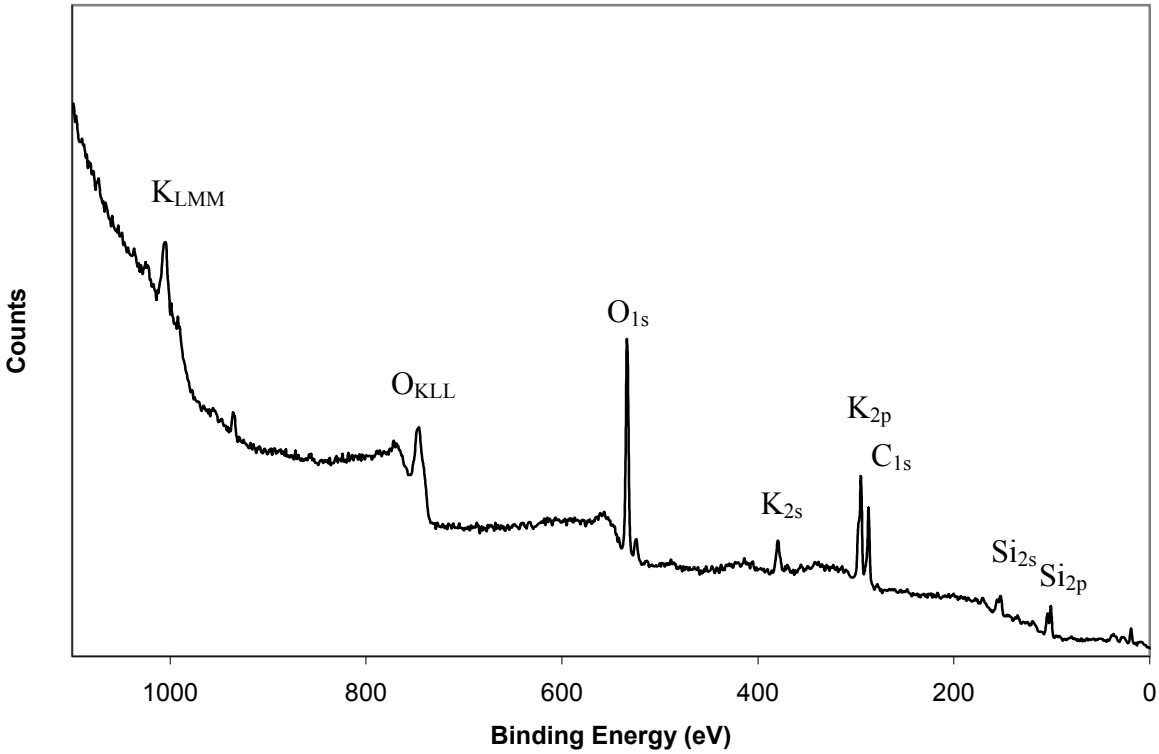

Fig. 4.3. XPS spectra of attempted TiO_2 deposition on Si at 900 °C for 30 min.

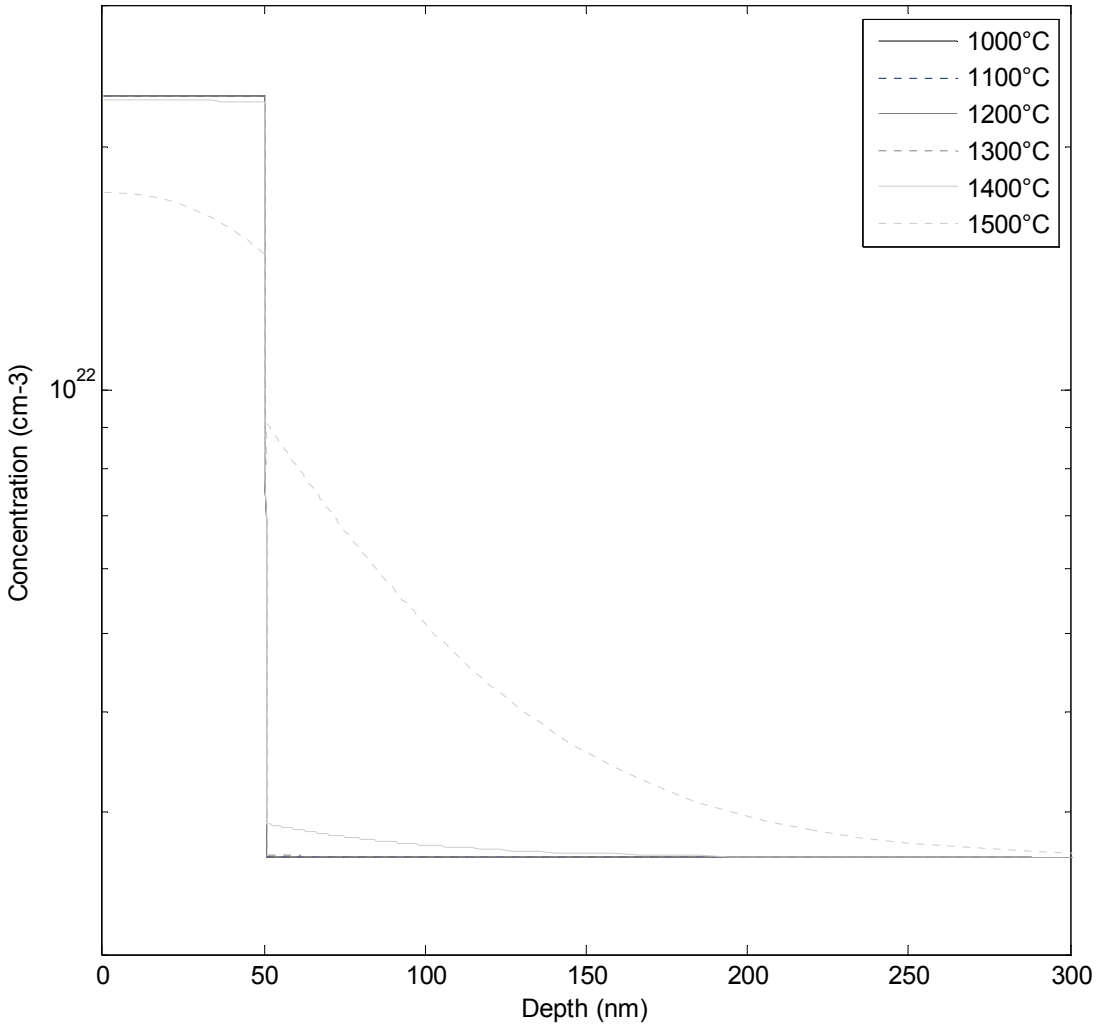

Fig. 4.4. Simulated diffusion profiles of ^{46}Ti with varying temperature. Diffusion time is 3 hr.

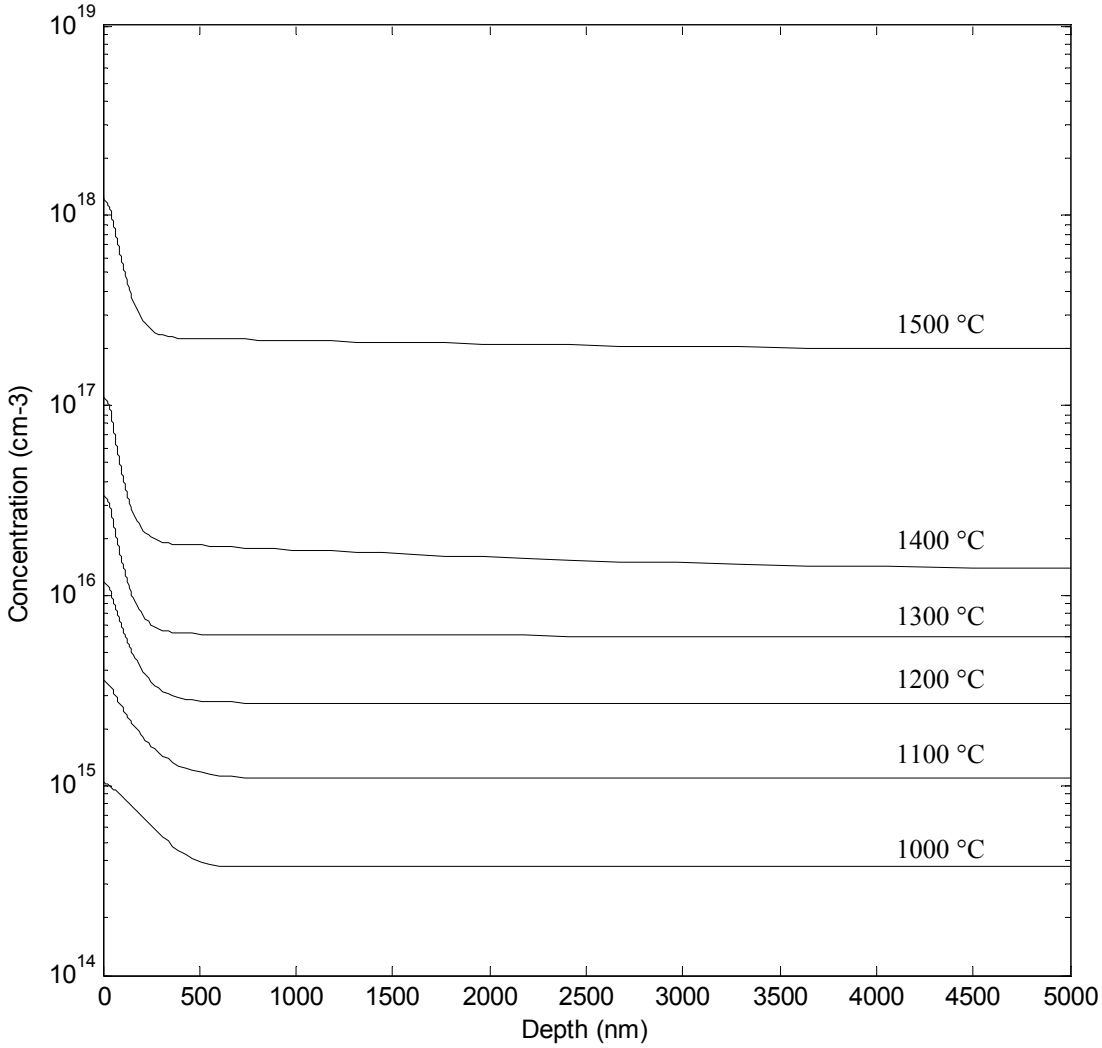

Fig. 4.5. Simulated ^{46}Ti interstitial profiles after 3 hr diffusion at various temperatures.

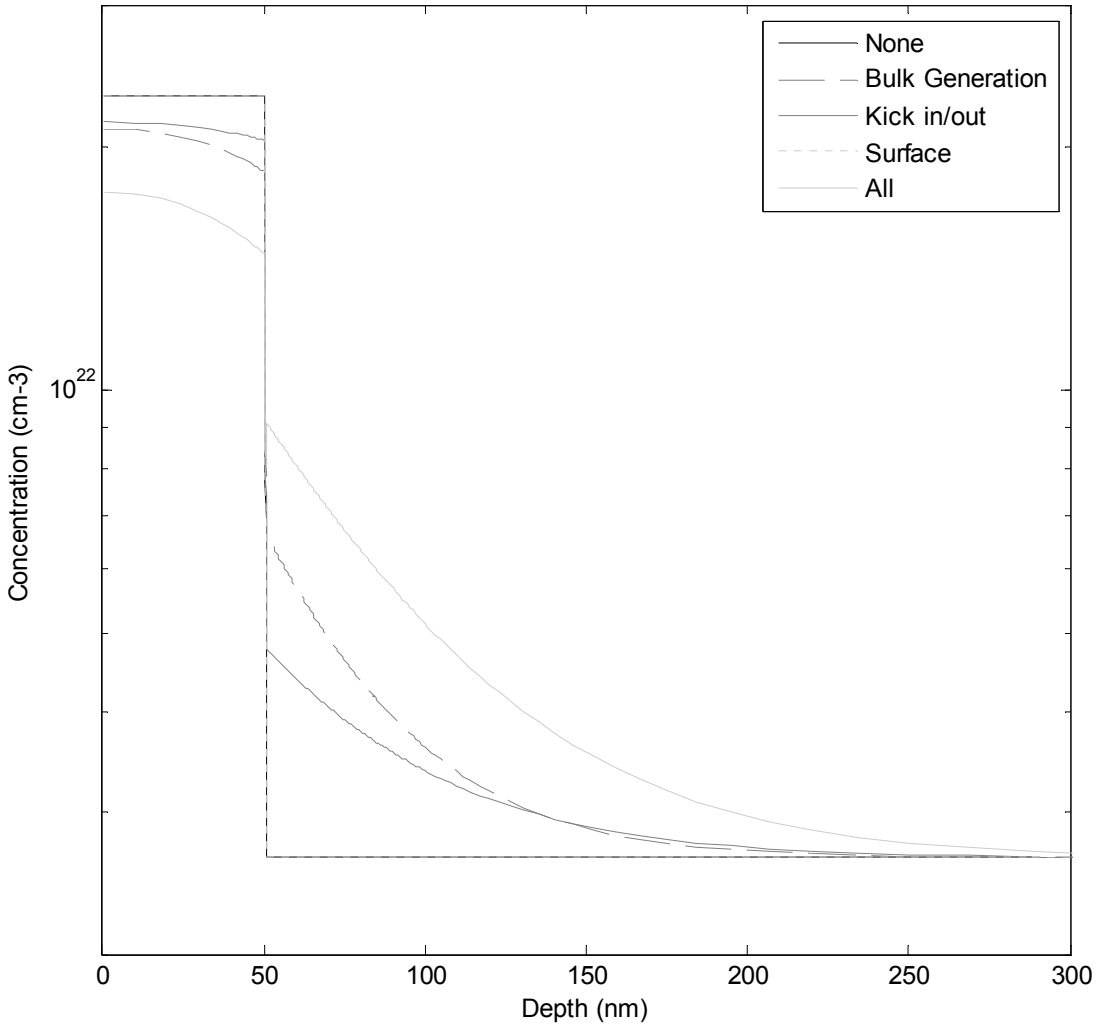

Fig. 4.6. Simulated diffusion profiles of ^{46}Ti when different mechanisms are active. After 3 hr at 1500 °C.

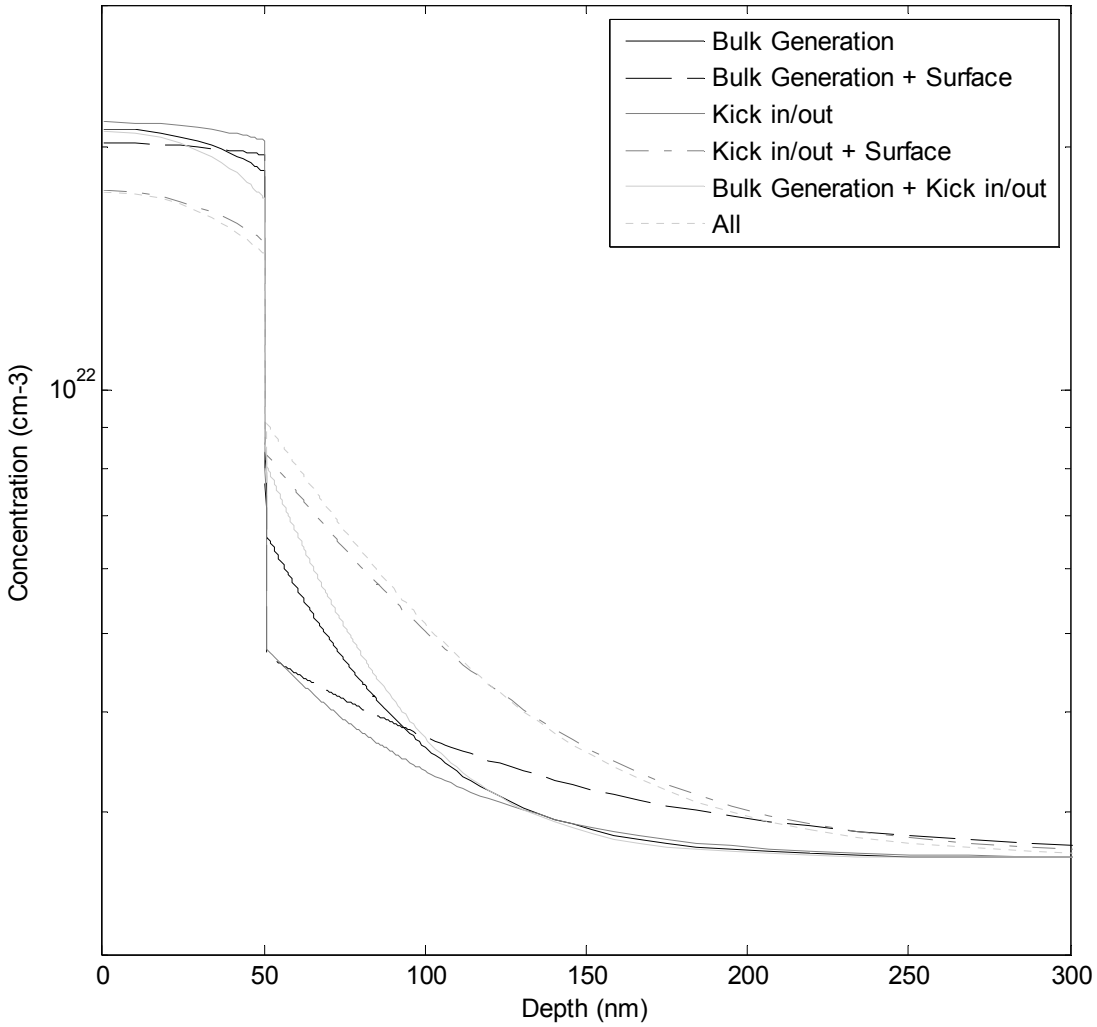

Fig. 4.7. Simulated diffusion profiles of ^{46}Ti with different combinations of mechanisms active. After 3 hr at 1500 °C.

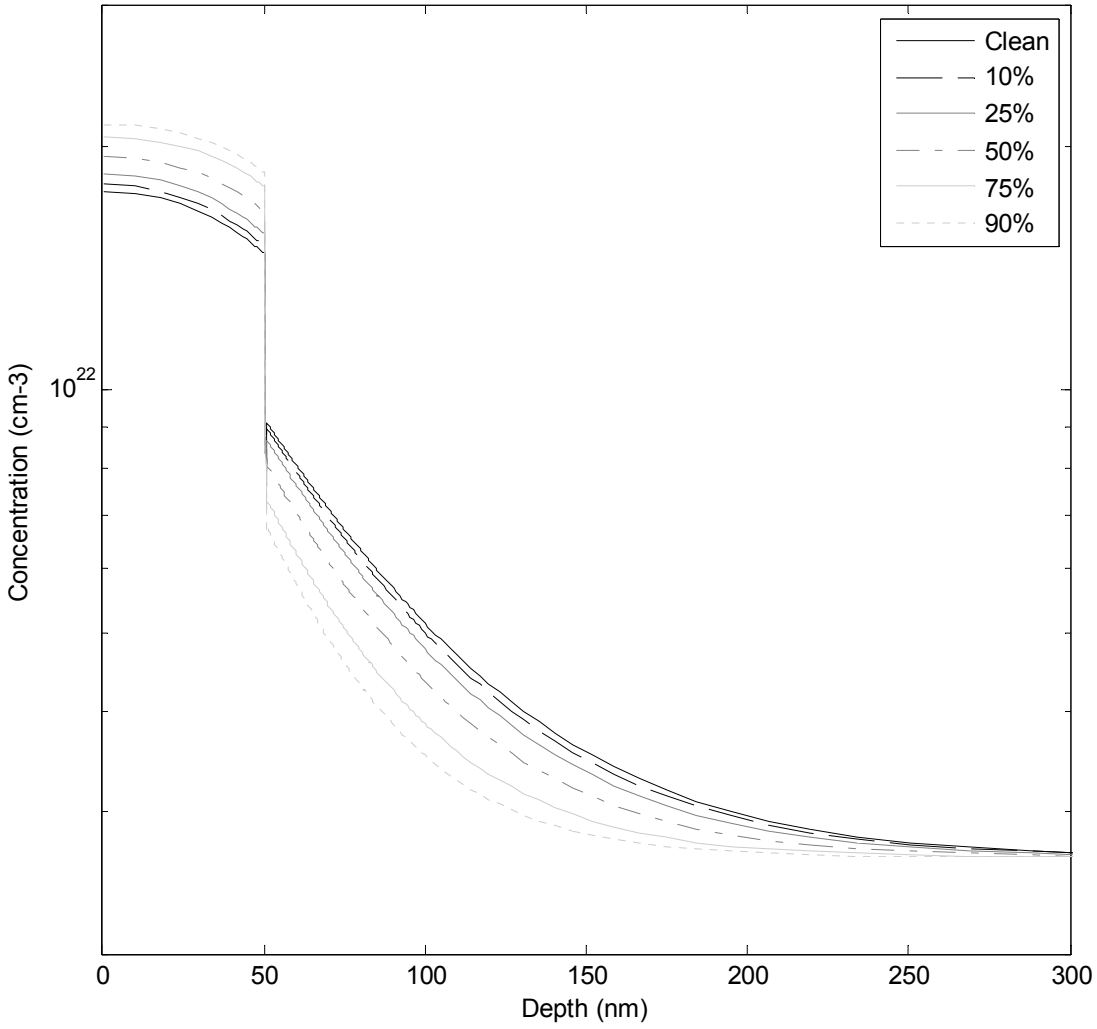

Fig. 4.8. Simulated diffusion profiles of ^{46}Ti with varying surface coverage. After 3 hr at 1500 °C.

4.8. References

1 A. Fujishima, K. Honda, *Nature* **238** (1972) 37-38.

2 P. Kofstad, *J. Less Common Met.* **13** (1967) 635.

3 M. K. Nowotny, T. Bak, J. Nowotny, *J. Phys. Chem. B* **110** (2006) 16302-16308.

4 M. K. Nowotny, L. R. Sheppard, T. Bak, J. Nowotny, *J. Phys. Chem. C* **112** (2008) 5275-5300.

5 R. Vaidyanathan, Ph.D. thesis, University of Illinois at Urbana-Champaign, 2007.

6 M. A. Henderson, *Surf. Sci.* **419** (1999) 174-187.

7 K. Hoshino, N. L. Peterson, C. L. Wiley, *J. Phys. Chem. Solids* **46** (1985) 1397-1411.

8 A. Hollister, Ph.D. thesis, University of Illinois at Urbana-Champaign, 2010.

9 S. M. Sze, *Semiconductor devices, physics and technology*, Wiley, New York, 2002.

10 V. N. Kuznetsov, *Kinet. Catal.* **43** (2002) 868-873.

11 M. Y. L. Jung, R. Gunawan, R. D. Braatz, E. G. Seebauer, *J. Appl. Phys.* **95** (2004) 1134-1140.

12 T. M. Kwok, Ph.D. thesis, University of Illinois at Urbana-Champaign, 2007.

13 See M. Law, University of Florida at Gainesville, http://www.swamp.tec.ufl.edu/

14 J. V. Beck, K. J. Arnold, *Parameter estimation in engineering and science*, Wiley, New York, 1977.

15 I. J. Myung, *J. Math. Psych.* **47** (2003) 90-100.

16 J. R. Leis, S. A. Gallagher, M. A. Kramer, *Comp. Chem. Eng.* **11** (1987) 409-421.

17 F. D. Van Voorhees, A. T. Bahill, in: *Proceedings of the IEEE International Conference on Systems, Man and Cybernetics*, (1995) pp. 971-976.

18 R. Tomović, M. Vukobratović, *General sensitivity theory*, American Elsevier Pub. Co., New York,, 1972.

19 A. Varma, M. Morbidelli, H. Wu, *Parametric sensitivity in chemical systems*, Cambridge University Press, Cambridge, U.K. ; New York, NY, 1999.

20 R. Vaidyanathan, M. Y. L. Jung, R. D. Braatz, E. G. Seebauer, *AIChE J.* **52** (2006) 366-370.

21 N. E. B. Cowern, G. F. A. van de Walle, D. J. Gravesteijn, C. J. Vriezema, *Phys. Rev. Lett.* **67** (1991) 212-215.

22 S. M. Tomlinson, C. M. Freeman, C. R. A. Catlow, H. Donnerberg, M. Leslie, *J. Chem. Soc., Faraday Trans. 2* **85** (1989) 367-383.

23 I. Dawson, P. D. Bristowe, J. A. White, M. C. Payne, in: *Materials Research Society Symposium - Proceedings*, (1997) pp. 203-208.

24 J. A. S. Ikeda, Y. M. Chiang, A. J. Garratt-Reed, J. B. Vander Sande, *J. Am. Ceram. Soc.* **76** (1993) 2447-2459.

25 D. M. Smyth, *The defect chemistry of metal oxides*, Oxford University Press, New York, 2000.

26 J. He, S. B. Sinnott, *J. Am. Ceram. Soc.* **88** (2005) 737-741.

27 J. He, R. K. Behera, M. W. Finnis, X. Li, E. C. Dickey, S. R. Phillpot, S. B. Sinnott, *Acta Mater.* **55** (2007) 4325-4337.

28 X. Li, M. W. Finnis, J. He, R. K. Behera, S. R. Phillpot, S. B. Sinnott, E. C. Dickey, *Acta Mater.* **57** (2009) 5882-5891.

29 R. N. Blumenthal, J. Coburn, J. Baukus, W. M. Hirthe, *J. Phys. Chem. Solids* **27** (1966) 643.

30 C. B. Alcock, S. Zador, B. C. H. Steele, *Proc. Br. Ceram. Soc.* **8** (1967) 231.

31 C. Picard, P. Gerdanian, *J. Solid State Chem.* **14** (1975) 66-77.

32 J. F. Baumard, E. Tani, *J. Chem. Phys.* **67** (1977) 857-860.

33 J. F. Baumard, E. Tani, *Phys. Status Solidi A* **39** (1977) 373-382.

34 J. F. Marucco, J. Gautron, P. Lemasson, *J. Phys. Chem. Solids* **42** (1981) 363-367.

35 D. K. Lee, J. L. Jeon, M. H. Kim, W. Choi, H. I. Yoo, *J. Solid State Chem.* **178** (2005) 185-193.

36 D. A. Venkatu, L. E. Poteat, *Mater. Sci. Eng.* **5** (1970) 258.

37 T. Lundy, R. Padgett, M. Banus, *Metall. Mater. Trans. B* **4** (1973) 1179-1180.

38 J. R. Akse, H. B. Whitehurst, *J. Phys. Chem. Solids* **39** (1978) 457-465.

39 D. K. Lee, H. I. Yoo, *Solid State Ionics* **177** (2006) 1-9.

APPENDIX A: RUNCODES

A.1. ^{46}Ti Diffusion Model

```
proc TiO2 {kdiffTi3 kdiffTi4 kdiffTivac Etrap EdiffTi3 EdiffTi4 EdiffTivac E1 E2 E3 Name} {

# Define grid

    line x loc=0.000000 tag=top spac=0.01
    line x loc=0.050000 spac=0.00005
    line x loc=0.075000 spac=0.0001
    line x loc=0.100000 spac=0.001
    line x loc=5.0 tag=bot spac=0.5
    region Silicon xlo=top xhi=bot
    init

# Initial conditions

    profile name=Ti46init inf=slope_profile.txt
    profile name=Ti48init inf=rev_slope_profile.txt

    sel z = Ti46init name=Ti46 store
    sel z = Ti48init name=Ti48 store
    sel z = Ti46*1.8683e17/2.3092e22 name=Ti463 store
    sel z = Ti46*1.7467e16/2.3092e22 name=Ti464 store
    sel z = Ti48*7.1221e16/8.8033e21 name=Ti3 store
    sel z = Ti48*5.6587e15/8.8033e21 name=Ti4 store

    sel z =(Ti48+Ti46)*2 name=Osub store
    sel z =Osub*3.27e16/6.38e22 name=Ovac store
    sel z =(Ti48+Ti46)*2.8217e17/3.18953e22 name=Tivac store

    sel z = Ti46-Ti463-Ti464 name=Ti46lat store
    sel z = Ti48-Ti3-Ti4 name=Tilat store

# define species to be simulated

    solution name=Tivac solve !damp !negative add
    solution name=Ti3 solve !damp !negative add
    solution name=Ti4 solve !damp !negative add
    solution name=Ti463 solve !damp !negative add
    solution name=Ti464 solve !damp !negative add
    solution name=Ti46lat solve !damp !negative add
    solution name=Tilat solve !damp !negative add

# Choosing Poisson Eqn and its boundary condition

    pdbSetBoolean Silicon Potential TEDmodel 1
    pdbSetBoolean Silicon Potential Pin 0
```

```
# Define all the parameters

    set tempK [pdbDelayDouble tempK]
    term name=kb add Silicon eqn = "8.617383e-05"
    term name=pi add Silicon eqn = "3.14159e0"
    term name=captr add Silicon eqn = "2.95e-8"
    term name=alpha add Silicon eqn = "kb*$tempK"
    term name=pre add Silicon eqn = "5e12"

# Energy levels

    term name=TO2Eg add Silicon eqn = "(3.09e0-(6.6e-4*$tempK))"
    term name=TO2ni add Silicon eqn = "2*((2*pi*$tempK*1.38e-23/(6.63e-34)^2)^1.5)*((30*
(9.11e-31)^2)^.75)*1.0e-6*exp(-1*TO2Eg/2/alpha)"
    term name=no_orig add Silicon eqn = "2*Ovac+((4*Ovac^2)+TO2ni^2)^0.5"
    term name=TO2Eib add Silicon eqn = "-1*alpha*log(no_orig/TO2ni)"
    term name=TO2Ei add Silicon eqn = "TO2Eib-Potential"
    term name=Ev add Silicon eqn = "TO2Ei-TO2Eg/2"
    term name=Ec add Silicon eqn = "TO2Ei+TO2Eg/2"
    term name=EFb add Silicon eqn = "0.0"

# Assume equilibrium electron and hole concentration

    term name=Myn add Silicon eqn = "TO2ni*exp((-TO2Ei)/alpha)"
    term name=Myp add Silicon eqn = "TO2ni*exp(TO2Ei/alpha)"

# Trap energies (ionization energy)

    term name=ETi3 add Silicon eqn = "((TO2Eg/3.09)*$Etrap)+Ev"

# Population of charged species

    term name=popTi3 add Silicon eqn = "1/(1+0.5e0*exp((ETi3-EFb)/(kb*$tempK)))"
    term name=popTi4 add Silicon eqn = "1-popTi3"

# Diffusivity

    term name=diffTi3 add Silicon eqn = "$kdiffTi3*exp(-$EdiffTi3/(kb*$tempK))"
    term name=diffTi4 add Silicon eqn = "$kdiffTi4*exp(-$EdiffTi4/(kb*$tempK))"
    term name=diffTivac add Silicon eqn = "$kdiffTivac*exp(-$EdiffTivac/(kb*$tempK))"

# Necessary terms to make diffusion equations readable by Floops

    term name=Ti41 add Silicon eqn = "grad(Potential*4.0e0*Ti4)"
    term name=Ti42 add Silicon eqn = "4.0e0*Ti4*grad(Potential)"
    term name=Ti43 add Silicon eqn = "Potential*grad(4.0e0*Ti4)"
    term name=Ti31 add Silicon eqn = "grad(Potential*3.0e0*Ti3)"
    term name=Ti32 add Silicon eqn = "3.0e0*Ti3*grad(Potential)"
    term name=Ti33 add Silicon eqn = "Potential*grad(3.0e0*Ti3)"
```

```
    term name=Ti4641 add Silicon eqn = "grad(Potential*4.0e0*Ti464)"
    term name=Ti4642 add Silicon eqn = "4.0e0*Ti464*grad(Potential)"
    term name=Ti4643 add Silicon eqn = "Potential*grad(4.0e0*Ti464)"
    term name=Ti4631 add Silicon eqn = "grad(Potential*3.0e0*Ti463)"
    term name=Ti4632 add Silicon eqn = "3.0e0*Ti463*grad(Potential)"
    term name=Ti4633 add Silicon eqn = "Potential*grad(3.0e0*Ti463)"

# Define the diffusion equations

    pdbSetString Silicon Ti4 Equation "ddt(Ti4)-diffTi4*(grad(Ti4)+0.5e0/alpha*(Ti41+Ti42-Ti43))"
    pdbSetString Silicon Ti3 Equation "ddt(Ti3)-diffTi3*(grad(Ti3)+0.5e0/alpha*(Ti31+Ti32-Ti33))"
    pdbSetString Silicon Ti464 Equation "ddt(Ti464)-diffTi4*(grad(Ti464)+0.5e0/alpha*(Ti4641+
Ti4642-Ti4643))"
    pdbSetString Silicon Ti463 Equation "ddt(Ti463)-diffTi3*(grad(Ti463)+0.5e0/alpha*(Ti4631+
Ti4632-Ti4633))"
    pdbSetString Silicon Tivac Equation "ddt(Tivac)-diffTivac*(grad(Tivac))"

# Reaction constants

    term name=K1 add Silicon eqn = "pre*exp(-$E1/(kb*$tempK))"
    term name=K2 add Silicon eqn = "4*pi*(diffTi3*popTi3+diffTi4*popTi4+diffTivac)*2.95e-8"
    term name=K3 add Silicon eqn = "pre*exp(-$E2/(kb*$tempK))"

# Reaction rates

    term name=Tii add Silicon eqn = "Ti3+Ti4"
    term name=Ti46i add Silicon eqn = "Ti463+Ti464"
    term name=RTivac add Silicon eqn = "K1*(Tilat+Ti46lat)-K2*(Tii+Ti46i)*Tivac"
    term name=RTii add Silicon eqn = "K1*Tilat-K2*Tii*Tivac+K3*Ti46i*Tilat-K3*Tii*Ti46lat"
    term name=RTilat add Silicon eqn = "-K1*Tilat+K2*Tii*Tivac-K3*Ti46i*Tilat+K3*Tii*Ti46lat"
    term name=RTi46i add Silicon eqn = "K1*Ti46lat-K2*Ti46i*Tivac-K3*Ti46i*Tilat+K3*Tii*
Ti46lat"
    term name=RTi46lat add Silicon eqn = "-K1*Ti46lat+K2*Ti46i*Tivac+K3*Ti46i*Tilat-K3*Tii*
Ti46lat"
    term name=RTi3 add Silicon eqn = "RTii*popTi3"
    term name=RTi4 add Silicon eqn = "RTii*popTi4"
    term name=RTi463 add Silicon eqn = "RTi46i*popTi3"
    term name=RTi464 add Silicon eqn = "RTi46i*popTi4"

    pdbSetString Silicon Tilat Equation "ddt(Tilat)-RTilat"
    pdbSetString Silicon Ti46lat Equation "ddt(Ti46lat)-RTi46lat"

    set Tivaceqn [pdbGetString Silicon Tivac Equation]
    set Ti3eqn [pdbGetString Silicon Ti3 Equation]
    set Ti4eqn [pdbGetString Silicon Ti4 Equation]
    set Ti463eqn [pdbGetString Silicon Ti463 Equation]
    set Ti464eqn [pdbGetString Silicon Ti464 Equation]

    pdbSetString Silicon Tivac Equation "$Tivaceqn-RTivac"
    pdbSetString Silicon Ti3 Equation "$Ti3eqn-RTi3"
    pdbSetString Silicon Ti4 Equation "$Ti4eqn-RTi4"
```

```
    pdbSetString Silicon Ti463 Equation "$Ti463eqn-RTi463"
    pdbSetString Silicon Ti464 Equation "$Ti464eqn-RTi464"

# Boundary Conditions

    if {[pdbGetBoolean Silicon Potential Pin]} {
    pdbSetBoolean Gas_Silicon Potential Fixed_Silicon 1
    pdbSetString Gas_Silicon Potential Equation_Silicon "1e20*Potential_Silicon"
    }

# Surface reaction

    pdbSetString Gas_Silicon Ovac Equation_Silicon "0.0e0"
    pdbSetString Gas_Silicon Tivac Equation_Silicon "0.0e0"
    pdbSetString Gas_Silicon Ti3 Equation_Silicon "3.6124e38*exp(-$E3/(8.617383e-05*$tempK))
*0.2524-Ti3*0.00002*3*$kdiffTi3*exp(-1*$EdiffTi3/(8.617383e-05*$tempK))/2.95e-8*2.9832e-4"
    pdbSetString Gas_Silicon Ti4 Equation_Silicon "3.6124e38*exp(-$E3/(8.617383e-05*$tempK))
*0.0236-Ti4*0.00002*3*$kdiffTi4*exp(-1*$EdiffTi4/(8.617383e-05*$tempK))/2.95e-8*2.9832e-4"
    pdbSetString Gas_Silicon Ti463 Equation_Silicon "3.6124e38*exp(-$E3/(8.617383e-05*$tempK))
*0.6621-Ti463*0.00002*3*$kdiffTi3*exp(-1*$EdiffTi3/(8.617383e-05*$tempK))/2.95e-8*2.9832e-4"
    pdbSetString Gas_Silicon Ti464 Equation_Silicon "3.6124e38*exp(-$E3/(8.617383e-05*$tempK))
*0.0619-Ti464*0.00002*3*$kdiffTi4*exp(-1*$EdiffTi4/(8.617383e-05*$tempK))/2.95e-8*2.9832e-4"

# Start diffusion

    diffuse time=180 temp=1500 press=0.0 init=1e-10

# Output results

    sel z=(Ti463+Ti464)
    print.2file outf=$Name.Ti46i.txt

    sel z=(Ti463+Ti464+Ti46lat)
    print.2file outf=$Name.Ti46.txt

}

# Run code

TiO2 3.8e-3 3.8e-3 1e-3 1.24 2.84 2.84 20.5 6.06 12.3 9.673 file_name
```

A.2. Parameter Sensitivity Analysis

```
% This code reads in simulated annealed profiles and computes total sensitivity

clear

% data = [E1 E2 E3 Ediff]
data = [6.06 12.3 9.673 2.84];

% Change in parameters
beta = data*0.05;

dat_ref = load (['mid.Ti46.txt']);
mat = [0 0 0 0];
for i = 1:4
        a = num2str(i);

        % Read in output
        mat_up = load (['E',a,'up.Ti46.txt']);
        mat_dn = load (['E',a,'dn.Ti46.txt']);
        mat_mid = load (['mid.Ti46.txt']);
        dat_up = interp1(mat_up(:,1),mat_up(:,2),dat_ref(:,1));
        dat_dn = interp1(mat_dn(:,1),mat_dn(:,2),dat_ref(:,1));
        dat_mid = interp1(mat_mid(:,1),mat_mid(:,2),dat_ref(:,1));

        % Calcualate sensitivity
        for p = 1:size(dat_ref,1)
                mat(i) = mat(i) + abs((dat_up(p)-dat_dn(p))*data(i)/(2*beta(i)*dat_mid(p)));
        end
end

%Save to file
mat = mat';
save ('SA_Ti46.txt', 'mat', '-ascii', '-double', '-tabs');
```